1 OF 2
AD
A101125

LEVEL

(4)

AFOSR-TR- 81 -0538

Viscous-Inviscid Interaction
in Transonic Flow

by

Laurence B. Wigton

Ph.D. Thesis
University of California, Berkeley
June 1981

SECURITY CLASSIFICATON OF THIS PAGE (When Data Entered)

REPORT DOCUMENTATION PAGE	READ INSTRUCTIONS BEFORE COMPLETING FORM

1. REPORT NUMBER	2. GOVT ACCESSION NO.	3. RECIPIENT'S CATALOG NUMBER
AFOSR-TR- 81 -0538 $AD-A101125$		

4. TITLE (and Subtitle)	5. TYPE OF REPORT & PERIOD COVERED
"VISCOUS-INVISCID INTERACTION IN TRANSONIC FLOW"	INTERIM JUNE 1981
	6. PERFORMING ORG. REPORT NUMBER

7. AUTHOR(s)	8. CONTRACT OR GRANT NUMBER(s)
L B WIGTON	AFOSR-80-0230

9. PERFORMING ORGANIZATION NAME AND ADDRESS	10. PROGRAM ELEMENT, PROJECT, TASK AREA & WORK UNIT NUMBERS
UNIVERSITY OF CALIFORNIA BERKELEY, CA	2307/A4 61102F

11. CONTROLLING OFFICE NAME AND ADDRESS	12. REPORT DATE
AIR FORCE OFFICE OF SCIENTIFIC RESEARCH/NA BOLLING AFB, DC 20332	JUNE 1981
	13. NUMBER OF PAGES 111

14. MONITORING AGENCY NAME & ADDRESS(if different from Controlling Office)	15. SECURITY CLASS. (of this report)
	UNCLASSIFIED
	15a. DECLASSIFICATION DOWNGRADING SCHEDULE

16. DISTRIBUTION STATEMENT (of this Report)

Approved for public release; distribution unlimited.

17. DISTRIBUTION STATEMENT (of the abstract entered in Block 20, if different from Report)

18. SUPPLEMENTARY NOTES

19. KEY WORDS (Continue on reverse side if necessary and identify by block number)

TRANSONIC FLOW
SUPERCRITICAL AIRFOILS
INVISCID FLOW
BOUNDARY LAYER COUPLING

20. ABSTRACT (Continue on reverse side if necessary and identify by block number)

The aim of this thesis is to couple an inviscid two dimensional steady transonic flow calculation with a boundary layer calculation. This interaction is especially important in transonic problems since the boundary layer has a significant effect on the inviscid portion of the flow. Here, the inviscid solution is obtained by an algorithm developed for the full potential equation by Holst and Ballhaus while the attached and separated turbulent boundary layer calculations are performed by Green's lag entrainment method. Guided by a

DD FORM 1473 1 JAN 73   EDITION OF 1 NOV 65 IS OBSOLETE

model problem suggested by Le Balleur, a viscous-inviscid coupling algorithm
is developed. Theoretical analysis indicates that it coverges rapidly for
attached flows and also performs well for separated flows. These conclusions
are confirmed through a series of challenging transonic calculations involving
both attached and separated flows. The coupling algorithm is remarkably
stable and allows computation of coupled viscous-inviscid flows within times
required to perform the inviscid calculations by themselves.

Viscous-Inviscid Interaction in Transonic Flow

By

Laurence Byron/Wigton

A.B. (University of California) 1969

DISSERTATION

Submitted in partial satisfaction of the requirements for the degree of

DOCTOR OF PHILOSOPHY

in

Applied Mathematics

in the

GRADUATE DIVISION

OF THE

UNIVERSITY OF CALIFORNIA, BERKELEY

Approved: Maurice Holt .... May 5. 1981
                    Chairman   Date

81 7 06 003

Viscous-Inviscid Interaction in Transonic Flow

by

Laurence B. Wigton

Abstract

The aim of this thesis is to couple an inviscid two
dimensional steady transonic flow calculation with a
boundary layer calculation. This interaction is especially
important in transonic problems since the boundary layer
has a significant effect on the inviscid portion of the
flow. Here, the inviscid solution is obtained by an
algorithm developed for the full potential equation by
Holst and Ballhaus while the attached and separated
turbulent boundary layer calculations are performed by
Green's lag entrainment method.

Guided by a model problem suggested by Le Balleur,
a viscous-inviscid coupling algorithm is developed.
Theoretical analysis indicates that it coverges rapidly
for attached flows and also performs well for separated
flows. These conclusions are confirmed through a series
of challenging transonic calculations involving both
attached and separated flows. The coupling algorithm
is remarkably stable and allows computation of coupled

viscous-inviscid flows within times required to perform
the inviscid calculations by themselves.

Approved: _Maurice Holt_
Maurice Holt, Chairman

Acknowledgments

I am indebted to Dr. Yoshihara for introducing me to the viscous-inviscid coupling problem, to Professor Holt for encouraging me to pursue this problem to a reasonable conclusion, and to my parents who impatiently waited while all this took place. I would also like to thank Mr. Oliver W. Miller for helping me prepare some of the figures (it is obvious which ones!) and Sheila Slavin who made it seem that typing a thesis is not so hard after all.

Table of Contents

LIST OF FIGURES

1. Introduction

The aim of this thesis is to couple an inviscid two dimensional steady transonic flow calculation with a boundary layer calculation. This interaction is especially important in transonic problems since the boundary layer can have a significant effect on the inviscid portion of the flow. An example of a purely inviscid pressure distribution and that computed as the result of coupling with the boundary layer is shown in Fig. 8.21. As can be seen, the change in the pressure distribution is quite dramatic. The viscous effects smooth out the pressure near the trailing edge and weaken the shock driving it upstream. The shock jump conditions appear to be affected as well. Indeed for the purely inviscid solution, the critical pressure coefficient C_p^* shown as a tick mark on the C_p axis, nearly splits the shock profile. For the coupled solution, on the other hand, C_p^* is much closer to C_p downstream of the shock than it is to C_p upstream of the shock. An intuitive understanding of this phenomenon is provided by the following argument.

For the purely inviscid case, the flow must be tangential to the airfoil, both upstream and downstream of the shock. Therefore, the shock must not deflect the flow, which forces the shock to be normal to the airfoil. In the viscous case, on the other hand, the shock subjects

the boundary layer to a strongly unfavorable pressure
gradient. The boundary layer responds by thickening and
forming a wedge as can be seen in Fig. 8.22. The wedge,
in turn, forces the inviscid flow to deflect. In order
to accommodate the deflecting flow the shock must be
oblique. Hence the difference in the shock jump conditions
observed in Fig. 8.21 is caused by the change from a
normal to an oblique shock.

There are two programs in common use for computing
coupled viscous-inviscid transonic flows. One is the
viscous Garabedian and Korn (VGK) program developed by
Collyer and Lock (see Collyer and Lock [1979] and Lock
[1980]). The other is GRUMFOIL, developed by Melnik, Chow,
Mead and Jameson (see Melnik [1980]). Both programs are
capable of predicting flows around airfoils far more
accurately than is possible with purely inviscid codes.
Each employs the classical iteration procedure to couple
the boundary layer with the outer inviscid flow. This is
set out below.

CLASSICAL ITERATION

```
  ┌────────────────────────────────────┐
  │ Given Geometry Calculate           │◄──┐
  │ Inviscid Flow                      │   │
  └────────────────┬───────────────────┘   │
                   │                        │
  ┌────────────────┴───────────────────┐   │
  │ Given Inviscid Velocity            │   │
  │ Calculate Boundary Layer           │   │
  └────────────────┬───────────────────┘   │
                   │                        │
  ┌────────────────┴───────────────────┐   │
  │ Use Result of Boundary Layer       │───┘
  │ Calculation to Update Geometry     │
  └────────────────────────────────────┘
```
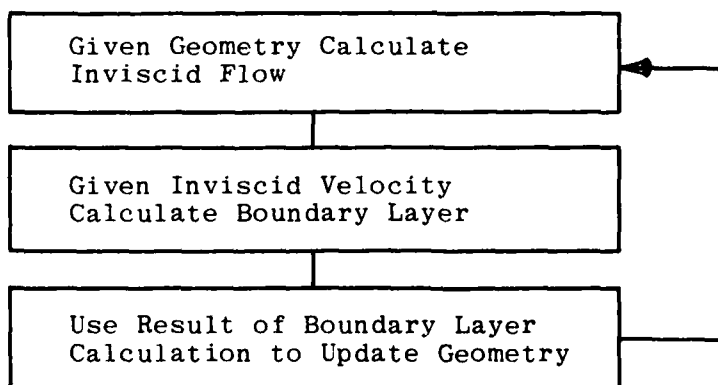
Unfortunately, as is well known, the classical iteration breaks down when the boundary layer separates or approaches separation. (The precise reasons for this failure will be explained below.) Accordingly, the authors of the VGK program and of GRUMFOIL expressed the need for alternative coupling procedures to handle separated flows more effectively. Such a coupling algorithm is developed in this thesis. The method is a modification of that proposed by Le Balleur [1978]. The modified method converges very rapidly in regions of attached flow and is also capable of handling regions of separated flow. Before describing this modification of Le Balleur's coupling algorithm, we will first discuss the boundary layer calculation and the inviscid flow calculation.

2. Green's Lag-Entrainment Method

In the present study the boundary layer is calculated using Green's lag-entrainment method (see Green et al. [1977] and East et al. [1977]). This is an integral method composed of a coupled system of first order ordinary differential equations. The turbulence modeling is derived from the Bradshaw-Ferriss [1971] turbulent energy equation. A useful feature of the method is the provision for performing wake calculations. The method has proven to be very fast and reliable, making it an ideal candidate for use in a viscous-inviscid coupling procedure. The method is in fact used by the VGK and GRUMFOIL programs.

When using the displacement thickness (δ^*) concept to represent the influence of the boundary layer on the outer inviscid flow, it is important to note that all integral boundary layer methods can be written in the form

$$A \frac{d\delta^*}{dx} = B \frac{\delta^*}{u} \frac{du}{dx} + C \qquad (2.1)$$

If $A = 0$, then it is impossible to use (2.1) to solve for $d\delta^*/dx$ in terms of du/dx. In this case it is not appropriate to integrate the boundary layer equations using a prescribed value of du/dx. This is referred to as the Goldstein or separation singularity. The separation singularity can be avoided by integrating the boundary layer equations with a prescribed value of $d\delta^*/dx$ and solving for du/dx. This is the so-called inverse mode of

calculating the boundary layer flow. On the other hand, if $B = 0$ somewhere in the interval of integration, then it becomes impossible to use (2.1) to solve for du/dx in terms of $d\delta^*/dx$. In this case it becomes inappropriate to integrate the boundary layer equations with prescribed values of $d\delta^*/dx$. This situation is referred to as the Crocco-Lees singularity.

A sharper criterion for deciding whether to prescribe $d\delta^*/dx$ or du/dx along the boundary layer edge is provided by considerations of numerical accuracy. If one is integrating numerically a differential equation of the form

$$\frac{dy}{dx} = Dy \qquad (2.2)$$

then the accuracy of the result depends on the size of Dh where h is the step size. To ensure numerical accuracy we would like to arrange for D to be as small as possible. Equation (2.1) can be rewritten in either of the forms

$$\frac{d\delta^*}{dx} = \left(\frac{B}{A}\frac{1}{u}\frac{du}{dx}\right)\delta^* + \frac{C}{A} \qquad (2.3)$$

$$\frac{du}{dx} = \left(\frac{A}{B}\frac{1}{\delta^*}\frac{d\delta^*}{dx}\right)u - \frac{C}{B} \qquad (2.4)$$

Comparing the coefficient of δ^* in Eq. (2.3) with the coefficient of u in Eq. (2.4) we see that from the viewpoint of numerical accuracy, it is better to prescribe du/dx at the boundary layer edge when

$$\left|\frac{A}{B}\frac{1}{\delta^*}\frac{d\delta^*}{dx}\right| > \left|\frac{B}{A}\frac{1}{u}\frac{du}{dx}\right| \qquad (2.5)$$

otherwise it is better to prescribe $d\delta^*/dx$.

It is shown by East [1977] that Green's lag-entrainment equations imply that

$$\frac{d\delta^*}{dx} = F_1 + F_2 \frac{\theta}{u} \frac{du}{dx} = F_1 + \frac{F_2}{H} \frac{\delta^*}{u} \frac{du}{dx} \qquad (2.6)$$

where θ is the momentum thickness. The third expression in Eq. (2.6) merely serves to define $H = \delta^*/\theta$. A plot of F_2/H versus a shape parameter $\bar{H}$ for both the standard Green's lag-entrainment method and for a modified method due to East is shown in Fig. 2.1. Separation normally occurs for $\bar{H} \geqslant 2.4$ (approximately). For $\bar{H} \leqslant 1.6$ the modified and standard method are identical. The modified method was introduced by East to improve the results based on Green's method for separated flows. As can be seen from Fig. 2.1, for separated flows this modification makes the value of $|F_2/H|$ larger than its corresponding value yielded by the standard method. For Mach numbers in the range of transonic interest, F_2/H is never 0 or ∞. In fact F_2/H is always a well-defined negative number. The Crocco-Lees singularity which corresponds to $F_2/H = 0$ does not occur until the Mach number exceeds 1.5. The separation singularity which corresponds to $F_2/H = \infty$ never occurs. However, in view of the analysis given above, if we are to expect accurate results when integrating the boundary layer equations with a prescribed velocity gradient, we must have

$$\left| \frac{F_2}{H} \frac{1}{u} \frac{du}{dx} h \right| \ll 1 \qquad (2.7)$$

where h is again the step size. This criterion is dif-
ficult to meet for separated flows because $|F_2/H|$ attains
such large values. This is all the more true for shock
induced separation because then $|du/dx|$ is also large.
Since the classical coupling procedure depends on inte-
grating the boundary layer equations with a prescribed
value of du/dx, the inequality (2.7) explains why trouble
can be expected for separated flows even though there is
no separation singularity. This demonstrates the need to
develop coupling procedures which allow one to integrate
the boundary layer equations with a prescribed $d\delta^*/dx$.
An additional reason for the failure of the classical
iteration will be given when we discuss Le Balleur's
method.

Using the same reasoning which led to inequality
(2.5) we see that we would prefer to integrate Green's
boundary layer equations with a prescribed $d\delta^*/dx$ whenever

$$\left| \frac{H}{F_2} \frac{1}{\delta^*} \frac{d\delta^*}{dx} \right| < \left| \frac{F_2}{H} \frac{1}{u} \frac{du}{dx} \right| \qquad (2.8)$$

For typical airfoil calculations Eq. (2.8) usually
indicates that Green's lag-entrainment equations should be
integrated with a prescribed value for $d\delta^*/dx$ everywhere
except in the far wake region.

In both the VGK and GRUMFOIL programs the effect of
the boundary layer on the inviscid flow is represented
through a surface transpiration condition

$$v_n = \frac{1}{\rho_e} \frac{d}{ds} (\rho_e u_e \delta^*) \qquad (2.9)$$

In this formula

v_n = normal velocity

ρ_e = density

u_e = tangential velocity

$\dfrac{d}{ds}$ = derivative in tangential direction

According to the analysis presented by Le Balleur [1977], use of Eq. (2.9) avoids the Crocco-Lees singularity; that is, if we define $m = \rho_e u_e \delta^*$ and use the integral boundary layer equations to derive an equation of the form

$$A' \frac{dm}{dx} = B' \frac{m}{u} \frac{du}{dx} + C' \qquad (2.10)$$

then the coefficient B' never vanishes (regardless of Mach number). This fact is easily verified for Green's lag-entrainment method by numerical computation.

Another advantage of the surface transpiration condition (2.9) is that it does not require the regeneration of a mesh after each iteration, as would be necessary if the displacement thickness concept were implemented exactly.

In the present study, both the displacement thickness and the surface transpiration concepts are implemented.

3.0   Inviscid Analysis

Calculation of steady inviscid transonic flows is a
formidable task. The equations governing transonic flow
are inherently nonlinear and change type within the solu-
tion domain, from elliptic in subsonic regions to hyper-
bolic in supersonic regions. Moreover, one must provide
for embedded shocks, the positions of which are to be
calculated as part of the solution. The most successful
numerical methods for calculating inviscid transonic flow
on a routine basis use finite difference schemes. There-
fore, only these methods were considered for use in the
viscous-inviscid coupling problem.

Magnus and Yoshihara [1970] solved the unsteady Euler
equations using an explicit second-order difference scheme
similar to that developed by Lax and Wendroff (see Lax
[1954]). The unsteady equations are always hyperbolic.
Thus the problem of dealing with equations of mixed type
was circumvented. The difference scheme effectively added
a numerical viscosity which allowed shocks to appear as
rapid but continuous changes in the flow. This allowed
shocks to be captured as a natural part of the solution.
The disadvantages of the method of Magnus and Yoshihara
are two-fold. Firstly, the equations were solved in
Cartesian coordinates which forced them to employ a
cumbersome set of embedded meshes to enforce the boundary
conditions on the airfoil. Secondly, the rate at which

the unsteady solution approaches the desired steady state
solution is very slow. Therefore, the method is computa-
tionally expensive. Of course, considerable progress has
since been made in solving the Euler equations (see for
example Beam and Warming [1976]). However the calcula-
tions are still very expensive. Therefore it was
decided not to solve the Euler equations as part of our
viscous-inviscid coupling problem, but to rely on the full
potential equations.

A significant forerunner to modern methods for solving
the latter was provided by Murman and Cole [1971]. In
this the small disturbance equations were solved with cor-
responding boundary conditions. Type dependent differencing
was introduced. Centered differences were used in elliptic
regions while upwind differences were employed in hyper-
bolic regions. A special shock point operator was incor-
porated to preserve the conservative nature of the scheme.
The difference equations were solved by successive line
over-relaxation (SLOR). The resulting calculation is
faster than the methods for solving the Euler equations
by several orders of magnitude.

Encouraged by the success of Murman and Cole, Jameson
[1974] developed methods for solving the non-conservative
form of the full potential equation:

$$(a^2 - \phi_x^2)\phi_{xx} - 2\phi_x\phi_y\phi_{xy} + (a^2 - \phi_y^2)\phi_{yy} = 0 \qquad (3.1)$$

(see for example Shapiro [1953]). A circle plane mapping

which transformed the exterior of the airfoil to the interior of the unit circle was employed. This allowed the exact boundary conditions at the airfoil to be easily enforced. Upwind differencing in the direction of the flow was used. Also artificial time terms guaranteed the stability of the method. The difference equations were also solved using SLOR.

Later Jameson [1975] extended his method to the conservative form of the full potential equations:

$$(\rho\phi_x)_x + (\rho\phi_y)_y = 0 \qquad (3.2)$$

This conservative form is to be preferred over the non-conservative form because it assures the proper jump conditions across shocks. If the non-conservative form (3.1) is used, then the shock location is mesh dependent.

In an attempt to improve the rate of convergence to the solution of inviscid transonic flows, Ballhaus, Jameson and Albert [1978] developed an implicit approximate factorization (AF) algorithm. The method was applied to the steady state transonic small disturbance equation and enjoyed a rate of convergence 5-7 times as great as that achievable by the SLOR algorithm. Holst and Ballhaus [1979] followed up on this success by applying the (AF) algorithm to the conservative full potential equation in Cartesian coordinates. Holst [1979] later extended the method to a numerically generated body fitted coordinate system, which allows the exact boundary conditions at the

airfoil to be implemented easily.

The fastest method for solving the full potential equation numerically was developed by Jameson [1979]. In this a multiple grid method developed by Achi Brandt [1979] is combined with an Alternating Directions Implicit (ADI) scheme similar to the (AF) scheme developed by Holst and Ballhaus. The ADI scheme acts as the smoothing algorithm necessary for the success of the Multiple Grid method. The resulting Multigrid Alternating Direction (MAD) method converges very rapidly indeed. A typical calculation requires only about 10 iterations to achieve convergence.

For the purpose of calculating a coupled viscous-inviscid flow it was decided not to use Jameson's MAD method. This decision was based on the difficulty in implementing multigrid methods. More importantly, it is difficult to construct a coupling algorithm which is sufficiently rapid to take advantage of the speed with which MAD calculates the inviscid flow. Thus using MAD would not necessarily improve the rate at which a coupled viscous-inviscid calculation can be carried out. Accordingly, it was decided to use the (AF) scheme developed by Holst. This method is also very fast and reliable. Moreover, it is well documented allowing it to be easily implemented on the computer.

3.1 Motivation for Approximate Factorization Schemes

An intuitive motivation for approximate factorization (AF) schemes is provided by the following considerations.

Suppose that it is required to solve a problem of the form

$$L\phi = 0 \qquad (3.3)$$

where L is an operator. Given an approximation ϕ^n to ϕ and an approximation N to L, we might be able to find a better approximation to ϕ by solving

$$N(\phi^{n+1} - \phi^n) = -L\phi^n \qquad (3.4)$$

Indeed, in the case where L is linear and $N = L$, then solving Eq. (3.4) for ϕ^{n+1} yields the exact solution to Eq. (3.3). We can introduce over-relaxation into the algorithm indicated by Eq. (3.4) by solving for

$$(\phi^{n+1})^* = \omega\phi^{n+1} + (1-\omega)\phi^n \qquad (3.5)$$

which implies that

$$(\phi^{n+1})^* - \phi^n = \omega(\phi^{n+1} - \phi^n) \qquad (3.6)$$

If N is linear, then Eqs. (3.4) and (3.6) yield

$$N((\phi^{n+1})^* - \phi^n) = \omega N(\phi^{n+1} - \phi^n) = -\omega L\phi^n \qquad (3.7)$$

Thus the version of Eq. (3.4) which includes over-relaxation can be written

$$N(\phi^{n+1} - \phi^n) = -\omega L\phi^n \qquad (3.8)$$

In this formula, $L\phi^n$ is the residual which is a measure of how well the operator is satisfied by the nth level solution

ϕ^n, ω is the relaxation parameter and $c^n = \phi^{n+1} - \phi^n$ is the correction. The iteration given by Eq. (3.8) can be regarded as an iteration in pseudo-time, where the super-script n indicates the time level of the iteration. In the approximate factorization scheme, N is chosen to be the product of two or more factors indicated by

$$N = N_1 N_2 \tag{3.9}$$

The factors N_1 and N_2 are chosen so that they are easily invertible, their product is an approximation to L, and the iteration indicated by Eq. (3.8) is stable.

3.2 Artificial Density

When solving the full potential equations in conservation form Eq. (3.2), the shock jump conditions are

$$[\rho \phi_x] n_x + [\rho \phi_y] n_y = 0 \tag{3.10}$$

In this formula (n_x, n_y) is normal to the shock and [ ] denotes the change in a quantity when crossing the shock. Unfortunately, Eq. (3.10) is not enough to ensure unique-ness of solutions. Non-admissible expansion shocks, for example, are not excluded by Eq. (3.10).

One method to ensure uniqueness is to add viscous terms. Viscous terms occur naturally in the Navier-Stokes equations. They guarantee that shocks are regions of rapid but continuous change and exclude the possibility of expan-sion shocks. When solving the inviscid flow equations involving shocks, it is customary to add numerically

convenient viscous terms which smear shocks over three to four mesh points and also exclude physically unrealistic solutions.

In earlier attempts to solve the inviscid transonic flow equations, artificial viscosity was explicitly added through type dependent difference schemes. Centered differences were used in elliptic regions and upwind differences were used in hyperbolic regions. Recently it has been discovered that it is more convenient to add artificial viscosity by retarding the density. The method used in the present study is to use $\tilde{\rho}$ given by

$$\tilde{\rho} = \rho - \mu \frac{\partial \rho}{\partial s} \Delta s \tag{3.11}$$

where:

$$\frac{\partial \rho}{\partial s} = \text{derivative of } \rho \text{ in the streamwise direction} \tag{3.12}$$

$$\Delta s = \text{mesh width} \tag{3.13}$$

$$\mu = \begin{cases} \text{Min}[C(M^2-1),1] & M > 1 \\ 0 & M \leqslant 1 \end{cases} \tag{3.14}$$

$$M = \text{Mach number} \tag{3.15}$$

$$C = \text{bias coefficient, usually 1.5} \tag{3.16}$$

For completeness we mention that

$$V^2 = \phi_x^2 + \phi_y^2 \tag{3.17}$$

$$\rho = (1-V^2)^{1/(\gamma-1)} \tag{3.18}$$

$$M^2 = \frac{2}{\gamma-1} V^2/(1-V^2) \qquad (3.19)$$

$$\gamma = \text{ratio of specific heats} = 1.4 \text{ for air} \qquad (3.20)$$

where the velocity V is normalized by the maximum velocity V_m and the density ρ is normalized by the stagnation density.

Numerical experiments reveal that in order to maintain stability, $\partial\rho/\partial s$ must be calculated using upwind differencing. Also pressure overshoots upstream of the shock can be avoided by using the Mach number M computed one mesh point upstream in Eq. (3.14).

From the above formulas it is evident that

$$\tilde{\rho} = \rho \quad \text{when} \quad M \leqslant 1 \qquad (3.21)$$

while for supersonic flow ρ is retarded in the upstream direction by an amount which increases with Mach number. Formula (3.14) ensures that ρ is never retarded for more than one mesh point. In place of Eq. (3.2) we now solve

$$(\tilde{\rho}\phi_x)_x + (\tilde{\rho}\phi_y)_y = 0 \qquad (3.22)$$

The new jump conditions become

$$[\tilde{\rho}\phi_x]n_x + [\tilde{\rho}\phi_y]n_y = 0 \qquad (3.23)$$

From Eq. (3.11) we see that as $\Delta s \to 0$, $\tilde{\rho} \to \rho$. Thus by comparing Eq. (3.23) with Eq. (3.10) we see that the exact shock jump conditions are enforced as the mesh width tends to 0.

The artificial density method is a convenient way of
introducing artificial viscosity which preserves the
proper shock jump conditions. Moreover, as we shall see,
it permits the full potential equations to be solved
using an approximate factorization scheme.

3.3 Approximate Factorization Applied to the Full Potential Equation

In order to solve Eq. (3.22) we introduce the finite
difference analog:

$$L\phi = (\overleftarrow{\delta}_x \, \tilde{\rho}_{i+\frac{1}{2},j} \, \overrightarrow{\delta}_x + \overleftarrow{\delta}_y \, \tilde{\rho}_{i,j+\frac{1}{2}} \, \overrightarrow{\delta}_y)\phi_{i,j} \qquad (3.24)$$

The first factorization introduced by Ballhaus, Jameson
and Albert [1978] referred to as AF1 corresponds to

$$\alpha N = - (\alpha - \overleftarrow{\delta}_x \, \tilde{\rho}_{i+\frac{1}{2}} \, \overrightarrow{\delta}_x)(\alpha - \overleftarrow{\delta}_y \, \tilde{\rho}_{j+\frac{1}{2}} \, \overrightarrow{\delta}_y) \qquad (3.25)$$

where α is a positive number which is part of a parameter
sequence chosen so as to optimize the rate of convergence
of the algorithm (3.8). In general large values of α
reduce high frequency errors while small values of α
reduce low frequency errors. The best sequence of
parameters to use for any particular problem must be
determined experimentally since the problem is non-linear.
However, Ballhaus et al. [1978] do provide rough guide-
lines based on a linear analysis. Fortunately, almost any
reasonable choice of parameter sequence leads to an algo-
rithm which converges much faster than SLOR.

The AF1 scheme indicated in Eq. (3.25) performs very

well for subsonic flows but not for supersonic flows. A
heuristic argument explaining this behavior will now be
presented.

If we regard $\phi^{n+1} - \phi^{n}$ to be ϕ_t, then the left-hand
side of Eq. (3.8) with N given by Eq. (3.25) contains a
ϕ_t term. In regions of subsonic flow the right-hand side
of Eq. (3.8) is an elliptic operator, whereas in regions
of supersonic flow it is hyperbolic. In subsonic regions
we can model the AF1 algorithm with the equation

$$\phi_t = \phi_{xx} + \phi_{yy} \tag{3.26}$$

while for supersonic flow we use the model equation

$$\phi_t = \phi_{xx} - \phi_{yy} \tag{3.27}$$

Assume solutions of the form

$$\phi = e^{\sigma t + i(ax+by)} \tag{3.28}$$

where a and b are real constants. Substitute Eq. (3.28)
into Eqs. (3.26) and (3.27) and solve for σ. We find

$$\sigma = \begin{cases} -(a^2+b^2) & \text{for subsonic flow} \\ b^2-a^2 & \text{for supersonic flow} \end{cases} \tag{3.29}$$

In the subsonic case we see that ϕ always remains bounded
with time but this is not true in the supersonic case.
This explains the behavior of the AF1 scheme. The ϕ_t
term, which is implicitly introduced, is compatible with
subsonic flows but not with supersonic flows.

Time dependent terms of the form ϕ_{xt} or ϕ_{yt}, on the other hand, are compatible with both subsonic and supersonic flows. Indeed, if we consider

$$\phi_{xt} = \phi_{xx} + \phi_{yy} \tag{3.30}$$

$$\phi_{xt} = \phi_{xx} - \phi_{yy} \tag{3.31}$$

and assume solutions of the form given in Eq. (3.28), then, in both cases, we find that σ is purely imaginary so that ϕ is bounded with time.

Accordingly, Ballhaus et al. [1978] developed a second approximate factorization scheme called AF2 which introduces the proper time dependent terms. The version of AF2 used in the present study is given by

$$\alpha N = (\alpha + \overset{\leftarrow}{\delta}_y \ \tilde{\rho}_{j+\frac{1}{2}})(\alpha \overset{\rightarrow}{\delta}_y + \overset{\leftarrow}{\delta}_x \ \tilde{\rho}_{i+\frac{1}{2}} \ \overset{\rightarrow}{\delta}_x) \tag{3.32}$$

In order to enhance further the stability of AF2, a term of the form

$$\pm \ \alpha \ \beta \ \overset{\leftrightarrow}{\delta}_x \tag{3.33}$$

is added to the second factor for N given in Eq. (3.32). For subsonic regions β is usually assigned the value 0.3. For supersonic regions β is a user defined constant attaining values as large as 9.0 for particularly challenging flows. The double arrow notation indicates that the difference is always upwind and the sign is chosen so as to increase the magnitude of the diagonal terms in the matrix for the second factor of N. The first factor for N

is a bidiagonal matrix while the second is a tridiagonal matrix. Thus both factors are easily inverted. Moreover, AF2 has proven to converge rapidly and reliably for many challenging inviscid flow calculations.

3.4 Extension to a General Coordinate System

In order to apply the boundary conditions accurately at the airfoil surface, we must use a body fitted co-ordinate system. The transformation of the full potential equation (3.2) to a general coordinate system will now be derived.

If we invoke the summation convention, then the conservative form of the full potential equation is

$$\delta_{ij} \frac{\partial}{\partial x_i} (\rho \frac{\partial \varphi}{\partial x_j}) = 0 \qquad (3.34)$$

where:

$$\delta_{ij} = \begin{cases} 0 & \text{if} \quad i \neq j \\ 1 & \text{if} \quad i = j \end{cases} \qquad (3.35)$$

Let the general coordinates be denoted by y_i. The Jacobian matrix of the transformation is given by

$$J = (\partial x_i / \partial y_j) \qquad (3.36)$$

Define the matrix (g_{ij}) by

$$(g_{ij}) = J^T J = (\frac{\partial x_k}{\partial y_i} \frac{\partial x_k}{\partial y_j}) \qquad (3.37)$$

The inverse matrix (g^{ij}) of (g_{ij}) is then

$$(g^{ij}) = J^{-1}(J^T)^{-1} = (\frac{\partial y_i}{\partial x_k} \frac{\partial y_j}{\partial x_k}) \tag{3.38}$$

Also set

$$g = \det(g_{ij}) = (\det J)^2 \tag{3.39}$$

An element of volume dV will be denoted by dx in the Cartesian coordinate system and will become $\sqrt{g}$ dy in y coordinates. If w is any infinitely differentiable function with compact support then we have:

$$\int \delta_{ij} \frac{\partial}{\partial x_i} (\rho \frac{\partial \phi}{\partial x_j}) w \, dx$$

$$= - \int \delta_{ij} \rho \frac{\partial \phi}{\partial x_j} \frac{\partial w}{\partial x_i} \, dx \quad \text{(integration by parts)}$$

$$= - \int \delta_{ij} \rho \frac{\partial \phi}{\partial y_k} \frac{\partial y_k}{\partial x_j} \frac{\partial w}{\partial y_\ell} \frac{\partial y_\ell}{\partial x_i} \sqrt{g} \, dy$$

$$= \int \rho \frac{\partial \phi}{\partial y_k} \frac{\partial w}{\partial y_\ell} g^{k\ell} \sqrt{g} \, dy$$

$$= \int \frac{\partial}{\partial y_\ell} (\rho \sqrt{g} \, g^{k\ell} \frac{\partial \phi}{\partial y_k}) w \, dy$$

$$= \int \frac{1}{\sqrt{g}} \frac{\partial}{\partial y_\ell} (\rho \sqrt{g} \, g^{k\ell} \frac{\partial \phi}{\partial y_k}) w \, dx$$

Comparing the first and last expressions we conclude that in y coordinates, the full potential equation is given by

$$\frac{\partial}{\partial y_\ell} (\rho \sqrt{g} \, g^{k\ell} \frac{\partial \phi}{\partial y_k}) = 0 \tag{3.40}$$

Once a mesh has been generated, the x coordinates are known in terms of the y coordinates. This allows us to

compute (g_{ij}) from Eq. (3.37) and hence (g^{ij}) from Eq. (3.38) and g from Eq. (3.39). This provides us with the metric coefficients required in Eq. (3.40). Also in y coordinates we have

$$v^2 = \delta_{ij} \frac{\partial \Phi}{\partial x_i} \frac{\partial \Phi}{\partial x_j} = g^{ij} \frac{\partial \Phi}{\partial y_i} \frac{\partial \Phi}{\partial y_j} \qquad (3.41)$$

allowing us to compute ρ and M^2.

Naturally, in solving Eq. (3.40) we replace ρ with $\tilde{\rho}$ and use the finite difference analog of Eq. (3.40). The precise algebraic details may be found in Holst [1979]. The AF2 scheme used in the present study was the finite difference version of

$$\alpha N = (\alpha + \frac{\partial}{\partial y_2} (\tilde{\rho} \sqrt{g} g^{22}))(\alpha \frac{\partial}{\partial y_2} + \frac{\partial}{\partial y_1} (\tilde{\rho} \sqrt{g} g^{11} \frac{\partial}{\partial y_1})) \qquad (3.42)$$

The finite difference operators were chosen so as to make the diagonal terms as large as possible in absolute value.

Two versions of the code exist. The first uses Cartesian coordinates and applies the boundary conditions according to

$$\Phi_y/\Phi_x = f' + \frac{d\delta^*}{dx} \quad \text{at} \quad y = 0 \qquad (3.43)$$

where f' is the slope of the airfoil and $d\delta^*/dx$ is the slope of the boundary layer displacement thickness. This version of the code is intended for testing various viscous-inviscid coupling techniques.

The more exact version of the code uses Eisman's [1979] method to generate a body fitted mesh and imposes

the boundary condition

$$v_n = \frac{1}{\rho_e} \frac{\partial}{\partial s} (\rho_e u_e \delta^*) \qquad (3.44)$$

at the airfoil surface and along the wake centerline.
Eisman's method was chosen to generate the mesh because
it is very fast and gives excellent control. A typical
mesh is shown in Figs. 3.1 and 3.2. Note that the mesh is
designed to conform with both the symmetric airfoil and
the wake at the centerline. This makes it easy to
implement the boundary conditions necessary to solve the
viscous-inviscid coupling problem.

4. Le Balleur's Model Problem

Although Le Balleur's [1978] method for analysing viscous-inviscid coupling algorithms is relatively easy, it has not yet received the recognition in this country that it deserves. Therefore, some aspects of his theory will be presented in detail.

In order to gain insight into coupling algorithms, Le Balleur considers a model problem. The inviscid flow is assumed to be governed, over the half plane $y \geqslant 0$, by the linearized small disturbance equation

$$(1-M^2)\phi_{xx} + \phi_{yy} = 0 \quad , \tag{4.1}$$

where the Mach number M is constant and the full potential Φ is given by

$$\Phi = u_\infty(x + \phi) \tag{4.2}$$

so that the inviscid velocity u is given by

$$u = \Phi_x = u_\infty(1 + \phi_x) \tag{4.3}$$

$$\frac{du}{dx} = u_\infty \phi_{xx} \tag{4.4}$$

The boundary layer is assumed to be governed by the equation

$$\frac{d\delta^*}{dx} = A + B \frac{du}{dx} \tag{4.5}$$

where A and B are constants. For convenience we introduce

$$\alpha = \frac{d\delta^*}{dx} \tag{4.6}$$

and rewrite the boundary layer equation as

$$\alpha = A + B \frac{du}{dx} \qquad (4.7)$$

The boundary conditions for the inviscid flow are applied
in a small disturbance fashion so that

$$\phi_y = f' + \alpha \quad \text{at} \quad y = 0 \qquad (4.8)$$

where f' is the slope of the body about which we are com-
puting the flow.

We will have a coupled viscous-inviscid solution if we
can determine α so that the inviscid velocity gradient
(evaluated at $y = 0$) agrees with the velocity gradient com-
puted from the boundary layer equation. Suppose that such
a distribution of α is given to us. In order to analyse a
particular algorithm for calculating a coupled solution,
Le Balleur perturbs the exact α by $\Delta\alpha = \epsilon e^{i\nu x}$. He then
applies the coupling algorithm to see if the error in α is
increased or decreased. The analysis of the classical
iteration, for example, is now described.

If we perturb the exact α by an amount $\Delta\alpha = \epsilon e^{i\nu x}$, it
follows from Eqs. (4.1) and (4.8) that the exact ϕ will be
perturbed by $\Delta\phi$ governed by

$$(1-M^2)(\Delta\phi)_{xx} + (\Delta\phi)_{yy} = 0 \qquad (4.9)$$

where

$$(\Delta\phi)_y = \epsilon e^{i\nu x} \quad \text{at} \quad y = 0 \qquad (4.10)$$

Introduce

$$\beta = |1-M^2|^{\frac{1}{2}} \qquad (4.11)$$

If the inviscid flow is subsonic, then Eq. (4.9) may be rewritten as

$$\beta^2 (\Delta\phi)_{xx} + (\Delta\phi)_{yy} = 0 \qquad (4.12)$$

The solution to Eq. (4.12), subject to the boundary condition (4.10), is

$$\Delta\phi = \frac{\varepsilon e^{i\nu x} e^{-\beta\nu y}}{-\beta\nu} \qquad (4.13)$$

The solution involving $e^{+\beta\nu y}$ is discarded because it is not well behaved for $y \to \infty$. Now, using Eq. (4.4), we see that this perturbation of ϕ causes the inviscid velocity gradient (at $y = 0$) *to be changed by the amount*

$$\Delta\left(\frac{du}{dx}\right) = \frac{u_\infty \nu}{\beta} \varepsilon e^{i\nu x} \qquad (4.14)$$

The velocity gradient which the inviscid flow imposes on the boundary layer differs from the exact velocity gradient by the amount shown in Eq. (4.14). Thus, by Eq. (4.7), the boundary layer is forced to respond by giving a value of α which is in error by

$$\Delta\alpha = \frac{\nu B u_\infty}{\beta} \varepsilon e^{i\nu x} \qquad (4.15)$$

Thus in the subsonic case, the classical iteration mutliplies the original error in α, namely $\Delta\alpha = \varepsilon e^{i\nu x}$, by a factor

$$\mu = \frac{\nu B u_\infty}{\beta} \quad \text{for} \quad M < 1 \qquad (4.16)$$

Similarly for the supersonic case we find

$$-\beta^2(\Delta\phi)_{xx} + (\Delta\phi)_{yy} = 0 \qquad (4.17)$$

$$\Delta\phi = \frac{\varepsilon e^{i\nu x}e^{-i\beta\nu y}}{-i\beta\nu} \qquad (4.18)$$

Only the right running wave is considered in Eq. (4.18).
Following the same steps as those used to derive Eq. (4.16)
we find

$$\mu = \frac{-i\nu Bu_\infty}{\beta} \qquad \text{for} \quad M > 1 \qquad (4.19)$$

The classical iteration will converge only if $|\mu| < 1$
for all possible values of ν. The latter lie in the
approximate range

$$\frac{\pi}{L} \leqslant \nu \leqslant \frac{\pi}{\Delta x} \qquad (4.20)$$

where Δx is the mesh width and L is the size of the computa-
tional domain. Also we should note that for separated flows,
Bu_∞ becomes large. Thus, for separated flows computed on
fine grids, we can easily expect that $|\mu| > 1$ in either the
subsonic or supersonic case. This provides the second
reason for expecting the classical iteration to fail for
separated flows. If we refine the mesh sufficiently so that
we can accurately integrate the boundary layer equations
with a prescribed velocity gradient when the flow separates,
we can easily force $|\mu| > 1$, so that the viscous-inviscid
coupling will diverge.

It is of interest to see how the classical iteration
operates when under-relaxation is employed. For this
purpose it is useful to note that, according to the above
analysis, the classical iteration can be viewed as a

linear operator $\mathcal{L}$ with eigenfunctions $e^{i\nu x}$

$$\mathcal{L}(e^{i\nu x}) = \mu e^{i\nu x} \tag{4.21}$$

where the eigenvalue μ is given by

$$\mu = \begin{cases} \dfrac{\nu B u_\infty}{\beta} & \text{for} \quad M < 1 \\[2ex] \dfrac{-i\nu B u_\infty}{\beta} & \text{for} \quad M > 1 \end{cases} \tag{4.22}$$

When relaxation is employed with relaxation factor ω the linear operator $\mathcal{L}$ is replaced by

$$\mathcal{L}_\omega = \omega \mathcal{L} + (1-\omega)I \tag{4.23}$$

where I is the identity operator. Note

$$\mathcal{L}_0 = I \tag{4.24}$$

$$\mathcal{L}_1 = \mathcal{L} \tag{4.25}$$

From (4.21) and (4.23) we see that

$$\mathcal{L}_\omega(e^{i\nu x}) = [\omega\mu + (1-\omega)]e^{i\nu x} \tag{4.26}$$

Thus $e^{i\nu x}$ is also an eigenfunction of $\mathcal{L}_\omega$ with corresponding eigenvalue

$$\mu_\omega = \omega\mu + (1-\omega) \tag{4.27}$$

Note that

$$\mu_0 = 1 \tag{4.28}$$

$$\mu_1 = \mu \tag{4.29}$$

As ω decreases from 1 to 0, μ_ω varies from μ to 1. Geometrically, if $0 < \omega < 1$, then the relationship between μ, μ_ω and 1 is as shown in Fig. 4.1. We can guarantee the convergence of the classical iteration if we can choose ω so that $\sigma(\mathcal{L}_\omega)$, the set of eigenvalues of $\mathcal{L}_\omega$, lies within the unit circle. From (4.22) we see that if $M > 1$ then conditions are as shown in Fig. 4.2. It is geometrically clear that if we make ω sufficiently small, we can arrange for $\sigma(\mathcal{L}_\omega)$ to lie within the unit circle and thus ensure the convergence of the classical iteration in this case. Similar remarks apply when $M > 1$ and $B > 0$. When the flow is subsonic, conditions are as shown in one or other of Figs. 4.3 and 4.4.

In the first case we can choose ω so that $\sigma(\mathcal{L}_\omega)$ lies within the unit circle, but in the second case this is not possible.
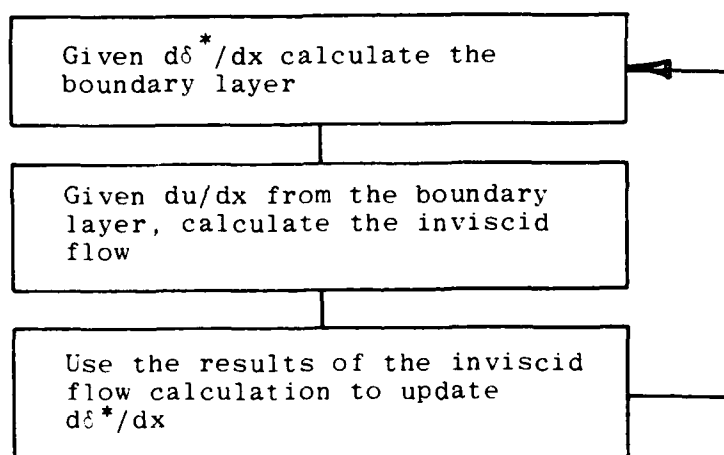
Summarizing these results we see that for supersonic flow the classical iteration can always be stabilized by under-relaxation. For subsonic flow the classical iteration can be stabilized by under-relaxation when $B < 0$ but not necessarily if $B > 0$.

For Green's lag-entrainment method we always have $B < 0$, so that the classical iteration can always be stabilized by under-relaxation. However, it is still not a good idea to use the classical iteration when the flow separates because in this case we cannot integrate the boundary layer equations accurately with a prescribed velocity gradient. Moreover, the under-relaxation parameter can become so

small that this method is rendered too slow for practical use. We really must search for a coupling algorithm which allows us to integrate the boundary layer equations with a prescribed value of $d\delta^*/dx$.

Perhaps the most natural coupling algorithm which allows one to integrate the boundary layer equations with a prescribed value of $d\delta^*/dx$ is the so-called inverse method:

Inverse Iteration

```
┌─────────────────────────────────┐
│ Given dδ*/dx calculate the      │◄──┐
│ boundary layer                  │   │
└─────────────────────────────────┘   │
           │                          │
┌─────────────────────────────────┐   │
│ Given du/dx from the boundary   │   │
│ layer, calculate the inviscid   │   │
│ flow                            │   │
└─────────────────────────────────┘   │
           │                          │
┌─────────────────────────────────┐   │
│ Use the results of the inviscid │   │
│ flow calculation to update      │───┘
│ dδ*/dx                          │
└─────────────────────────────────┘
```

Since we can associate a linear operator $\mathcal{L}$ with the classical iteration, we can associate the inverse operator $\mathcal{L}^{-1}$ with the inverse iteration. If we apply $\mathcal{L}^{-1}$ to both sides of Eq.(4.21)., we find that

$$\mathcal{L}^{-1}(e^{i\nu x}) = \mu_I e^{i\nu x} \tag{4.30}$$

where

$$\mu_I = \begin{cases} \dfrac{\beta}{\nu B u_\infty} & \text{for} \quad M < 1 \\[3ex] \dfrac{i\beta}{\nu B u_\infty} & \text{for} \quad M > 1 \end{cases} \tag{4.31}$$

Thus $\mathcal{L}^{-1}$ has the same eigenfunctions as $\mathcal{L}$ with corresponding eigenvalues which are the reciprocals of those of $\mathcal{L}$. The largest values for $|\mu_I|$ occur for low frequencies. In view of Eqs. (4.20) and (4.31) it follows that

$$\max_\nu |\mu_I| = \frac{\beta}{|B| u_\infty} \frac{L}{\pi} \tag{4.32}$$

Thus $\max |\mu_I|$ is proportional to the size of the computational domain L. In cases where $\max |\mu_I| \gg 1$, the size of the relaxation parameter ω required to produce convergence should vary inversely with L.

Confirmation of this result is provided by a calculation performed by Melnik [1976]. In this the boundary layer equations are integrated using a prescribed value of $d\delta^*/dx$ to yield du/dx. Since the flow considered by Melnik is incompressible, the inviscid flow can be solved with a prescribed distribution of du/dx using a Hilbert integral. Convergence of this inverse iteration scheme was first achieved over a computational domain [0,3] using $\omega = .15$. When the size of the computational domain was increased to [0,20.791] Melnik found it necessary to reduce ω to the value .02. Hence a seven-fold increase in the size of the computational domain did indeed require roughly a seven-fold decrease in the size of ω.

In general the size of the relaxation parameter required to stabilize the inverse iteration over a reasonable sized computation domain is disappointingly small. Also the inverse iteration requires that the inviscid flow be computed with a prescribed value of du/dx. This requires performing a design calculation which is particularly difficult in transonic flow involving shock waves. Accordingly, Le Balleur develops a semi-inverse method which allows one to calculate the boundary layer with a prescribed $d\delta^*/dx$ (inverse mode for the boundary layer) but also allows the inviscid flow to be calculated with a prescribed geometry (direct mode for the inviscid flow).

5. Semi-Inverse Method

Our derivation of the semi-inverse method differs from that given by Le Balleur. Moreover, as we shall see the formula we derive for use in supersonic regions differs from his.

Let α^e denote the value of α which is the solution of the viscous-inviscid coupling problem. The corresponding velocity gradient will be denoted by du^e/dx. Then it follows from Eq. (4.7) that

$$\alpha^e = A + B \frac{du^e}{dx} \qquad (5.1)$$

Suppose as in our previous analysis

$$\alpha = \alpha^e + \Delta\alpha = \alpha^e + \varepsilon e^{i\nu x} \qquad (5.2)$$

The corresponding velocity gradient du/dx calculated from the boundary layer equation satisfies

$$\alpha = A + B \frac{d\tilde{u}}{dx} \qquad (5.3)$$

Subtract Eq. (5.1) from Eq. (5.3) and use Eq. (5.2). Then

$$\frac{\varepsilon e^{i\nu x}}{B} = \frac{d\tilde{u}}{dx} - \frac{du^e}{dx} \qquad (5.4)$$

For $M < 1$, it follows from Eq. (4.14) that

$$\frac{u_\infty \nu}{\beta} \varepsilon e^{i\nu x} = \frac{du}{dx} - \frac{du^e}{dx} \qquad (5.5)$$

where du/dx is the velocity gradient calculated from the inviscid flow (at $y = 0$). Now subtract Eq. (5.5) from

Eq. (5.4). Then

$$(\frac{1}{B} - \frac{u_\infty \nu}{\beta})\varepsilon e^{i\nu x} = \frac{d\tilde{u}}{dx} - \frac{du}{dx} \qquad (5.6)$$

which can be written as

$$\Delta\alpha = \varepsilon e^{i\nu x} = \frac{\beta B}{\beta - u_\infty B\nu}[\frac{d\tilde{u}}{dx} - \frac{du}{dx}] \qquad (5.7)$$

If at the nth iteration $\alpha = \alpha^n$, then the $(n+1)^{th}$
iteration provides the required solution if $\alpha^{n+1} = \alpha^e$.
According to Eqs. (5.7) and (5.2) this will be the case
if

$$\alpha^{n+1} - \alpha^n = \frac{\beta B}{u_\infty B\nu - \beta} [\frac{d\tilde{u}}{dx} - \frac{du}{dx}] \qquad (5.8)$$

where $M < 1$.

Similarly if we start with Eq. (4.18) and use Eq.
(4.4), we find that for $M > 1$

$$-\frac{iu_\infty \nu}{\beta} \varepsilon e^{i\nu x} = \frac{du}{dx} - \frac{du^e}{dx} \qquad (5.9)$$

Subtract Eq. (5.9) from Eq. (5.4)

$$(\frac{1}{B} + \frac{iu_\infty \nu}{\beta})\varepsilon e^{i\nu x} = \frac{d\tilde{u}}{dx} - \frac{du}{dx} \qquad (5.10)$$

In order to eliminate the annoying imaginary term
$iu_\infty \nu/\beta$ we first differentiate Eq. (5.10) with respect
to x:

$$i\nu(\frac{1}{B} + \frac{iu_\infty \nu}{\beta})\varepsilon e^{i\nu x} = \frac{d^2 u}{dx^2} - \frac{d^2 u}{dx^2} \qquad (5.11)$$

Multiply Eq. (5.11) by $u_\infty B/\beta$ and subtract from Eq. (5.10).
Then

$$\left(\frac{1}{B} + \frac{u_\infty^2 B\nu^2}{\beta^2}\right)\varepsilon e^{i\nu x} = \frac{d\tilde{u}}{dx} - \frac{du}{dx}$$

$$- \frac{u_\infty B}{\beta}\left[\frac{d^2\tilde{u}}{dx} - \frac{d^2 u}{dx}\right] \qquad (5.12)$$

We now use the same reasoning which led to Eq. (5.8) to obtain

$$\alpha^{n+1} - \alpha^n = \frac{B\beta}{u_\infty^2 B^2\nu^2 + \beta^2}\left\{u_\infty B\left[\frac{d^2\tilde{u}}{dx^2} - \frac{d^2 u}{dx^2}\right]\right.$$

$$\left. - \beta\left[\frac{d\tilde{u}}{dx} - \frac{du}{dx}\right]\right\} \qquad (5.13)$$

where $M > 1$.

6. Analysis of Semi-Inverse Method

When the error in α is simple harmonic with frequency ν, it can be eliminated, with use of formulas (5.8) and (5.13), for our model problem, in one iteration. Unfortunately, however, the error in α will actually be a superposition of harmonics with frequencies ν' limited only by the mesh width and the size of the computational domain. Accordingly it behooves us to investigate the performance of Eqs. (5.8) and (5.13) when

$$\alpha^n = \alpha^e + \varepsilon e^{i\nu'x} \qquad (6.1)$$

where ν' can be any frequency in the range

$$\frac{\pi}{L} \leq \nu' \leq \frac{\pi}{\Delta x} \qquad (6.2)$$

Consider the subsonic case first. Since $M < 1$ it follows from Eq. (5.7) that

$$\varepsilon e^{i\nu'x} = \frac{B\beta}{\beta - u_\infty B\nu'} \left[\frac{d\tilde{u}}{dx} - \frac{du}{dx}\right] \qquad (6.3)$$

If we substitute Eqs. (6.1) and (6.3) in Eq. (5.8) we obtain

$$\alpha^{n+1} = \alpha^e + \left(1 - \frac{\beta - Bu_\infty\nu'}{\beta - Bu_\infty\nu}\right)\varepsilon e^{i\nu'x} \qquad (6.4)$$

Thus, the error in α due to a frequency ν' is multiplied by the factor

$$\mu(\nu') = 1 - \frac{\beta - Bu_\infty\nu'}{\beta - Bu_\infty\nu} \qquad (6.5)$$

Since $B < 0$ for Green's lag-entrainment method, it is apparent that $|\mu(\nu')| < 1$ for all possible ν' if we croose ν to be the maximum possible frequency:

$$\nu = \nu_{max} = \pi/\Delta x \tag{6.6}$$

With this substitution Eq. (6.5) becomes

$$\mu(\nu') = 1 - \frac{\beta - Bu_\infty \nu'}{\beta - Bu_\infty \nu_{max}} \tag{6.7}$$

For attached flows it is usually found that $|Bu_\infty \nu| \ll \beta$ for all possible ν unless a very fine mesh is used. From Eq. (6.7) we see that for attached flows we would expect

$$\mu(\nu') \approx 0 \tag{6.8}$$

indicating that Eq. (5.8) works very well in this case.

For separated flows, on the other hand, we can expect $|Bu_\infty \nu_{max}| \gg \beta$ so that

$$\mu(\nu') = 1 - \frac{Bu_\infty \nu' - \beta}{Bu_\infty \nu_{max}} \tag{6.9}$$

For high values of the frequency ν' this becomes

$$\mu(\nu') \simeq 1 - \nu'/\nu_{max} \tag{6.10}$$

while for low frequencies

$$\mu(\nu') \simeq 1 + \frac{\beta}{Bu_\infty \nu_{max}} \tag{6.11}$$

(We recall that $B < 0$ so that $|\mu(\nu')| < 1$.) Hence in the separated case high frequency errors are reduced substantially with each iteration, while low frequency errors

are also reduced but only slowly. Experimental verification of these results will be given later.

Now consider the performance of the supersonic iteration formula (5.13) when α^n is given by Eq. (6.1). It follows from (5.12) that

$$(\frac{1}{B} + \frac{u_\infty^2 B(\nu')^2}{\beta^2})\epsilon\,e^{i\nu'x}$$

$$= \frac{d\tilde{u}}{dx} - \frac{du}{dx} - \frac{u_\infty B}{\beta}\,[\frac{d^2\tilde{u}}{dx^2} - \frac{d^2u}{dx^2}] \qquad (6.12)$$

Substitute Eqs. (6.1) and (6.12) into Eq. (5.13). Then

$$\alpha^{n+1} = \alpha^e + (1 - \frac{\beta^2 + u_\infty^2 B^2(\nu')^2}{\beta^2 + u_\infty^2 B^2 \nu^2})\epsilon\,e^{i\nu'x} \qquad (6.13)$$

Again it follows that if we choose $\nu = \nu_{max}$, then errors of all frequencies will be reduced. Moreover, just as in the subsonic case, high frequency errors are always substantially reduced, while low frequency errors are reduced only slowly when separation occurs.

When actually implementing formulas (5.8) and (5.13) we use

$$\nu = \pi/\Delta x \quad , \quad u_\infty = u \quad , \quad \beta = |1-M^2|^{\frac{1}{2}} \qquad (6.14)$$

where Δx is the local mesh width, u is the local inviscid velocity and M is the local Mach number. Formula (5.8) can be written in a form which agrees with that of Le Balleur [1980] if we introduce the non-dimensional parameter $\tilde{B}$

$$B = \tilde{B}\,\frac{\delta^*}{\tilde{u}} \qquad (6.15)$$

Substitute Eqs. (6.14) and (6.15) into Eq. (5.8). Then

$$\alpha^{n+1} - \alpha^n = \frac{\delta^*\tilde{B}\beta u}{u\delta^*\tilde{B}\pi/\Delta x - \beta\tilde{u}} \left[\frac{1}{\tilde{u}}\frac{d\tilde{u}}{dx} - \frac{1}{\tilde{u}}\frac{du}{dx}\right] \qquad (6.16)$$

As convergence is achieved, $\tilde{u} \rightarrow u$. Therefore, Eq. (6.16) is equivalent to using

$$\alpha^{n+1} - \alpha^n = \frac{\delta^*\tilde{B}\beta}{\delta^*\tilde{B}\pi/\Delta x - \beta} \left[\frac{1}{\tilde{u}}\frac{d\tilde{u}}{dx} - \frac{1}{u}\frac{du}{dx}\right] \qquad (6.17)$$

which is precisely Le Balleur's result.

For supersonic flow, on the other hand, Le Balleur gives a formula which is equivalent to

$$\alpha^{n+1} - \alpha^n = \frac{B\beta}{u_\infty^2 B^2 \nu^2 + \beta^2} \left\{u_\infty B\left[\frac{d^2\tilde{u}}{dx^2} - \frac{d^2 u}{dx^2}\right]\right\} \qquad (6.18)$$

That is, the term involving

$$\frac{d\tilde{u}}{dx} - \frac{du}{dx} \qquad (6.19)$$

is omitted. Le Balleur's formula (6.18) can be analysed in the same manner as Eqs. (5.8) and (5.13). Indeed if we assume that α^n is given by Eq. (6.1), then from Eq. (5.11) we have

$$i\nu'\left(\frac{1}{B} + \frac{iu_\infty\nu'}{\beta}\right)\varepsilon e^{i\nu'x} = \frac{d^2\tilde{u}}{dx^2} - \frac{d^2 u}{dx^2} \qquad (6.20)$$

If we substitute Eqs. (6.1) and (6.20) into Eq. (6.18) we find that the error in α^n, namely $e^{i\nu'x}$, is multiplied by the factor

$$\mu(\nu') = 1 + \frac{i\beta Bu_\infty\nu' - (Bu_\infty\nu')^2}{\beta^2 + (u_\infty B\nu_{max})^2} \qquad (6.21)$$

If $|Bu_\infty\nu'| \gg \beta$ for all possible ν' (this is

characteristic of separated flows) then Eq. (6.21) yields:

$$\mu(\nu') \simeq 1 - (\nu'/\nu_{max})^2 \qquad (6.22)$$

In this case $|\mu(\nu')| < 1$ and we would expect convergence.
If, however, for some frequency ν' we have $|Bu_\infty\nu'| \ll \beta$
(which is characteristic of attached flows), then Eq.
(6.21) gives

$$\mu(\nu') \simeq 1 + \frac{i\beta Bu_\infty\nu'}{\beta^2 + (u_\infty B\nu_{max})^2} \qquad (6.23)$$

In this case $|\mu(\nu')| > 1$ so that we would not expect
convergence.

In summary we would expect Le Balleur's formula
Eq. (6.18) to converge for separated or nearly separated
flows, but note that it may fail to converge when the
boundary layer is attached.

Naturally, both Eqs. (5.13) and (6.18) were tested
numerically in a transonic calculation. In the super-
sonic region ahead of the shock, where the boundary layer
is firmly attached, formula (5.13) converged very quickly.
On the other hand, (6.18) failed to converge. This
numerical test confirms the theoretical analysis given
above.

7. Connection with the Carter Algorithm

At the 1979 AIAA Conference held in Williamsburg, Carter [1979] proposed a simple coupling algorithm of the form

$$(\delta^*)^{n+1} = (\delta^*)^n \frac{\tilde{u}}{u} \qquad (7.1)$$

Multiply Eq. (7.1) by u and differentiate. Then

$$\alpha^{n+1} u + \frac{du}{dx} (\delta^*)^{n+1} = \alpha^n \tilde{u} + (\delta^*)^n \frac{d\tilde{u}}{dx} \qquad (7.2)$$

As convergence is achieved $\tilde{u} \rightarrow u$ and $(\delta^*)^{n+1} \rightarrow (\delta^*)^n$. Accordingly Eq. (7.2) is equivalent to using

$$\alpha^{n+1} - \alpha^n \approx \frac{\delta^*}{u} [\frac{d\tilde{u}}{dx} - \frac{du}{dx}] \qquad (7.3)$$

If we compare Eq. (7.3) with Eq. (5.8) we see that we would expect the Carter algorithm to be valid for subsonic flows if

$$\frac{\delta^*}{u} \leqslant \frac{\beta B}{u_\infty B \nu_{max}^{-\beta}} \qquad (7.4)$$

In cases where Eq. (7.4) is satisfied strongly we would expect the Carter algorithm to work even when over-relaxation is employed.

If we compare Eq. (7.3) with Eq. (5.13) we see that, for supersonic flow, the Carter algorithm omits the term containing the expression

$$\frac{d^2\tilde{u}}{dx^2} - \frac{d^2u}{dx^2} \qquad (7.5)$$

Accordingly it is of interest to analyse Eq. (5.13) with this term deleted. Then

$$\alpha^{n+1} - \alpha^n = \frac{-B\beta^2}{\beta^2 + B^2 u_\infty^2 \nu^2} \left[\frac{d\tilde{u}}{dx} - \frac{du}{dx}\right] \qquad (7.6)$$

If we assume that α^n is given by Eq. (6.1) it follows from Eq. (5.10) that

$$\left(\frac{1}{B} + \frac{iu_\infty \nu'}{\beta}\right)\varepsilon e^{i\nu'x} = \frac{d\tilde{u}}{dx} - \frac{du}{dx} \qquad (7.7)$$

If we substitute Eqs. (6.1) and (7.7) into Eq. (7.6) we find that the original error in α^n is multiplied by the factor

$$\mu(\nu') = 1 - \frac{\beta^2 + i\beta u_\infty B\nu'}{\beta^2 + u_\infty^2 B^2 \nu_{max}^2} \qquad (7.8)$$

If $|u_\infty B\nu| \ll \beta$ for all possible ν (which is characteristic of attached flows) then

$$\mu(\nu') \approx 0 \qquad (7.9)$$

so that the Carter algorithm is simulating a convergent algorithm. On the other hand if $|u_\infty B\nu| \gg \beta$ (which is characteristic of separated flows) then

$$\mu(\nu') \simeq 1 - \frac{i\nu'\beta}{u_\infty B\nu_{max}^2} \qquad (7.10)$$

In this case $|\mu(\nu')| > 1$ so that we would not expect convergence.

In summary, we would expect the Carter algorithm to converge for attached supersonic flows but not for separated supersonic flows.

A coupling procedure employing Eqs. (5.8) and (5.13) is to be preferred over the Carter algorithm in any case because it has a sounder theoretical basis.

8.0   Numerical Tests

In order to assess the performance of Eqs. (5.8) and
(5.13), transonic calculations about an 18% thick
circular arc airfoil at zero degrees angle of attack were
carried out. A Cartesian computational grid of size
110×30 was used for the inviscid analysis. In the x-
direction 50 equally spaced mesh points were placed on
the airfoil, while 30 mesh points were placed both up-
stream and downstream of the airfoil, exponentially
stretched to a distance of five chord lengths away from
the airfoil in each direction. The mesh was also expo-
nentially stretched in the y-direction to a distance of
five chord lengths from the airfoil. The size of the mesh
in the y-direction near the airfoil was 1% of chord. Free
stream conditions were assumed to prevail at the far field
boundaries, while the boundary condition at $y = 0$ was
imposed in accordance with Eq. (3.42).

Equations (5.8) and (5.13) were implemented in their
integrated forms. Given the local inviscid velocity u and
the velocity $\tilde{u}$ calculated from the boundary layer, we
updated δ^* using the following equations. For $M < 1$

$$(\delta^*)^{n+1} - (\delta^*)^n = \frac{\beta B}{u_\infty B \nu - \beta} [\tilde{u} - u] \qquad (8.1)$$

While for $M > 1$

$$(\delta^*)^{n+1} - (\delta^*)^n = \frac{B\beta}{u_\infty^2 B^2 \nu^2 + \beta^2} \{ u_\infty B [\frac{d\tilde{u}}{dx} - \frac{du}{dx}] $$

$$- \beta [\tilde{u} - u] \} \qquad (8.2)$$

We point out for emphasis that ν, u_∞ and β are given in Eq. (6.14) and B is the coefficient of $d\tilde{u}/dx$ occurring in the boundary layer equation. Green's lag entrainment method yields

$$B = F_2 \delta^* / (H\tilde{u}) \qquad (8.3)$$

The boundary layer was calculated in the inverse mode (prescribed $d\delta^*/dx$) everywhere using the same mesh as used by the inviscid code. Equation (2.8) indicated that for the sake of numerical accuracy in integrating the boundary layer equations, the inverse mode was to be preferred over the direct mode everywhere except in the far wake region.

Once δ^* is updated using Eqs. (8.1) and (8.2) it is important to calculate $d\delta^*/dx$ required by the boundary layer equations in the appropriate manner. Usually for M < 1 we used a centered scheme

$$(\frac{d\delta^*}{dx})_i = \frac{\delta^*_{i+1} - \delta^*_{i-1}}{x_{i+1} - x_{i-1}} \qquad (8.4)$$

However, at the trailing edge, δ^* suffers a slope discontinuity necessitating the use of one-sided differences. To calculate the boundary layer upstream of the trailing edge (occurring at i = ITE) we used

$$\left(\frac{d\delta^*}{dx}\right)_{i=ITE} = \frac{\delta^*_i - \delta^*_{i-1}}{x_i - x_{i-1}} \qquad (8.5)$$

While for the wake calculation downstream of the trailing edge we used

$$\left(\frac{d\delta^*}{dx}\right)_{i=ITE} = \frac{\delta^*_{i+1} - \delta^*_i}{x_{i+1} - x_i} \qquad (8.6)$$

The boundary layer equations were integrated up to the trailing edge using Eq. (8.5) to supply $d\delta^*/dx$ at the trailing edge. The boundary layer calculation was then restarted using (8.6) to give $d\delta^*/dx$ at the trailing edge. This procedure also allows us to deal with the slope discontinuities due to switching from the boundary layer mode to the wake mode in Green's method.

For $M > 1$ it was found best to calculate $d\delta^*/dx$ using a difference scheme with upwind bias. Consider the formula

$$\left(\frac{d\delta^*}{dx}\right)_i = \lambda\left[\frac{\delta^*_i - \delta^*_{i-1}}{x_i - x_{i-1}}\right] + (1-\lambda)\left[\frac{\delta^*_{i+1} - \delta^*_i}{x_{i+1} - x_i}\right] \qquad (8.7)$$

Using $\lambda = .75$ to introduce upwind bias gave much better convergence in the supersonic zone upstream of the shock than did the centered scheme indicated in Eq. (8.4). On the other hand, using $\lambda = .25$ which introduced a downwind bias produced very poor results.

A series of plots relating to test calculations appear at the end of the paper. The first sequence covers the case where $M_\infty = .7425$ and the Reynolds number based on chord

length is 4.10^6. The standard Green's lag entrainment
method was used for this calculation. Figure 8.11 shows
the pressure distribution which arises from a purely
inviscid calculation. Figure 8.12 shows the pressure
distribution which arises from viscous-inviscid coupling.
Figures 8.11 and 8.12 are superimposed in Fig. 8.13. As
can be seen, the boundary layer drives the shock a small
distance upstream and slightly lowers the maximum Mach
number which is obtained. Also it smooths out the pressure
distribution at the trailing edge. A plot of δ^* appears
in Fig. 8.14. Note that δ^* rises dramatically in response
to the strongly unfavorable pressure gradient supplied by
the shock wave. This wedging effect accounts for the
weakening of the shock and its upstream displacement.
Also note the cusp in δ^* which occurs at the trailing
edge. A graph of the skin friction coefficient appears in
Fig. 8.15. This drops dramatically in response to the
shock wave and actually becomes negative (indicating
separated flow) near the trailing edge. Downstream of the
trailing edge, Green's method is applied to a wake calcula-
tion which demands that the skin friction coefficient vanish.
Figure 8.16 compares the pressure calculated by the boundary
layer code with that determined by the inviscid code.
Ideally of course our coupling algorithm should ensure that
these are identical. However, as might be expected some
trouble is experienced within the shock profile and to a
minor extent near the trailing edge. Despite this dif-
ficulty, the pressure distribution as calculated by the

boundary layer is in excellent agreement with the solutions to the Navier-Stokes equations presented by Deiwert [1976]. Wind tunnel interference corrections were not applied to the experimental data. As a consequence, there is a small discrepancy between the calculated and observed results (Mehta and Lomax [1981]).

It should be pointed out that for this example the original Le Balleur algorithm given by equation (6.18) fails to converge in the supersonic region ahead of the shock. Le Balleur overcomes this problem by resorting to the classical iteration (suitably under-relaxed in accordance with his theory presented in section 4) in regions of attached flow. The modified method on the other hand, is rapidly convergent in this region of attached supersonic flow. The decision as to when one should switch to the classical iteration can now be made on the basis of numerical accuracy in computing the boundary layer and need not be influenced by considerations of coupling algorithm convergence.

As a more severe test of our coupling procedures we also considered the case $M_\infty = .788$. The Reynolds number based on chord was again taken to be 4.10^6. The standard Green's lag entrainment method was used. Figure 8.21 shows the purely inviscid pressure distribution together with the pressure calculated from the viscous-inviscid coupling. In this case the boundary layer has quite a profound effect on the outer inviscid flow. The corresponding δ^* and skin friction coefficient are plotted in Figs. 8.22 and 8.23.

Note that we have shock induced separation, which accounts for the strong influence of the boundary layer. A convergence history of the coupling algorithm is presented in Figs. (8.24) through (8.28). As predicted by the theory presented in section 6, the algorithm does converge quite rapidly in regions of attached flow and the rate of convergence is slower in regions of separated flow. Considerable difficulty is experienced within the shock profile. However the graceful recovery downstream of the shock is a tribute to the basic stability of the coupling algorithm. In order to achieve convergence for this case it was found necessary to under-relax the coupling algorithm in the supersonic region. A relaxation factor of $\omega = .5$ was used, although a larger value probably would have sufficed. In the subsonic region a slight amount of over-relaxation, say $\omega = 1.2$, is generally helpful, although none was employed in this calculation.

The pressure distribution downstream of the shock predicted by this calculation does not agree well with experiment. The experimental data indicate that there is a supersonic plateau downstream of the shock. This example was recalculated using the modified Green's lag entrainment method due to East [1977]. The results are presented in Figs. 8.31 through 8.34. As can be seen, the C_p distribution downstream of the shock is augmented and the shock is moved further upstream. The calculated shock location is in excellent agreement with experiment, but the supersonic plateau downstream of the shock is still

not predicted. The Navier-Stokes solutions presented by Deiwert [1976] experienced the same difficulty. It is currently believed that the only way to overcome this problem is to prescribe the experimentally measured pressures at the downstream boundary (Mehta and Lomax [1981]).

Each of the three calculations presented here was run for 200 iterations, although the final answer was obtained, for all practical purposes, after 100 iterations. The computer time required for each case was approximately 18 seconds on the CDC 7600. Only about 20% of this time was devoted to the boundary layer calculation. Thus the total time required to compute a coupled viscous-inviscid solution is comparable to that required to compute the inviscid flow alone.

8.1 Remarks Concerning Numerical Tests

In the above numerical tests the coupling algorithm permits us to adjust δ^* in such a way that u, calculated from the inviscid code, agrees with $\tilde{u}$, calculated from the boundary layer equations. As we have seen there is a small discrepancy at the trailing edge and sometimes a rather large discrepancy on the downstream side of the shock. It should be pointed out, however, that in these regions the coefficient B in the boundary layer equation

$$\frac{d\delta^*}{dx} = A + B \frac{d\tilde{u}}{dx} \qquad (8.8)$$

becomes large. Rewrite Eq. (8.8) as

$$\frac{d\tilde{u}}{dx} = \frac{1}{B} \frac{d\delta^*}{dx} - \frac{A}{B} \qquad (8.9)$$

Errors in $d\delta^*/dx$ are ameliorated by the small factor $1/B$. Hence even though the coupling algorithm introduces errors in $d\delta^*/dx$, the value of $d\tilde{u}/dx$ is still close to that which would be calculated from the exact value of δ^*. This explains why the pressure coefficients, calculated by the boundary layer, always appear to be so reasonable, even though the inviscid pressure coefficients do not.

It may be desirable to introduce more sophisticated procedures in the regions around the shock and the trailing edge, such as triple deck theory (see Inger [1981] and Melnik [1980]). In this case our coupling algorithm provides a stable framework in which to embed these more sophisticated techniques.

9.   Calculations with the Exact Code

Encouraged by the success of our numerical tests in section 8, we now perform calculations using the exact code. The effect of the boundary layer on the inviscid flow is represented through the surface transpiration condition

$$v_n = \frac{1}{\rho_e} \frac{d}{ds} (\rho_e u_e \delta^*) \qquad (9.1)$$

(see Eq. (2.9)). In order to apply the semi-inverse method for this case we cast the boundary layer equations in the form

$$\frac{dm}{dx} = A_m + B_m \frac{du}{dx} \qquad (9.2)$$

where $m = \rho_e u_e \delta^*$. We define

$$\alpha_m = \frac{dm}{dx} \qquad (9.3)$$

It is then easily shown that formulae (5.8) and (5.13) apply, provided that:

α is replaced by α_m

B is replaced by B_m

β is replaced by $\beta \rho_e u_e$

As in section 8, the algorithm was implemented in its integrated form. In Eqs. (8.1) and (8.2) we make the replacements mentioned above and also note that

δ^* is replaced by m

A series of calculations were carried out for an NACA 0012 airfoil at zero angle of attack. A body-fitted mesh of size 110×30 generated by Eisman's method [1979] was used. This mesh is finer than the mesh displayed in Figs. 3.1 and 3.2. Eighty mesh points were placed on the airfoil. The mesh was concentrated near the leading edge but the largest mesh width, which occurred near the trailing edge, was only 1.8% of chord. Thirty mesh points were used in the wake, exponentially stretched to a distance of five chord lengths away from the airfoil. The mesh was also exponentially stretched in the pseudo radial direction to a distance of five chord lengths away from the airfoil. The size of the mesh in the pseudo radial direction near the airfoil and wake centerline is 1% of chord. Free stream conditions were assumed to prevail at the far field boundaries.

Five sets of calculations with corresponding experimentally measured pressure distributions are presented in Figs. 9.11 through 9.55. The experiments were carried out at the National Aeronautical Establishment (NAE) facility in Ontario, Canada (see Thibert, Grandjacques and Öhman [1979]). The pressure coefficients measured on the lower surface of the airfoil are plotted as O's while those pertaining to the upper surface are plotted with Δ's. The experiments were conducted at high Reynolds numbers, so in the calculations it was assumed that the boundary layer

was in a fully developed turbulent state at 5% of chord.

The first set of data corresponded to $M_\infty = .490$. The flow is strictly subsonic so that potential theory should be valid. Indeed the purely inviscid calculation is in excellent agreement with experiment. The effect of the boundary layer is totally negligible except very close to the trailing edge.

The second set of data was run for $M_\infty = .693$. The flow still remains subsonic with the maximum experimentally measured Mach number being .932. Thus, once again, potential theory should be valid for the inviscid portion of the flow. In this case, however, there is a small discrepancy between calculated and measured pressures near the leading edge. The effect of the boundary layer is predicted to be negligible in this region. Therefore, the coupled solution is in only slightly better agreement with experiment than is the purely inviscid calculation.

A possible explanation for the discrepancy between theory and experiment is that the boundary layer remains laminar. In the experiment the transition to turbulence was left free and, unfortunately, the position of the free transition was not established. If the boundary layer managed to remain laminar over, say, the first 20% of chord then the viscous effects would be more profound than those calculated assuming the boundary layer to be turbulent. Evidence supporting this conjecture is provided by the third set of data run at $M_\infty = .776$. In this case the flow becomes

supercritical and we have a weak shock near the leading
edge. However, the calculated shock position is 10% of
chord aft of the experimentally measured position. More-
over, the experiments show that the pressure coefficient
C_p just downstream of the shock is nearly equal to C_p^*.
This indicates that viscous effects are seriously affecting
the shock. The calculations based on the turbulent boundary
layer assumption show that the shock is too weak to produce
a substantial wedging effect (see Fig. 9.32). Therefore,
a turbulent boundary layer should not cause a dramatic
change in the shock jump conditions. Thus, we conclude
that the boundary layer may still be laminar when it
interacts with the shock.

In the last two data sets run at $M_\infty = .814$ and $M_\infty = .835$, respectively, the boundary layer is certainly
turbulent by the time it interacts with the shock.
However, the shock locations are still not properly
predicted by the calculations. For the $M_\infty = .835$ case, for
example, the purely inviscid solution predicts the shock
location to be at 20% of chord aft of that measured experi-
mentally (see Fig. 9.51). The coupled solution drives the
shock forward 5% of chord (see Fig. 9.54) so the difference
between theoretical and observed positions is still 15% of
the chord length.

The most likely cause of this discrepancy is explained
by Fig. 9.60 taken from Lock [1980]. Here we see that for
$M_\infty = .85$, the shock location predicted by the conservative
form of the full potential equation does in fact lie 15%

of chord downstream of that predicted by the Euler equations. Thus it appears that if we are to expect the coupled viscous-inviscid calculation to agree with experimental data for all flows of transonic interest we really must solve the Euler equations.

10.   Conclusion

A viscous-inviscid coupling procedure, which is a
modification of that proposed by Le Balleur, has been
presented. Using a model problem suggested by Le Balleur,
we showed that the modified algorithm converges rapidly
for attached flows and also works well for separated
flows. This theoretical analysis was confirmed by
numerical tests for a series of challenging transonic
calculations involving attached and separated flows. The
calculations attest to the remarkable stability of the
coupling algorithm, but also point out problems which
occur near the shock and the trailing edge. Nevertheless,
the method developed in this thesis to compute coupled
viscous-inviscid flows should provide a suitable vehicle
in which to incorporate more sophisticated treatments of
these regions.

References

Ballhaus, W. F., Jameson, A. and Albert, J., "Implicit Approximate Factorization Schemes for the Efficient Solution of Steady Transonic Flow Problems," AIAA Journal, 16, 573-579, 1978.

Beam, R. M. and Warming, R. F., "An Implicit Finite-Difference Algorithm for Hyperbolic Systems in Conservation-Law Fcrm," J. Comp. Phys. 22 (1), 1976.

Bradshaw, P. and Ferriss, D., "Calculation of Boundary Layer Development Using Turbulent Energy Equation, Compressible Flow on Adiabatic Walls," J. Fluid Mech. 46, 1971.

Brandt, A., "Multi-Level Adaptive Computations in Fluid Mechanics," AIAA Computational Fluid Dynamics Conference, July 1979, Williamsburg, VA.

Carter, J. E., "A New Boundary-Layer Inviscid Iteration Technique for Separated Flow," AIAA Computational Fluid Dynamics Conference, July 1979, Williamsburg, VA.

Collyer, M. R. and Lock, R. C., "Prediction of Viscous Effects in Steady Transonic Flow Past an Aerofoil," Aeronautical Quarterly, 30, p. 485, 1979.

Deiwert, G. S., McDevitt, J. B. and Levy, Jr., L. L., "Simulation of Turbulent Transonic Separated Flow Over an Airfoil," Conference on Aerodynamic Analyses Requiring Advanced Computers, NASA Langley Research Center, 1976, NASA SP-347.

East, L. F., Smith, P. D. and Merryman, P. J., "Prediction of the Development of Separated Turbulent Boundary Layers by the Lag-Entrainment Method," British Royal Aircraft Establishment Technical Report 77046, 1977.

Eisman, P. R., "A Multi-Surface Method of Coordinate Generation," J. Comp. Phys., 33, 118-150, 1979.

Green, J. E., Weeks, D. J. and Brooman, J. W. F., "Prediction of Turbulent Boundary Layers and Wakes in Incompressible Flow by a Lag-Entrainment Method," British Aeronautical Research Council Reports and Memoranda No. 3791, 1977.

Holst, T. L. and Ballhaus, Jr., W. F., "Fast Conservative
    Schemes for the Full Potential Equations Applied to
    Transonic Flows," AIAA Journal, 17, 145-152, 1979.

Holst, T. L., "Implicit Algorithm for the Conservative
    Transonic Full Potential Equation Using an Arbitrary
    Mesh," AIAA Journal, 17, 1038-1045, 1979.

Inger, G. R., "Application of a Shock-Turbulent Boundary
    Layer Interaction Theory in Transonic Flow Field
    Analysis," paper presented at "Transonic Perspective
    – A Critique of Transonic Flow Research," NASA Ames
    Research Center, Feb. 1981.

Jameson, A., "Iterative Solution of Transonic Flows Over
    Airfoils and Wings, Including Flows at Mach 1," Comm.
    Pure Appl. Math., 27, 283-309, 1974.

Jameson, A., "Transonic Potential Flow Calculations Using
    Conservation Form," Proc. Second AIAA Computational
    Fluid Dynamics Conference, Hartford, 148-161, June
    1975.

Jameson, A., "Accleration of Transonic Potential Flow
    Calculation on Arbitrary Meshes by the Multiple Grid
    Method," AIAA Computational Fluid Dynamics Conference,
    July 1979, Williamsburg, VA.

Lax, P. D., "Weak Solutions of Nonlinear Hyperbolic Equations
    and their Numerical Computation," Comm. Pure Appl.
    Math., 7, 159-193, 1954.

Le Balleur, J. C., "Couplage Visqueux-Non Visqueux:
    Analyse du Probleme Incluant Decollements et Ondes
    de Choc," La Recherche Aerospatiale, No. 6, pp. 349-
    358, 1977.

Le Balleur, J. C., "Couplage Visqueux-Non Visqueux: Methode
    Numerique et Applications Aux Ecoulements Bidimensionnels
    Transsoniques et Supersoniques," La Recherche Aerospatiale,
    pp. 67-76, Mar.-Apr. 1978.

Le Balleur, J. C., "Calcul des Ecoulements a Forte Inter-
    action Visqueuse au Moyen de Methodes de Couplage,"
    AGARD Conference on Computation of Viscous-Inviscid
    Interactions, Preprint No. 291, Paper 1, Colorado
    Springs, 1980.

Lock, R. C., "A Review of Methods for Predicting Viscous
    Effects on Aerofoils and Wings at Transonic Speeds,"
    AGARD Conference on Computation of Viscous-Inviscid
    Interactions, Preprint No. 291, Paper 2, Colorado
    Springs, 1980.

Magnus, R., and Yoshihara, H., "Inviscid Transonic Flow Over Airfoils," AIAA Journal, 8, 2157-2162, 1970.

Mehta, U., and Lomax, H., "Numerical Prediction Methods (Reynolds-Averaged Navier-Stokes Simulations of Transonic Separated Flows)," p. 43. Paper presented at "Transonic Perspective — A Critique of Transonic Flow Research," NASA Ames Research Center, Feb. 1981.

Melnik, R. E., "Turbulent Interactions on Airfoils at Transonic Speeds — Recent Developments," AGARD Conference on Computation of Viscous-Inviscid Interactions, Preprint No. 291, Paper 10, Colorado Springs, 1980.

Melnik, R. E., and Chow, R., "Asymptotic Theory of Two-Dimensional Trailing-Edge Flows," NASA SP-347, p. 197, 1976.

Murman, E. M., and Cole, J. D., "Calculation of Plane Steady Transonic Flows," AIAA Journal, 9, 114-121, 1971.

Shapiro, A. H., The Dynamics and Thermodynamics of Compressible Fluid Flow, pp. 286-289, Ronald Press Company, 1953.

Thibert, J. J., Grandjacques, M., and Öhman, L. H., "NACA 0012 Airfoil," Section A1, AGARD Advisory Report No. 138, Experimental Data Base for Computer Program Assessment, 1979.
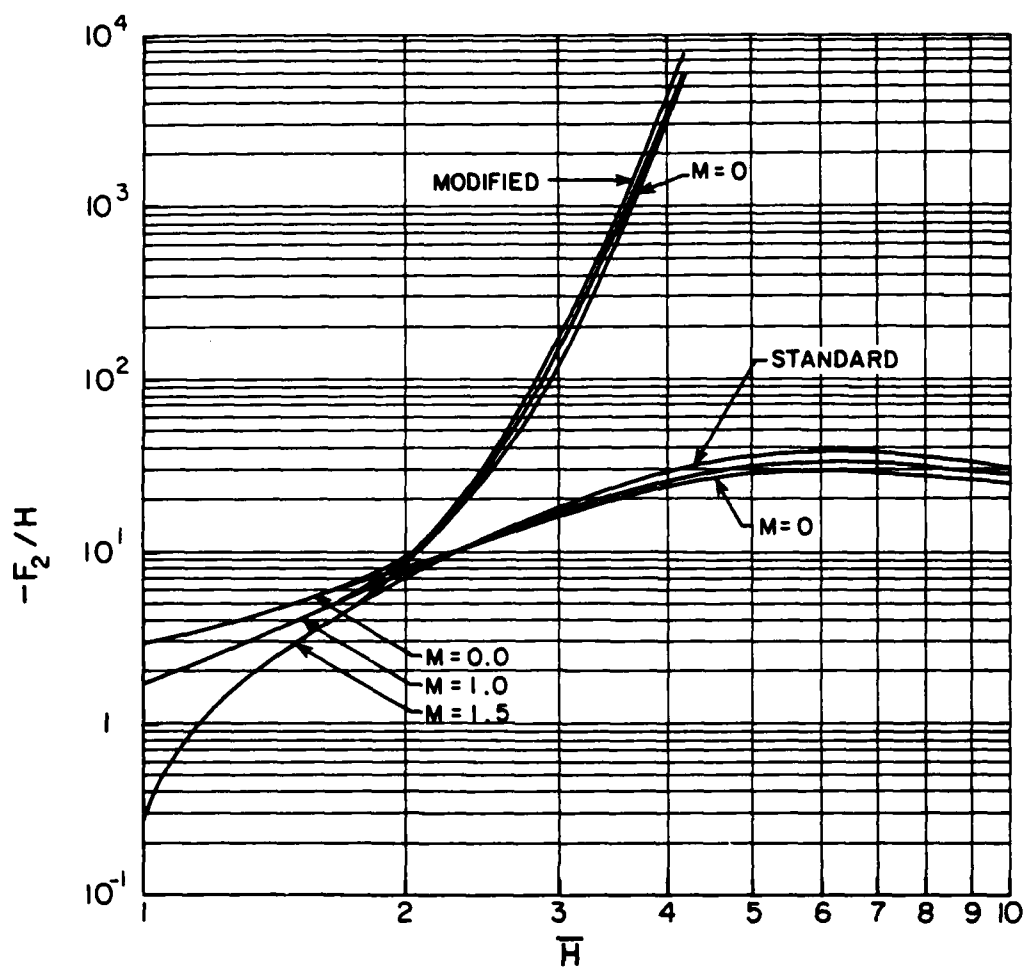
Fig. 2.1 Variation of $-F_2/H$ with $\bar{H}$ at Mach Numbers M=0.0, 1.0, 1.5 for Standard and Modified Green's Lag - Entrainment Method.
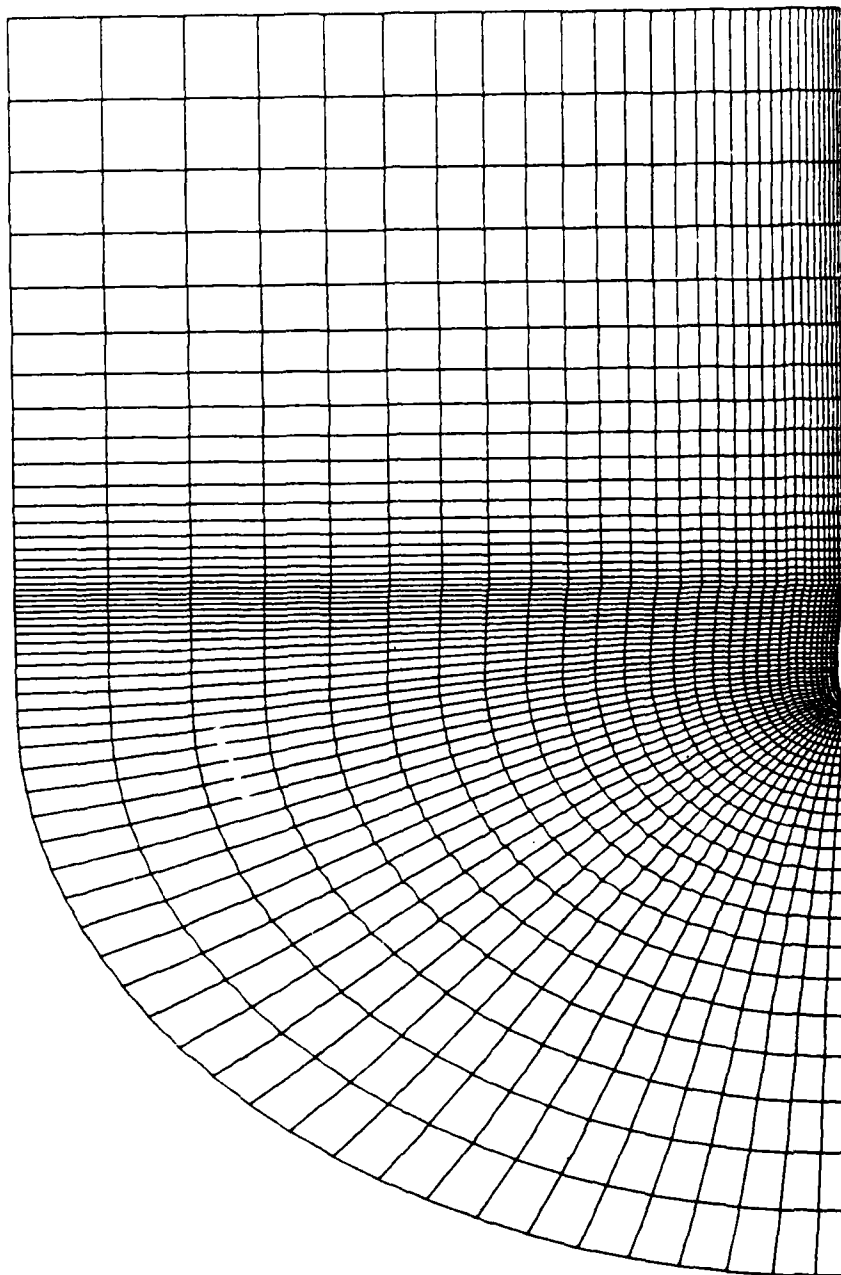
FIG. 3.1 MESH GENERATED ABOUT NACA 0012 AIRFOIL
MESH IS 61 BY 30
VIEW OF ENTIRE MESH
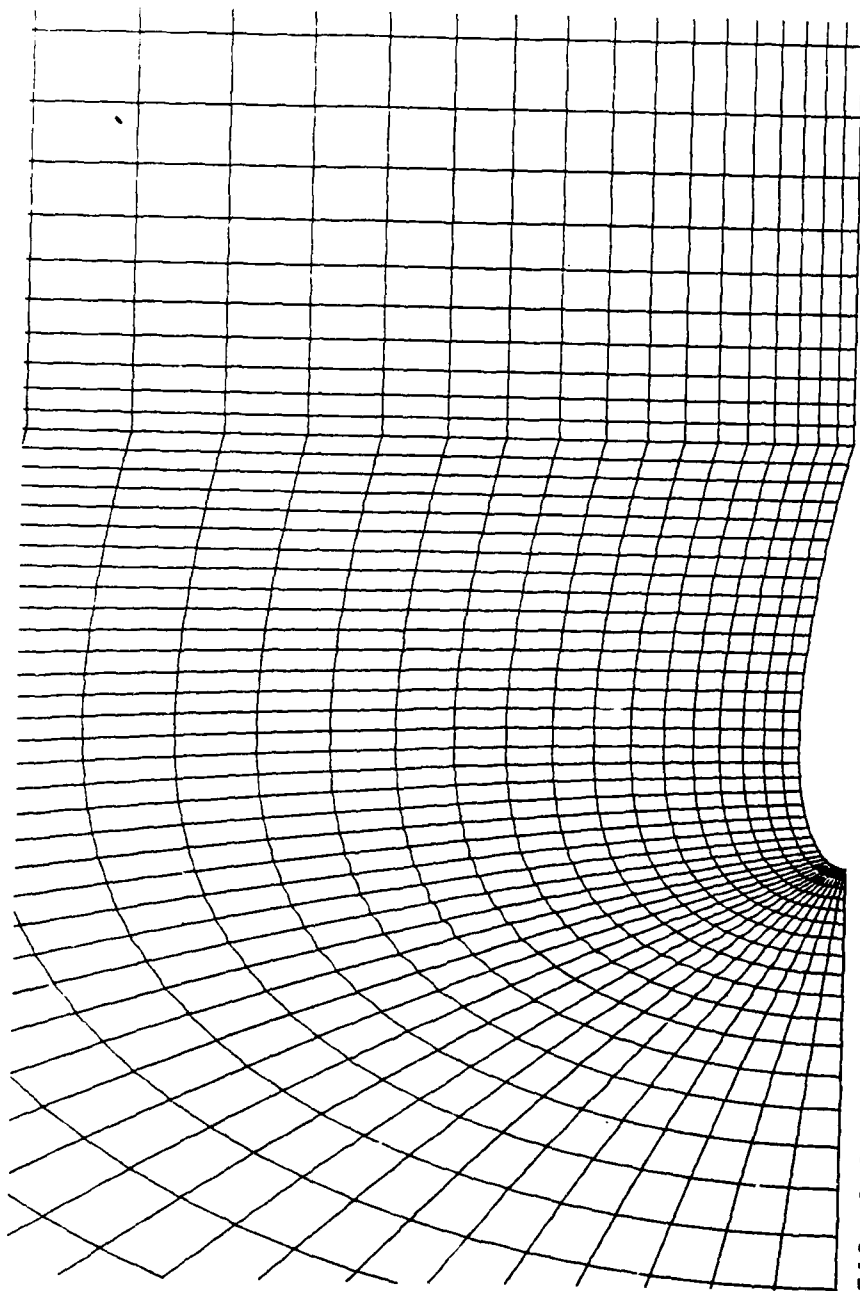
FIG. 3.2 MESH GENERATED ABOUT NACA 0012 AIRFOIL
MESH IS 61 BY 30
VIEW CLOSE TO AIRFOIL
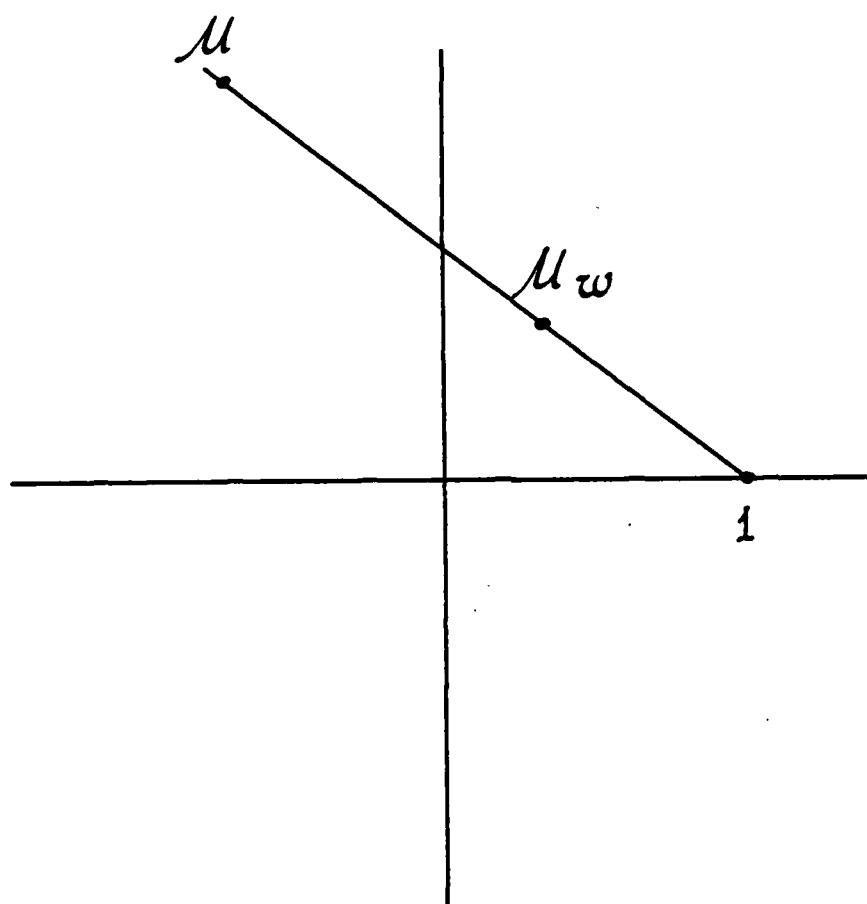
Fig. 4.1 Geometric Representation
of Equation (4.27),
$$\mu_w = w\mu + (1-w).$$
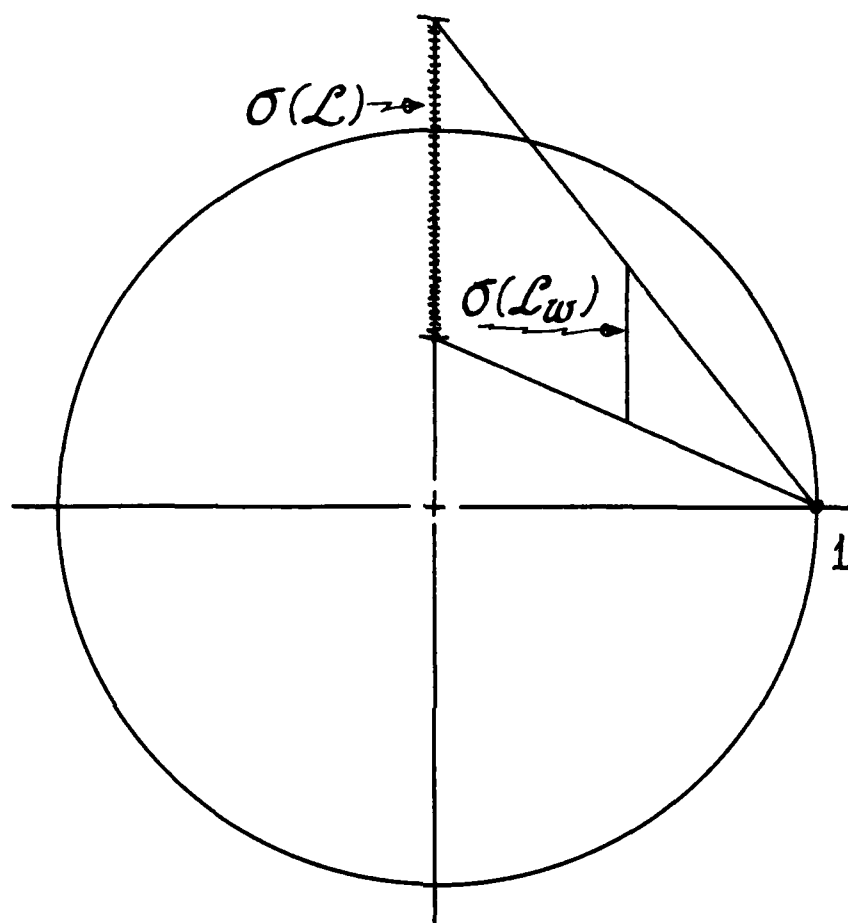
Fig. 4.2 $\sigma(\mathcal{L})$ and $\sigma(\mathcal{L}_w)$ in
Supersonic Case $B < 0$.
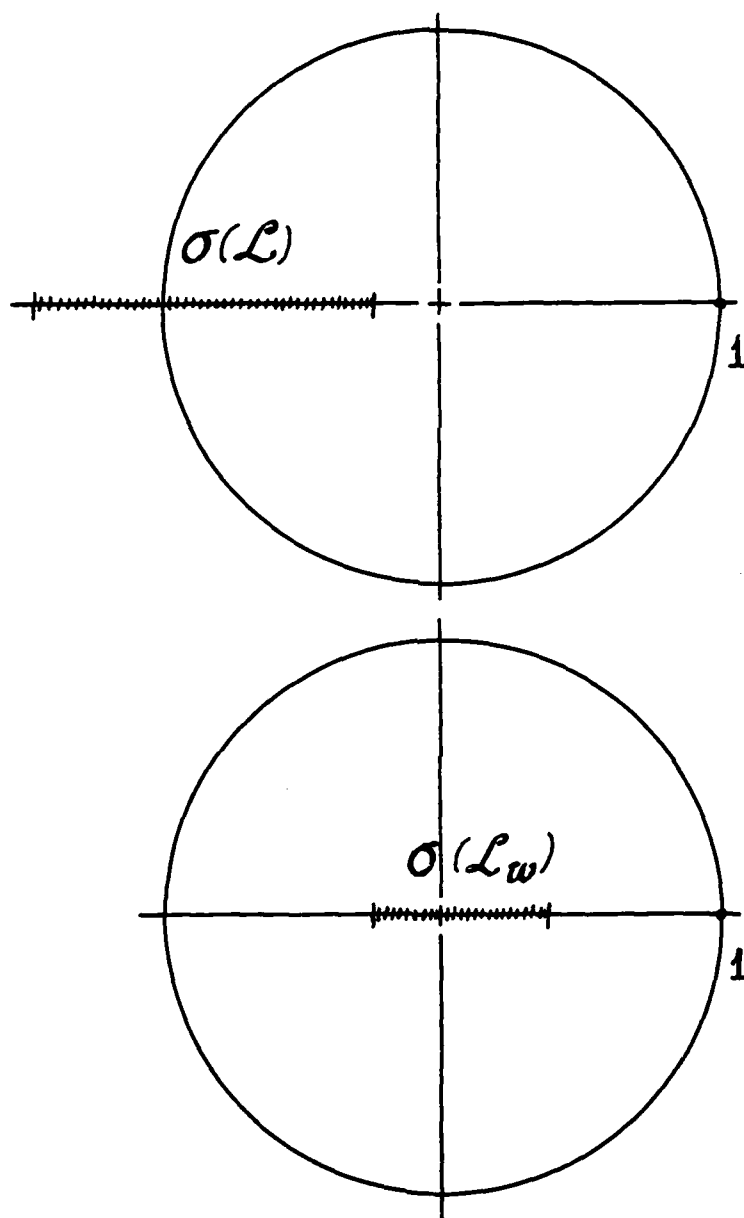
Fig. 4.3 $\sigma(\mathcal{L})$ and $\sigma(\mathcal{L}_w)$ in
Subsonic Case $B < 0$.
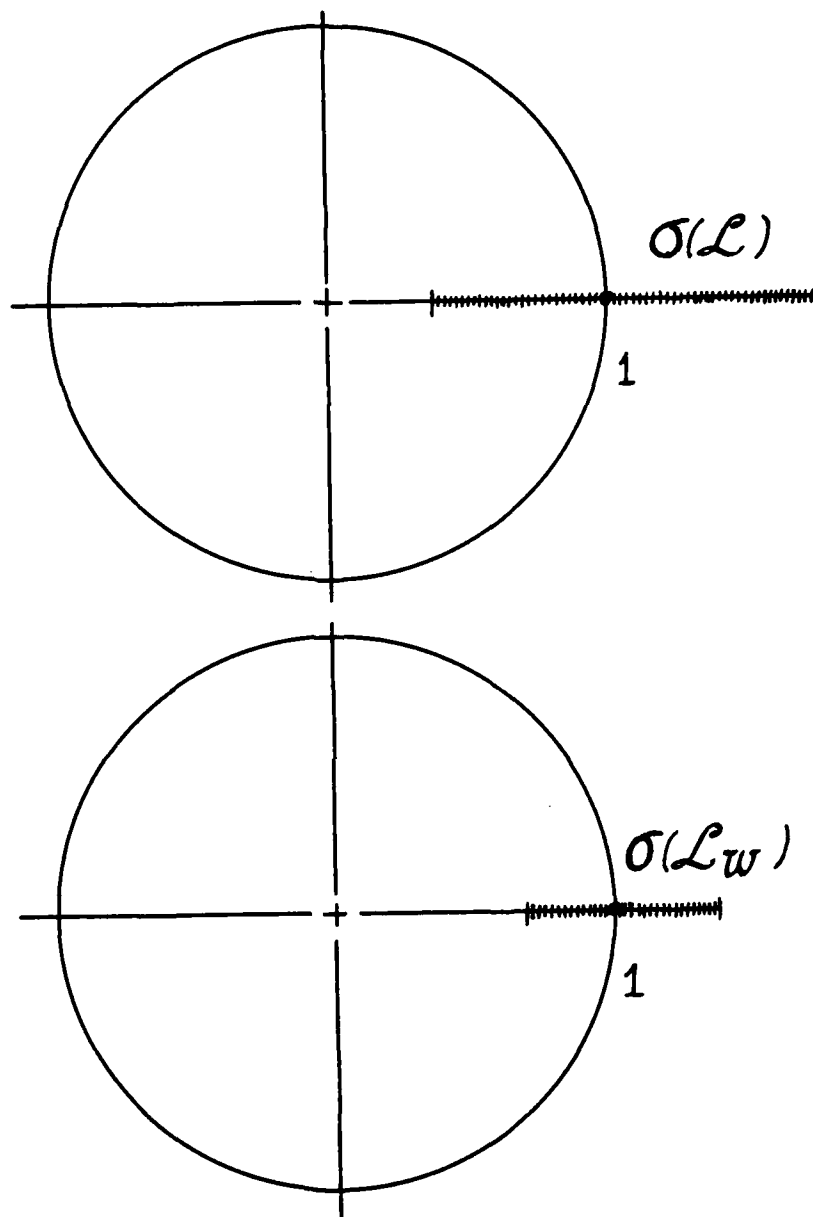
Fig. 4.4 $\sigma(\mathcal{L})$ and $\sigma(\mathcal{L}_W)$ in Subsonic Case $B > 0$.
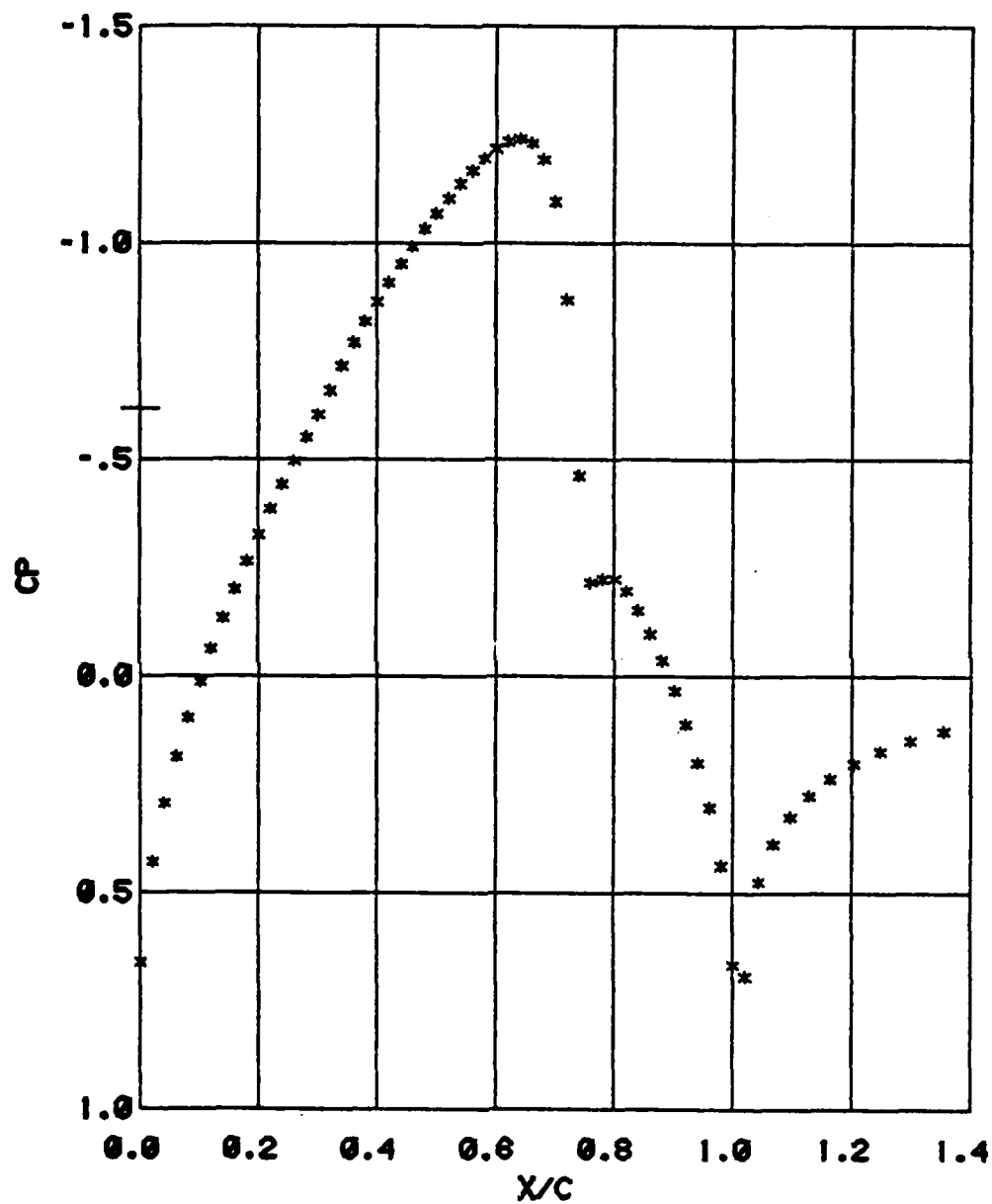
FIG. 8.11   18% THICK CIRCULAR ARC AIRFOIL
PURE INVISCID PRESSURE DISTRIBUTION
MINF=.7425   RECH=4E06
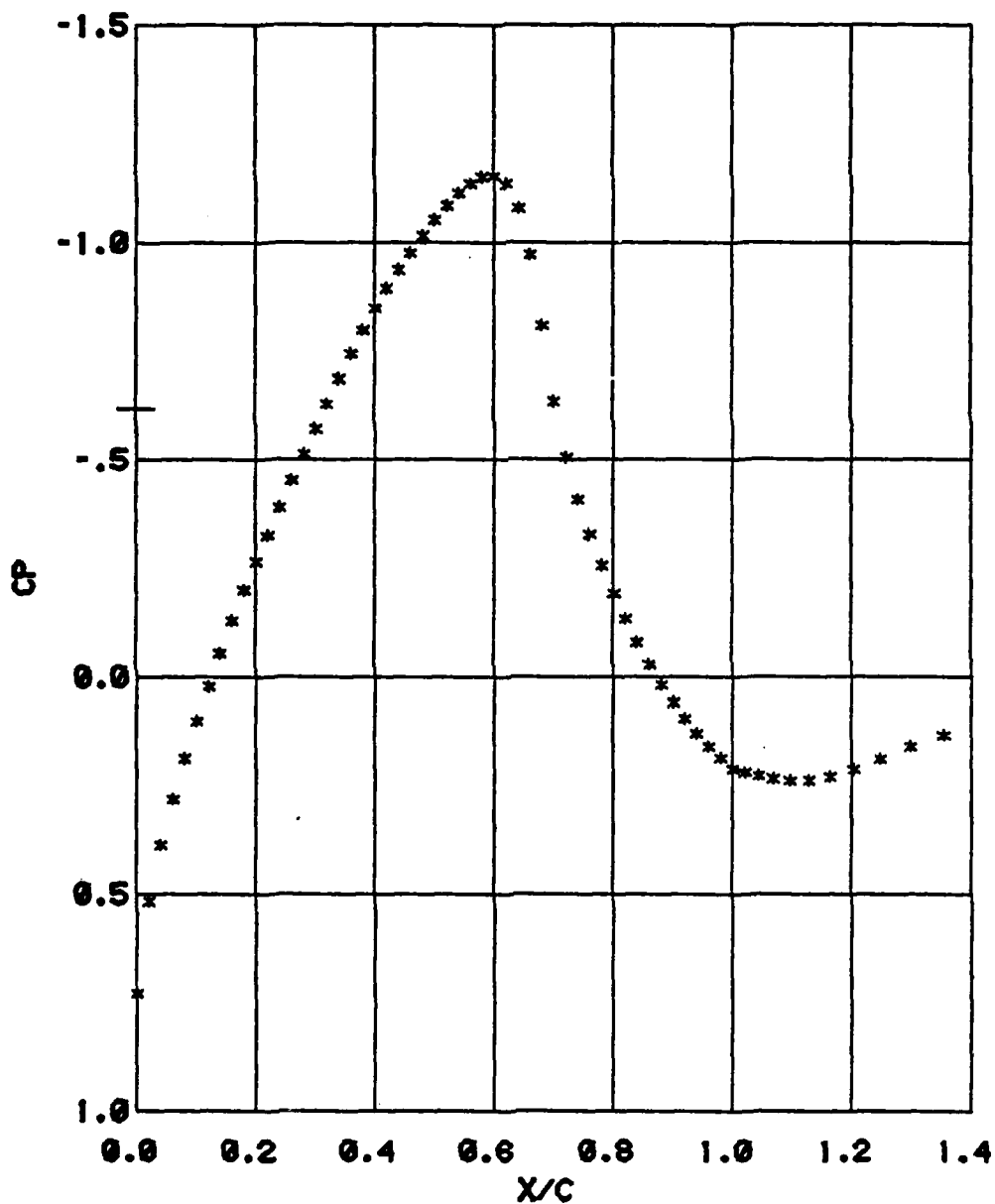
FIG. 8.12   18% THICK CIRCULAR ARC AIRFOIL
            PRESSURE AFTER VISCOUS-INVISCID
            COUPLING IS PERFORMED
            MINF=.7425   RECH=4E06
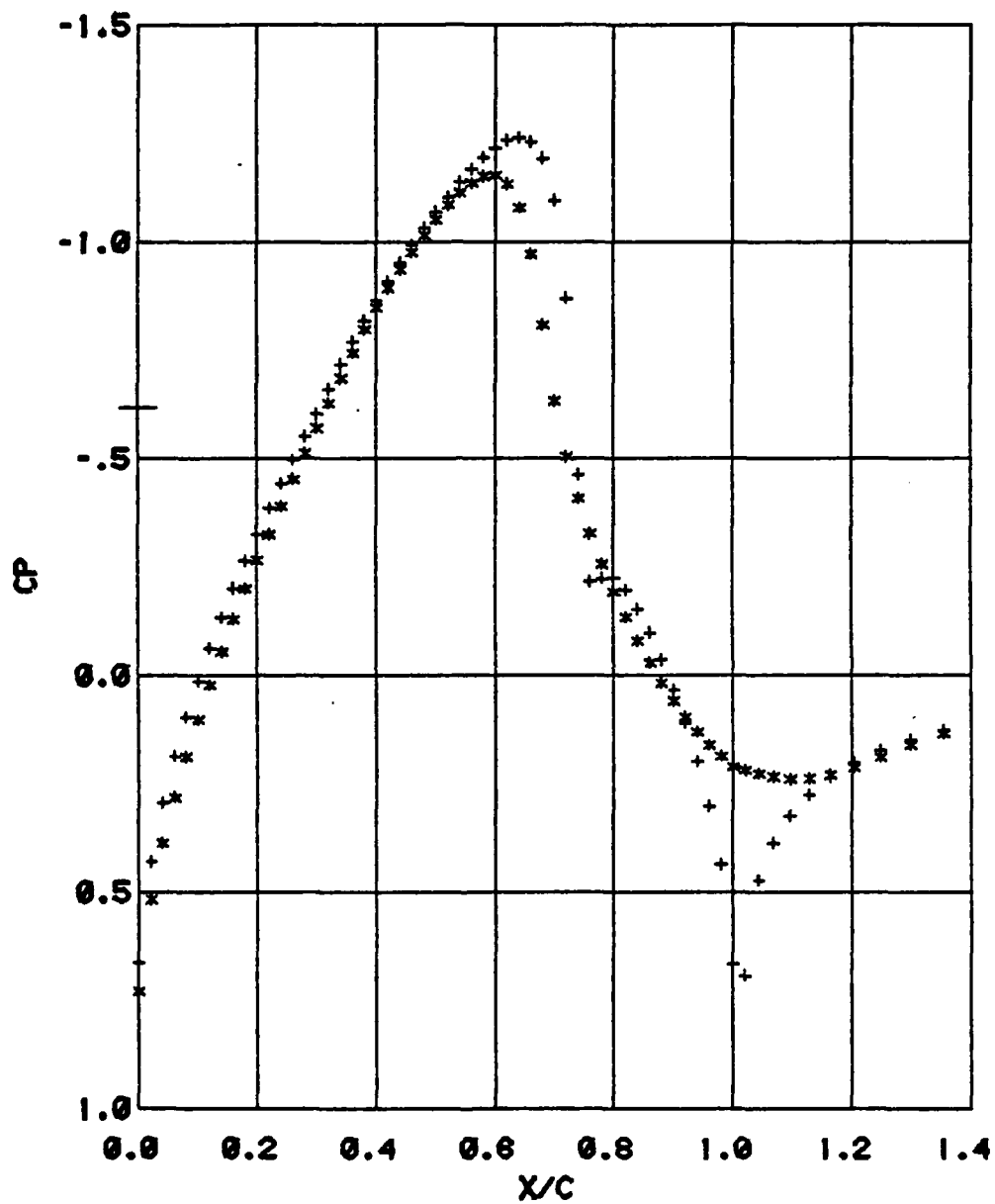
FIG. 8.13 18% THICK CIRCULAR ARC AIRFOIL
PURE INVISCID PRESSURE DISTRIBUTION
AND PRESSURE AFTER COUPLING
MINF=.7425   RECH=4E06
=COUPLED   +INVISCID
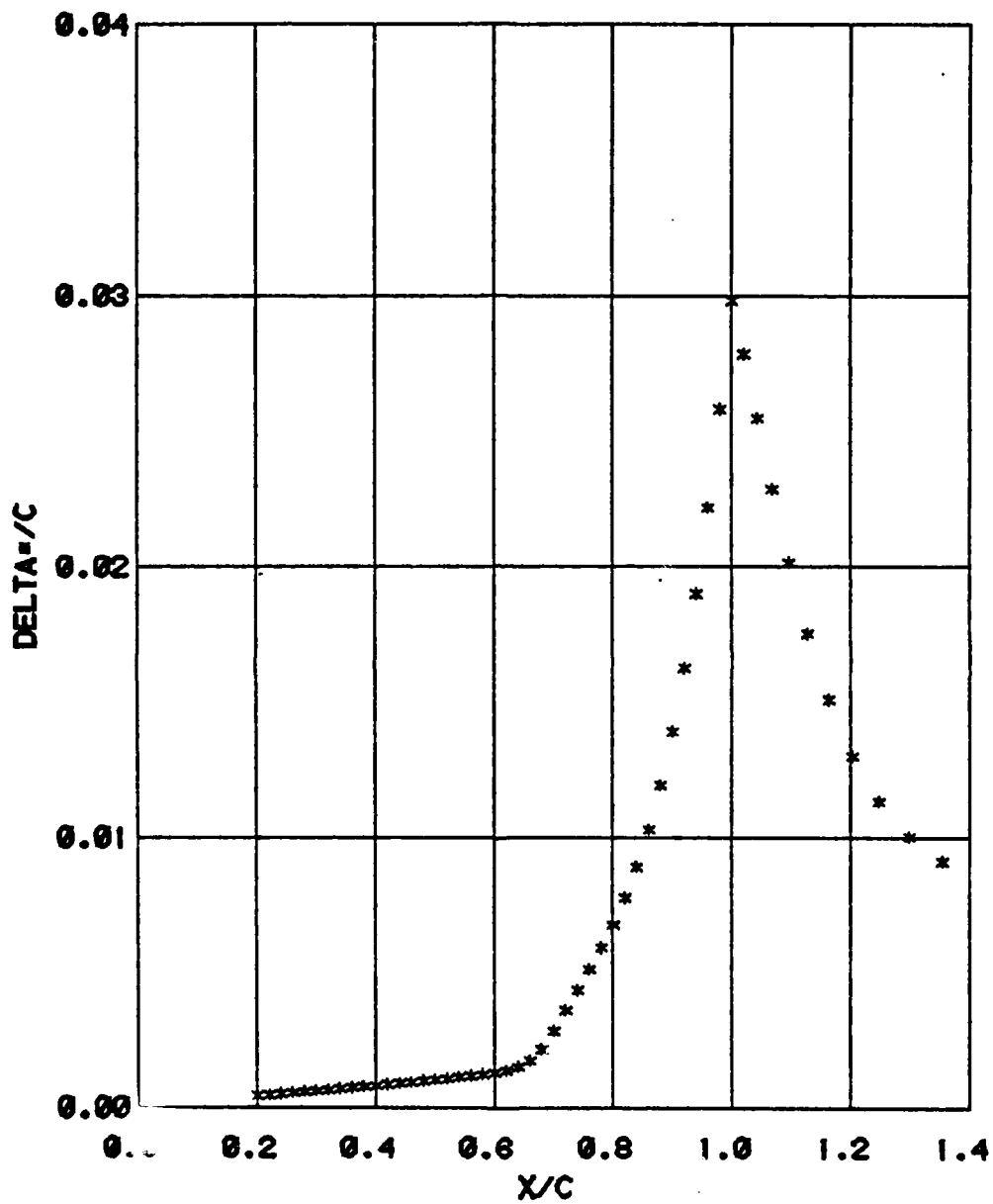
FIG. 8.14   18% THICK CIRCULAR ARC AIRFOIL
DISPLACEMENT THICKNESS
MINF=.7425   RECH=4E06
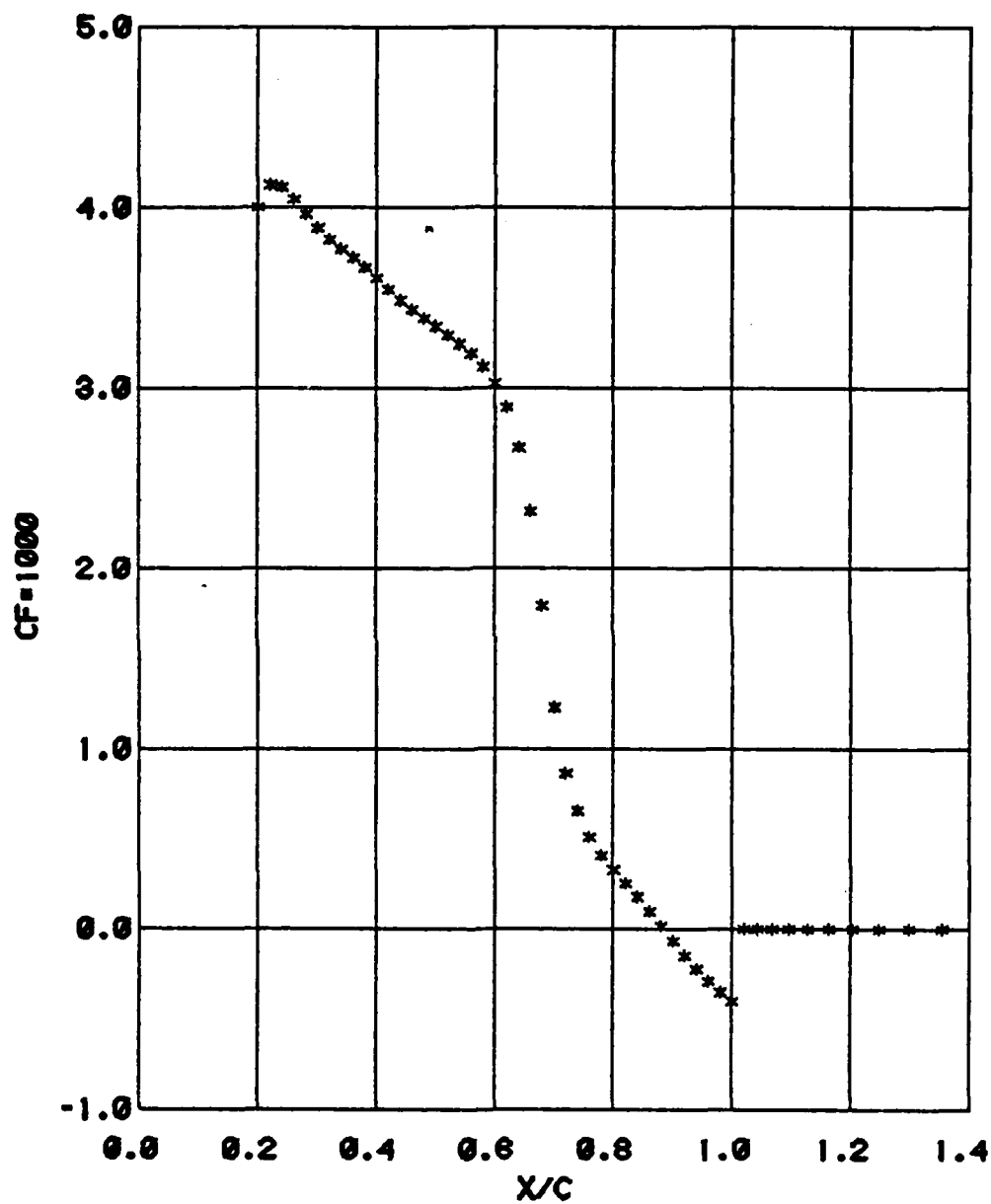
FIG. 8.15   18% THICK CIRCULAR ARC AIRFOIL
SKIN FRICTION COEFFICIENT
MINF=.7425   RECH=4E06
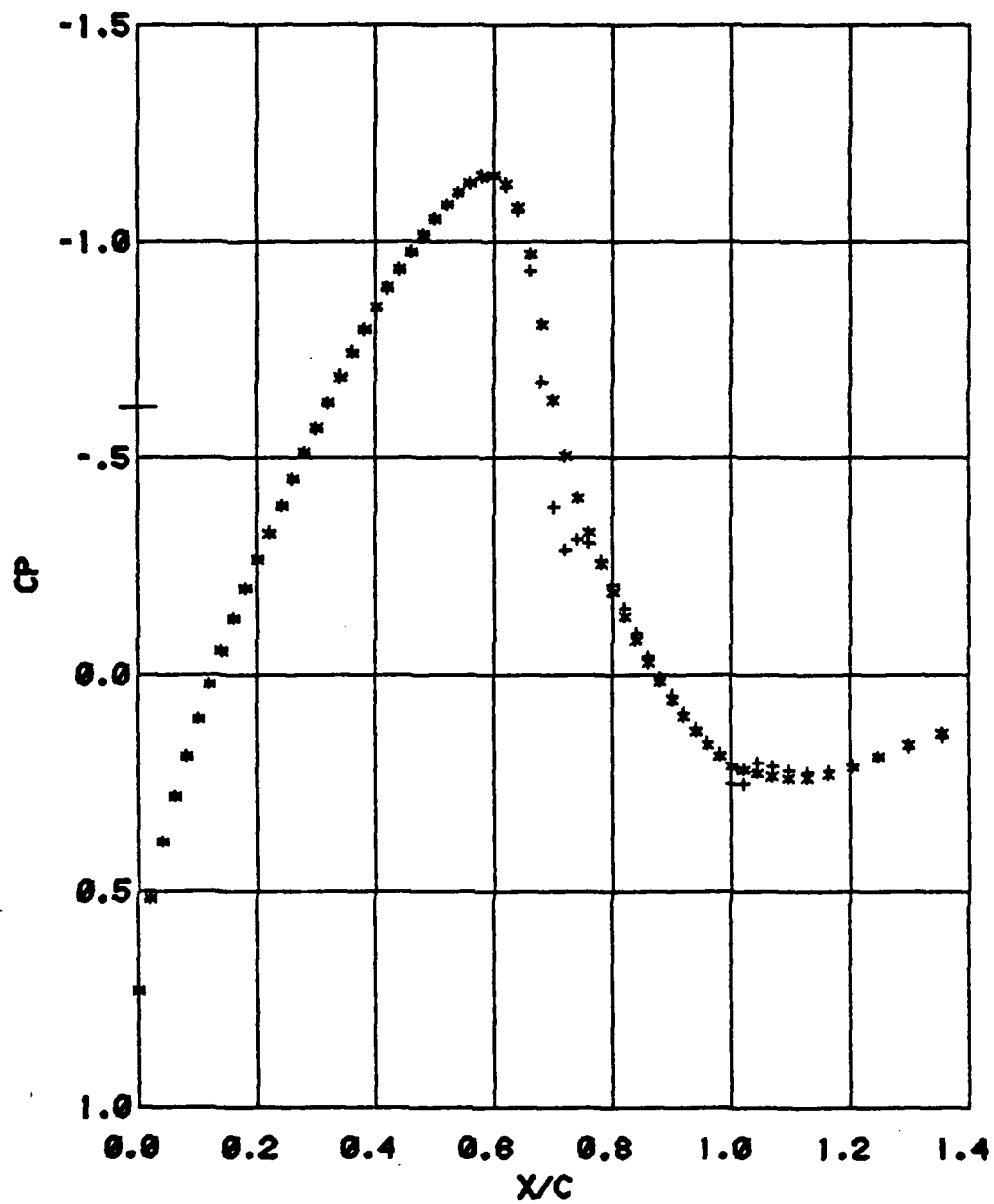
FIG. 8.16   18% THICK CIRCULAR ARC AIRFOIL
VISCOUS AND INVISCID PRESSURE
AFTER COUPLING
MINF=.7425   RECH=4E06
■VISCOUS   •INVISCID
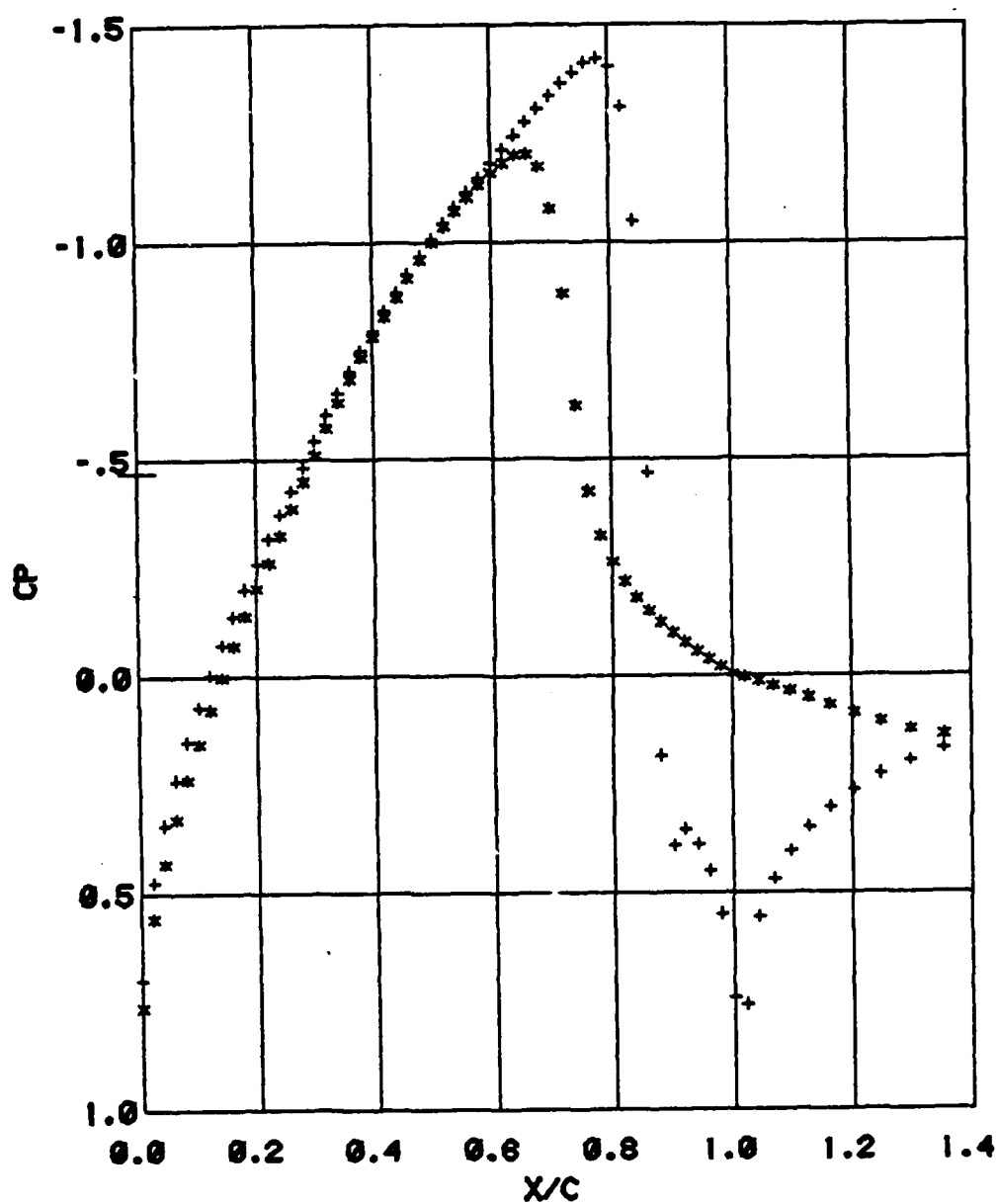
FIG. 8.21 18% THICK CIRCULAR ARC AIRFOIL
PURE INVISCID PRESSURE DISTRIBUTION
AND PRESSURE AFTER COUPLING
MINF=.788   RECH=4E06
=COUPLED   +INVISCID
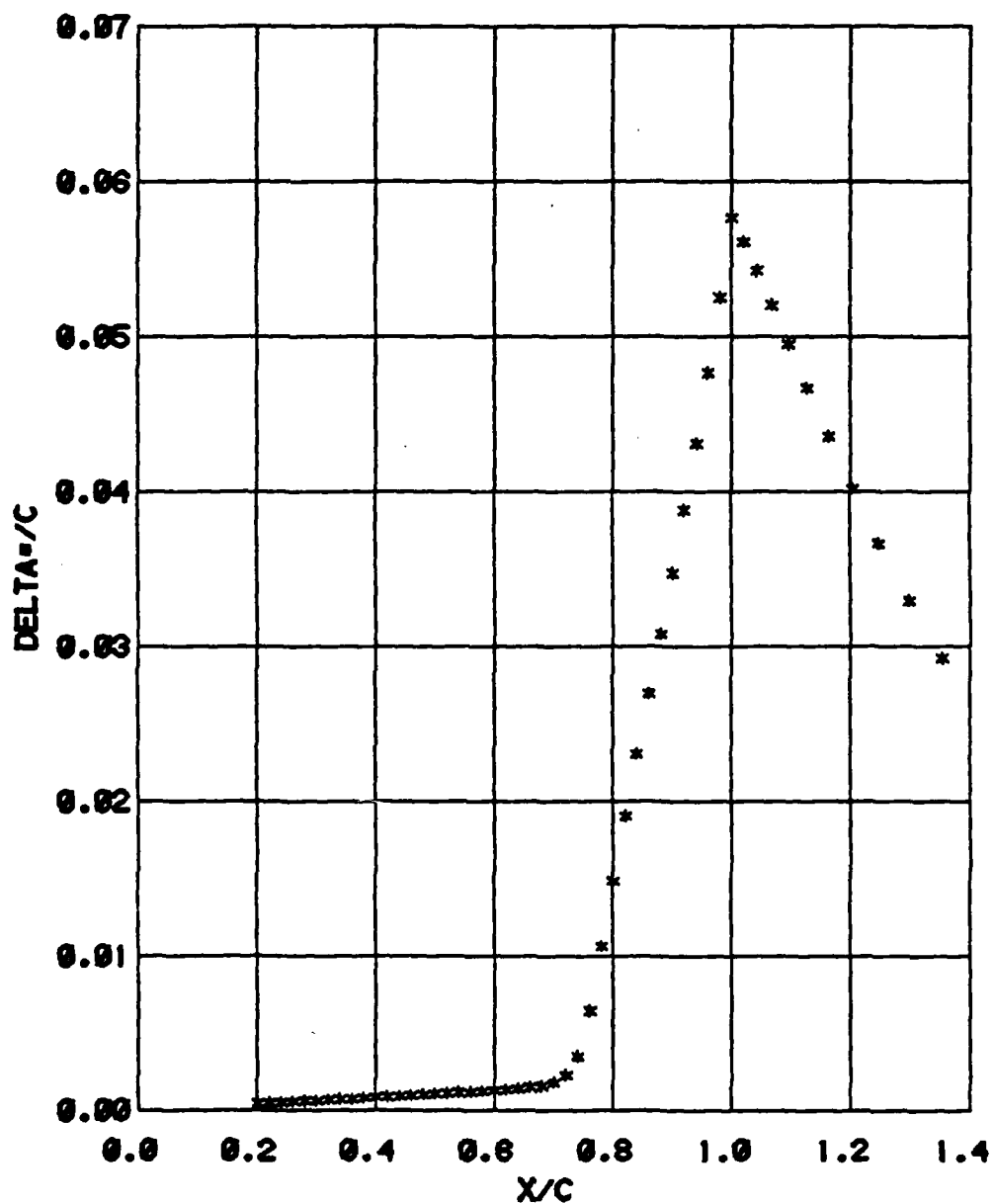
FIG. 8.22   18% THICK CIRCULAR ARC AIRFOIL
DISPLACEMENT THICKNESS
MINF=.788   RECH=4E06
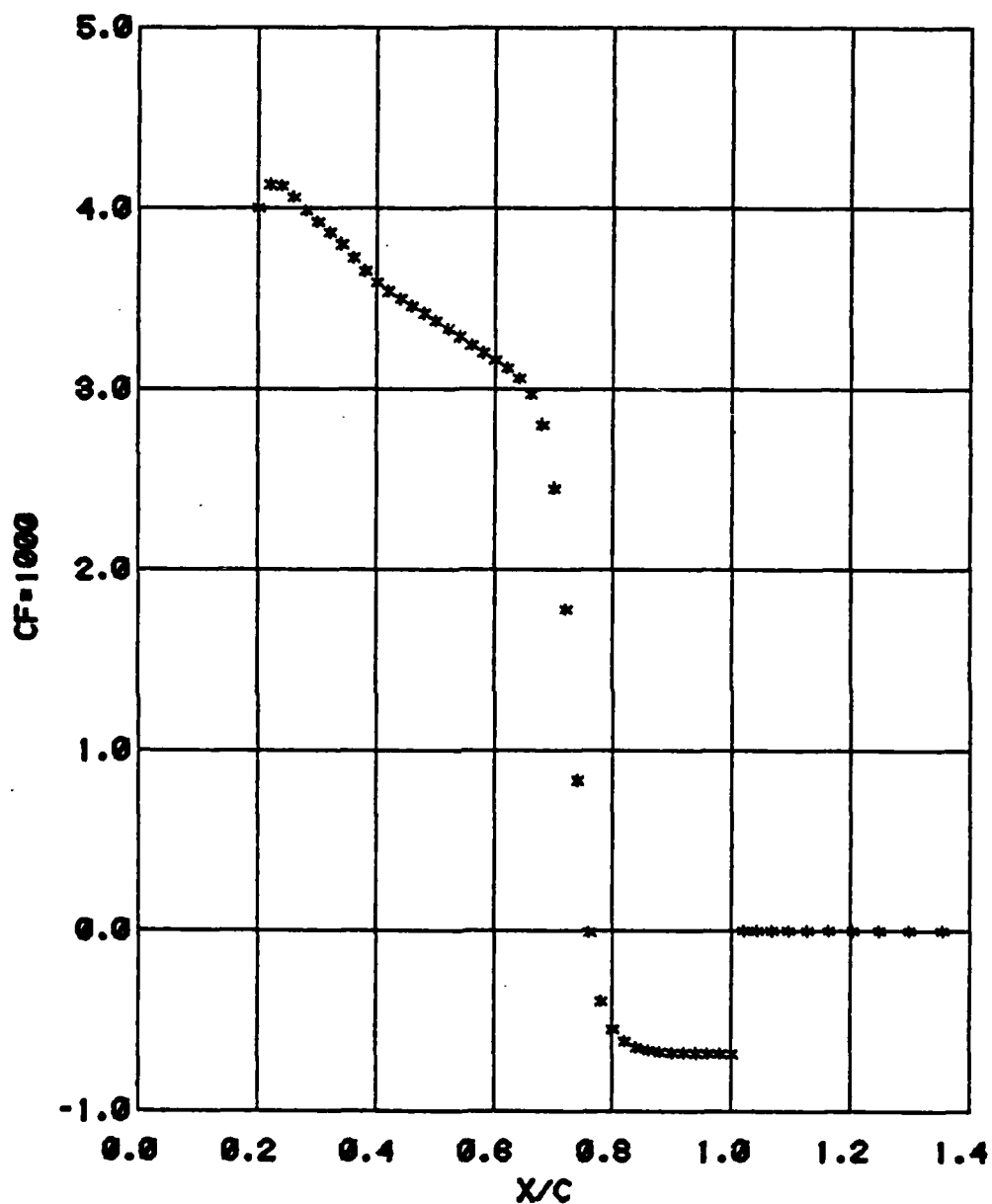
FIG. 8.23   18% THICK CIRCULAR ARC AIRFOIL
SKIN FRICTION COEFFICIENT
MINF=.788   RECH=4E06
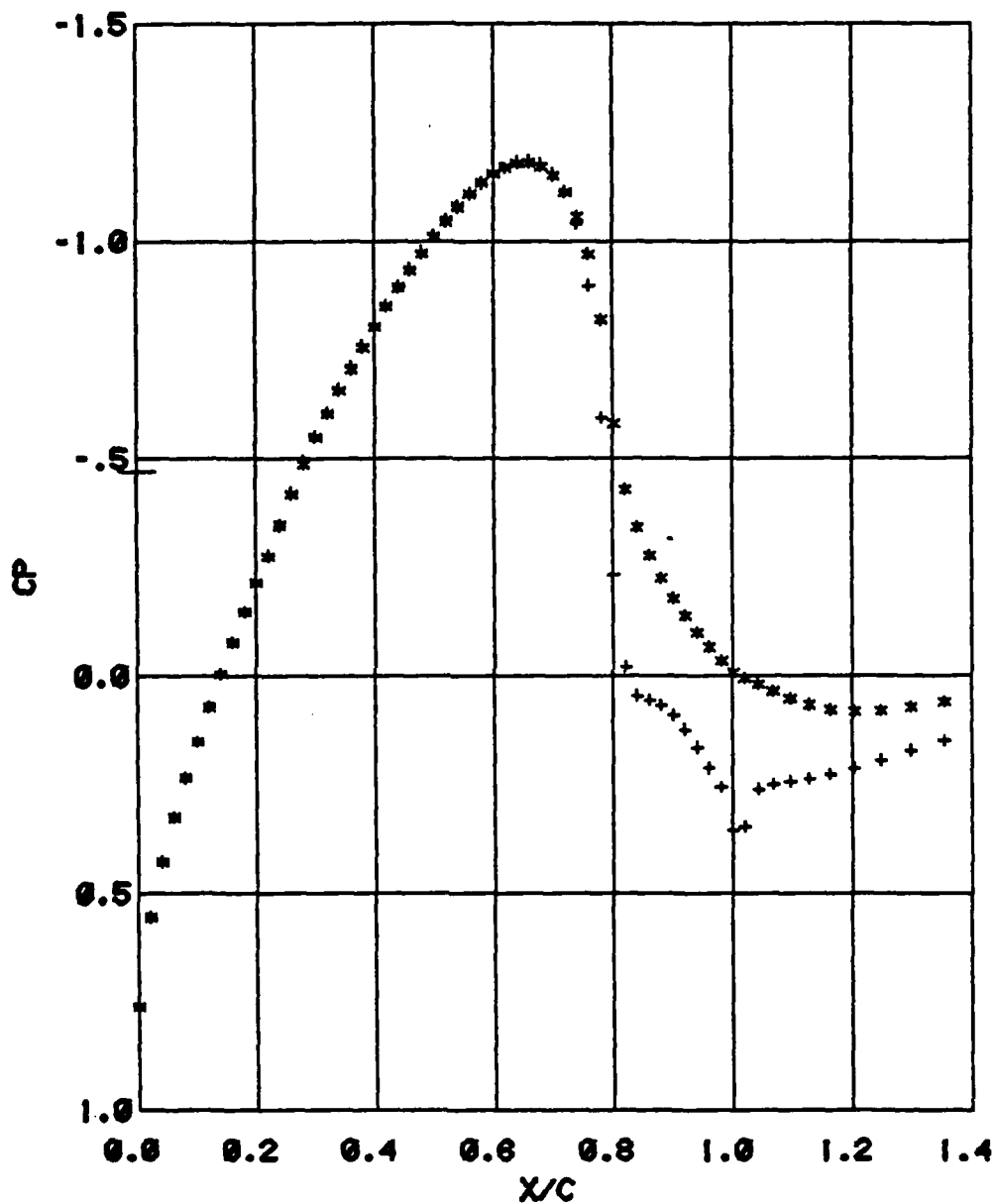
FIG. 8.24   18% THICK CIRCULAR ARC AIRFOIL
VISCOUS AND INVISCID PRESSURE
AFTER 20 ITERATIONS
MINF=.788   RECH=4E06
=VISCOUS   +INVISCID
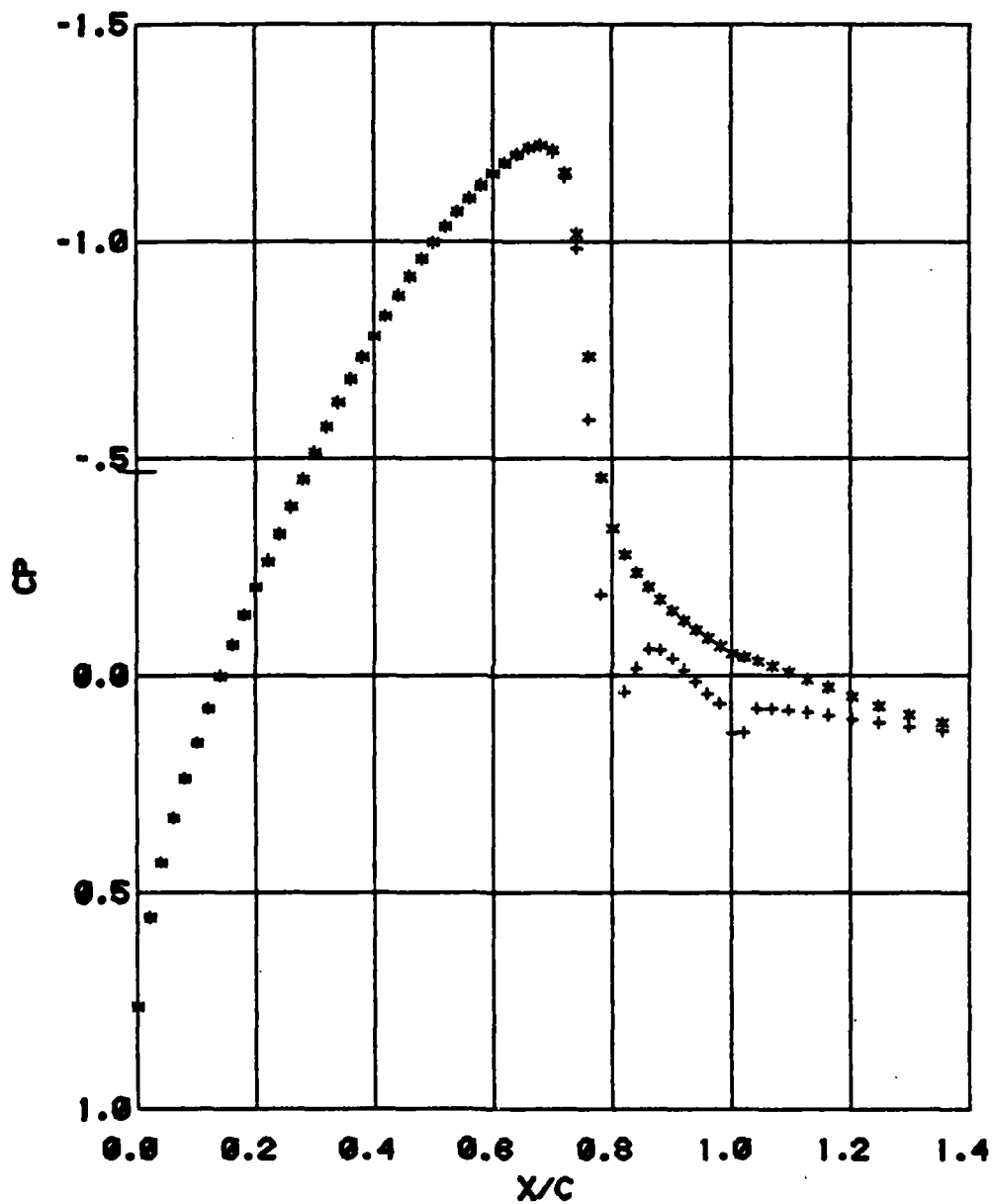
FIG. 8.25 18% THICK CIRCULAR ARC AIRFOIL
VISCOUS AND INVISCID PRESSURE
AFTER 50 ITERATIONS
MINF=.788   RECH=4E06
■VISCOUS   +INVISCID
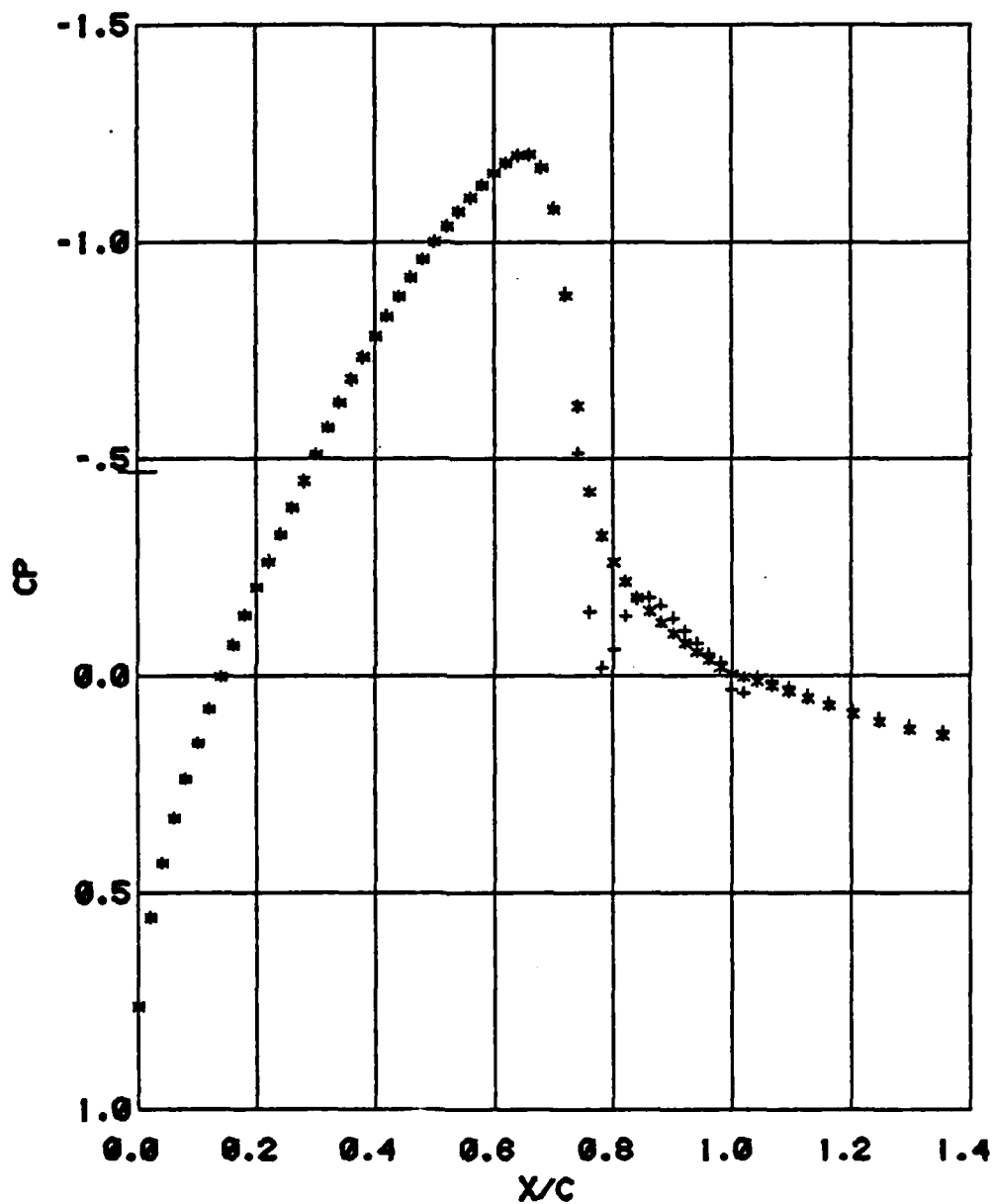
FIG. 8.26   18% THICK CIRCULAR ARC AIRFOIL
VISCOUS AND INVISCID PRESSURE
AFTER 100 ITERATIONS
MINF=.788   RECH=4E06
*VISCOUS   +INVISCID
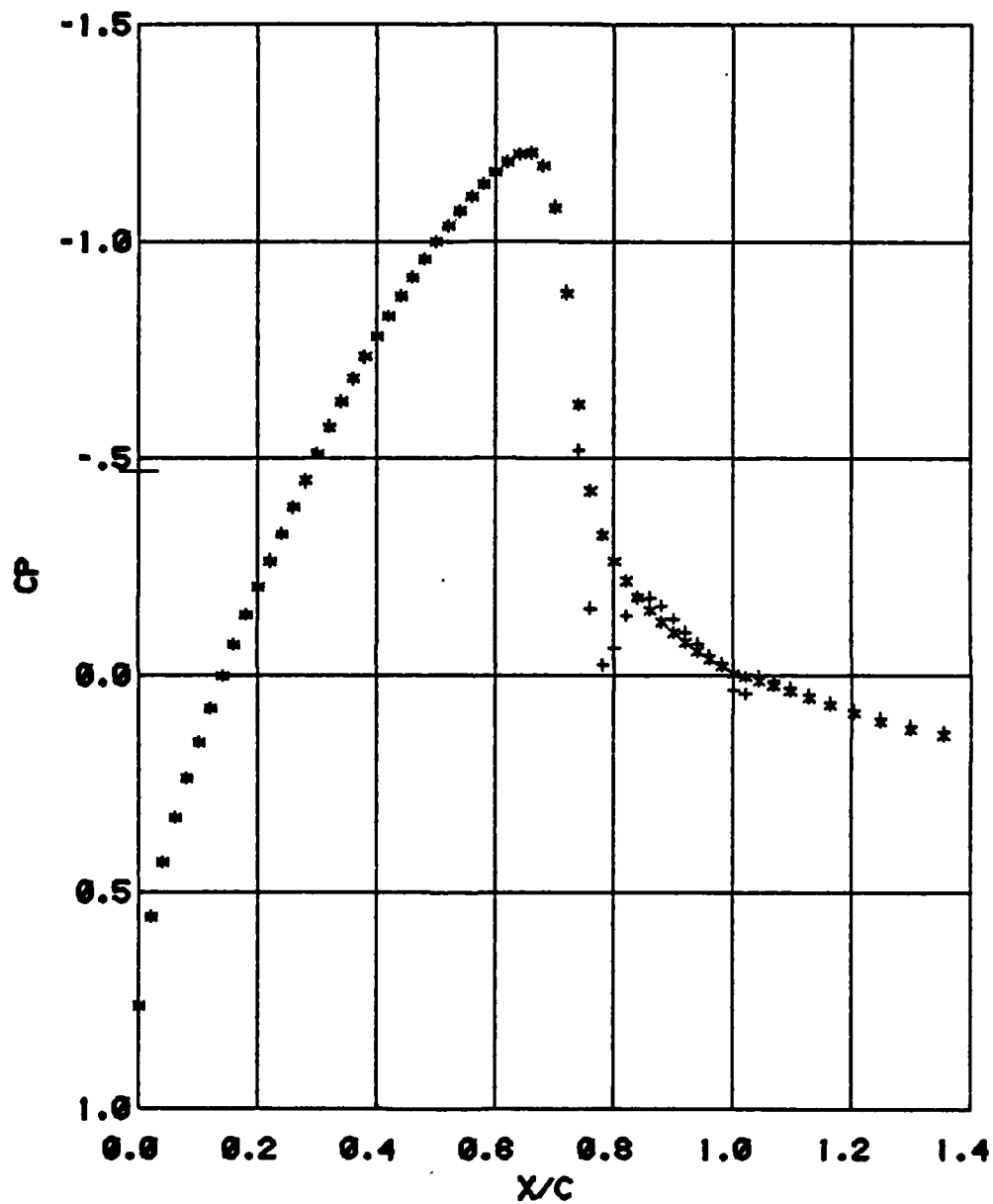
FIG. 8.27   18% THICK CIRCULAR ARC AIRFOIL
VISCOUS AND INVISCID PRESSURE
AFTER 150 ITERATIONS
MINF=.788   RECH=4E06
=VISCOUS   +INVISCID
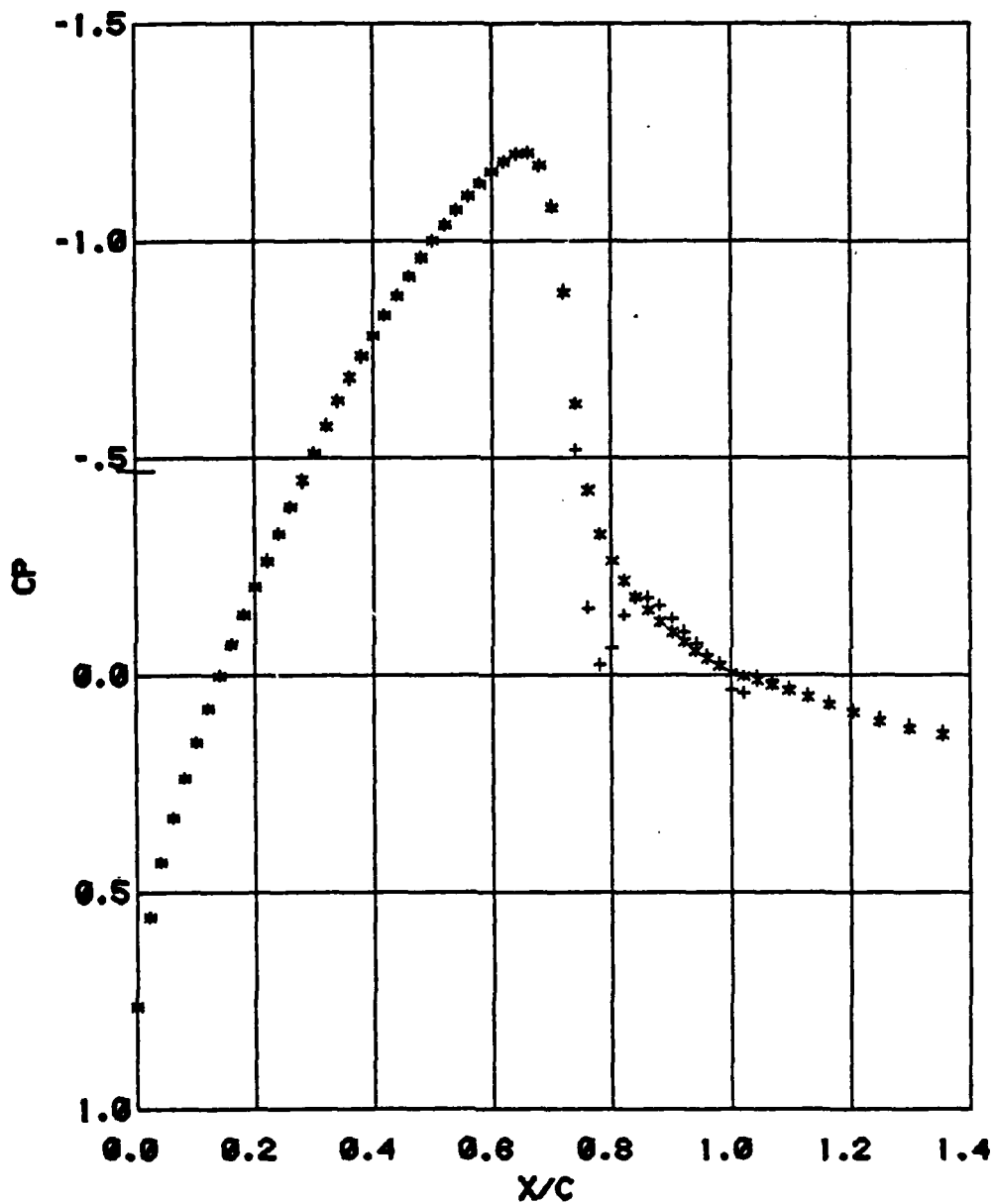
FIG. 8.28 18% THICK CIRCULAR ARC AIRFOIL
VISCOUS AND INVISCID PRESSURE
AFTER 200 ITERATIONS
MINF=.788 RECH=4E06
=VISCOUS +INVISCID
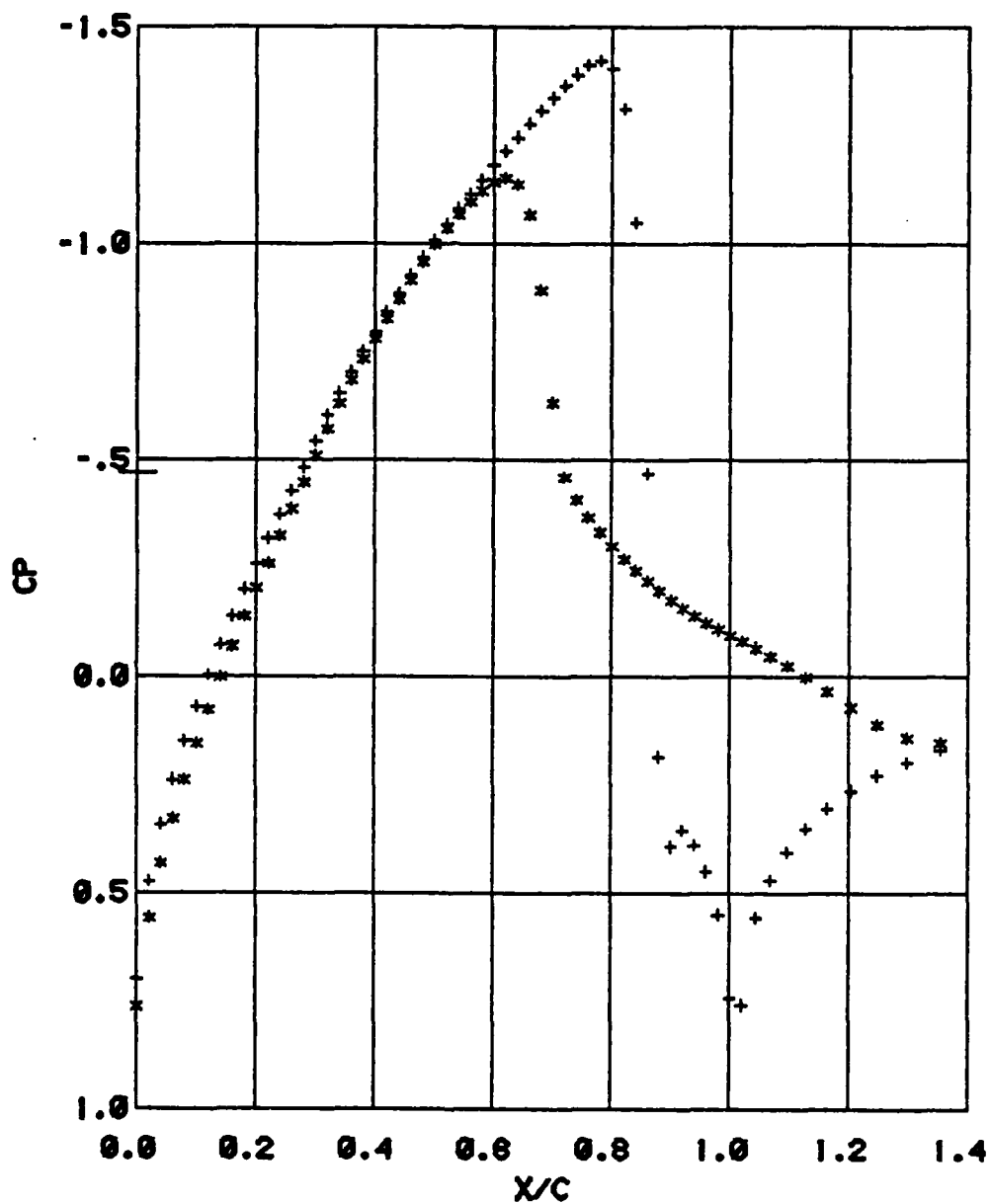
FIG. 8.31   18% THICK CIRCULAR ARC AIRFOIL
PURE INVISCID PRESSURE DISTRIBUTION
AND PRESSURE AFTER COUPLING WITH
EAST'S MODIFIED BOUNDARY LAYER CODE
MINF=.788   RECH=4E06
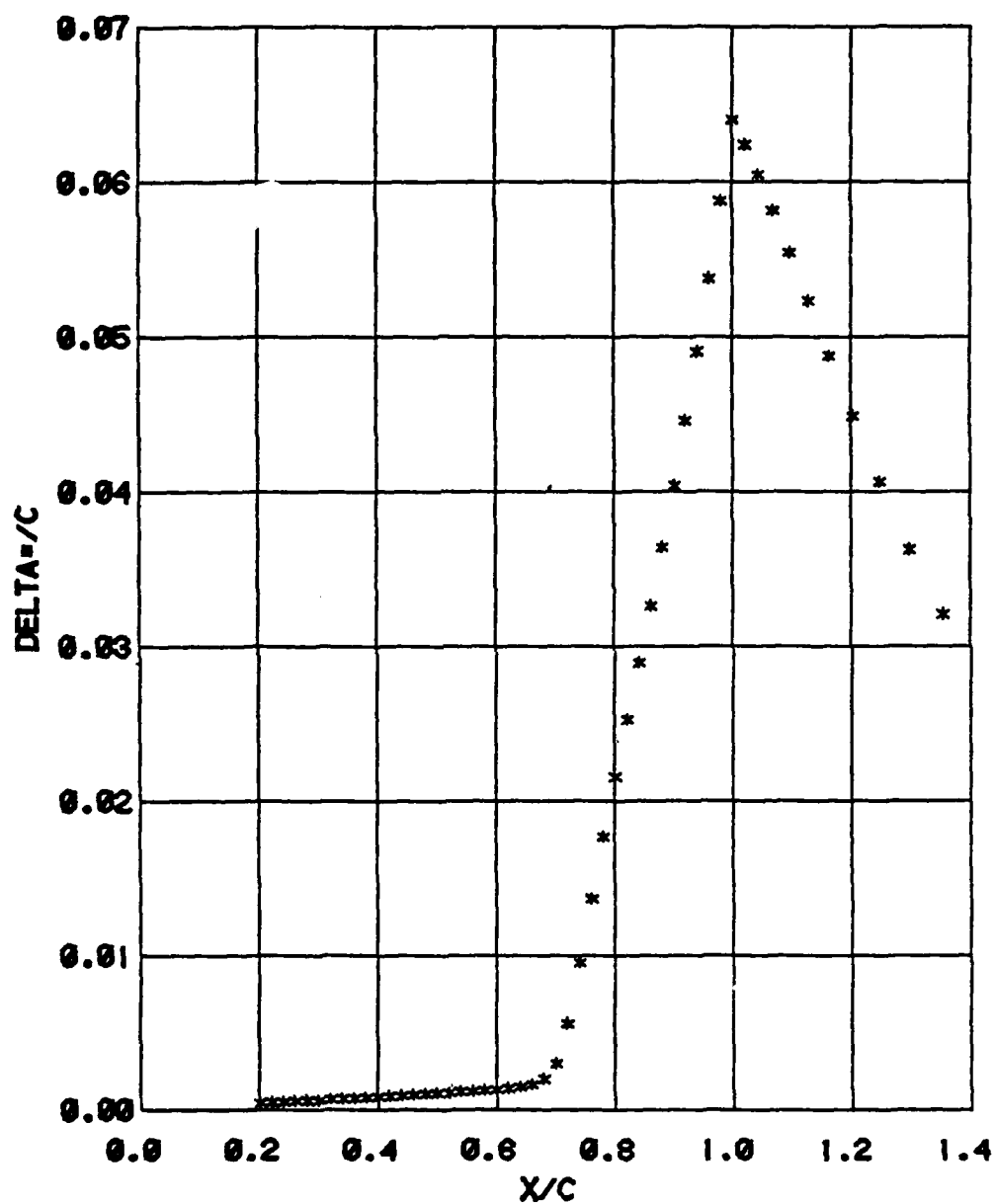
FIG. 8.32   18% THICK CIRCULAR ARC AIRFOIL
DISPLACEMENT THICKNESS USING
MODIFIED BOUNDARY LAYER METHOD
MINF=.788   RECH=4E06
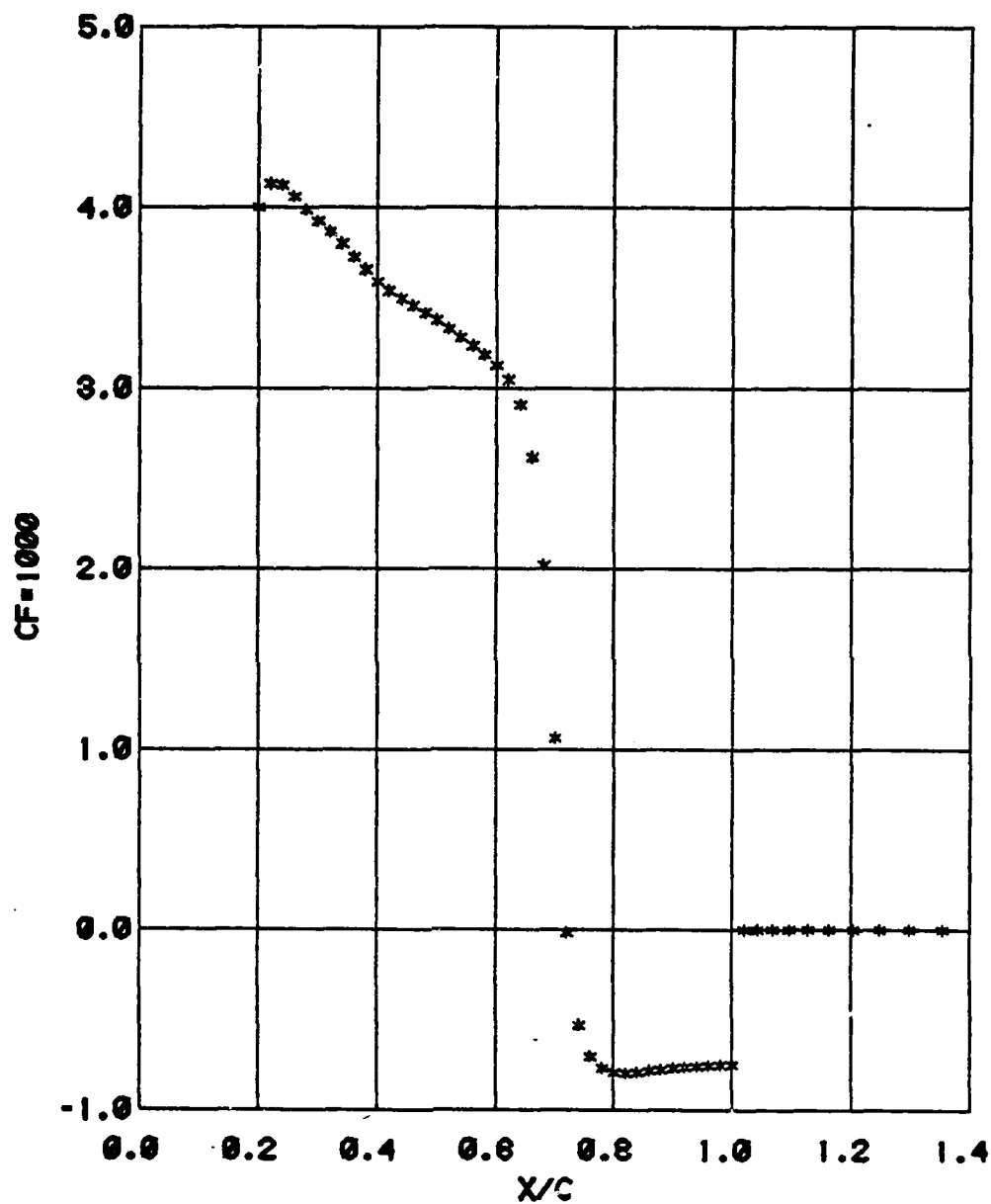
FIG. 8.33 18% THICK CIRCULAR ARC AIRFOIL
SKIN FRICTION COEFFICIENT USING
MODIFIED BOUNDARY LAYER METHOD
MINF=.788   RECH=4E06
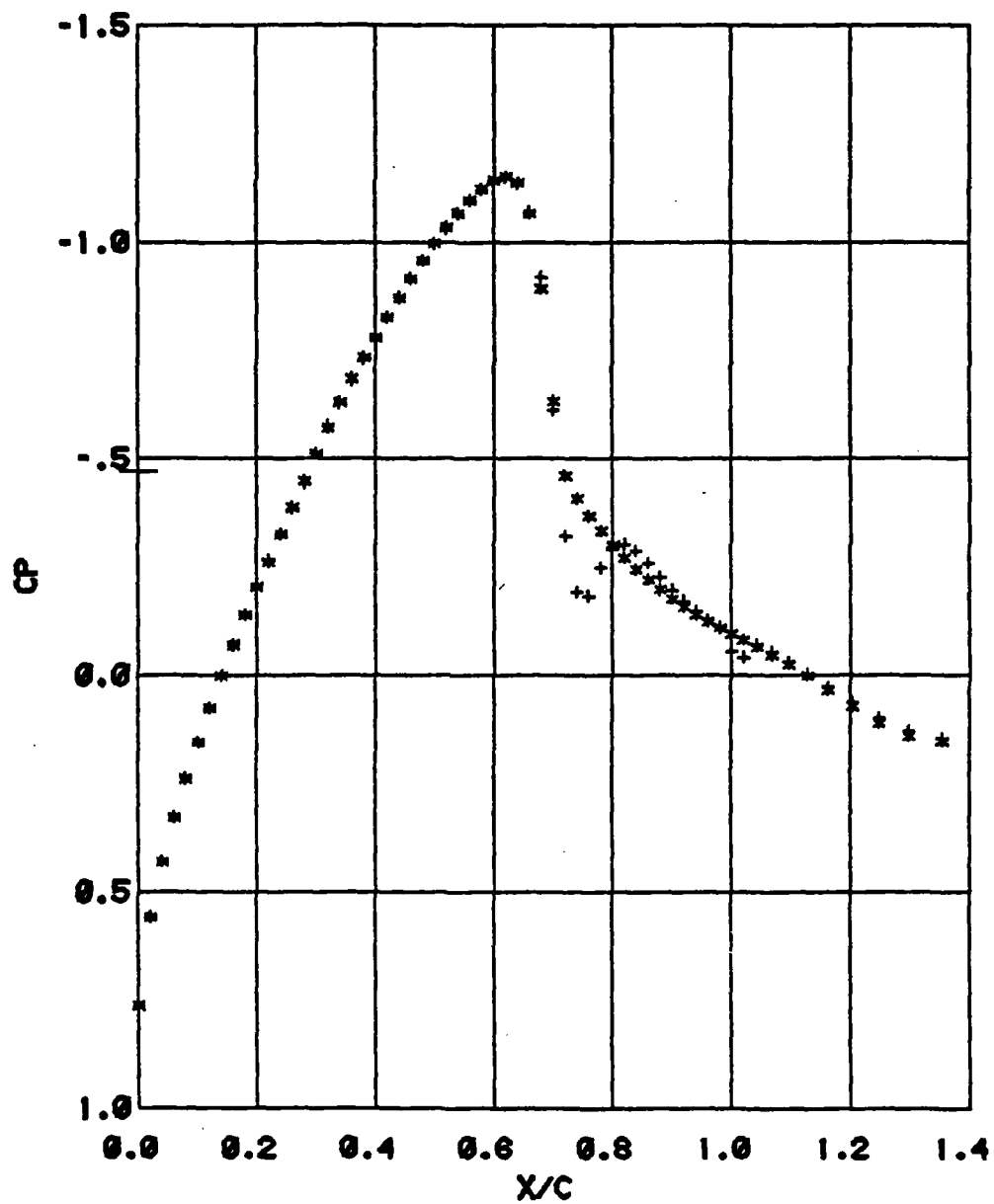
FIG. 8.34   18% THICK CIRCULAR ARC AIRFOIL
VISCOUS AND INVISCID PRESSURE AFTER
COUPLING MODIFIED BOUNDARY LAYER
MINF=.788   RECH=4E06
=VISCOUS   +INVISCID
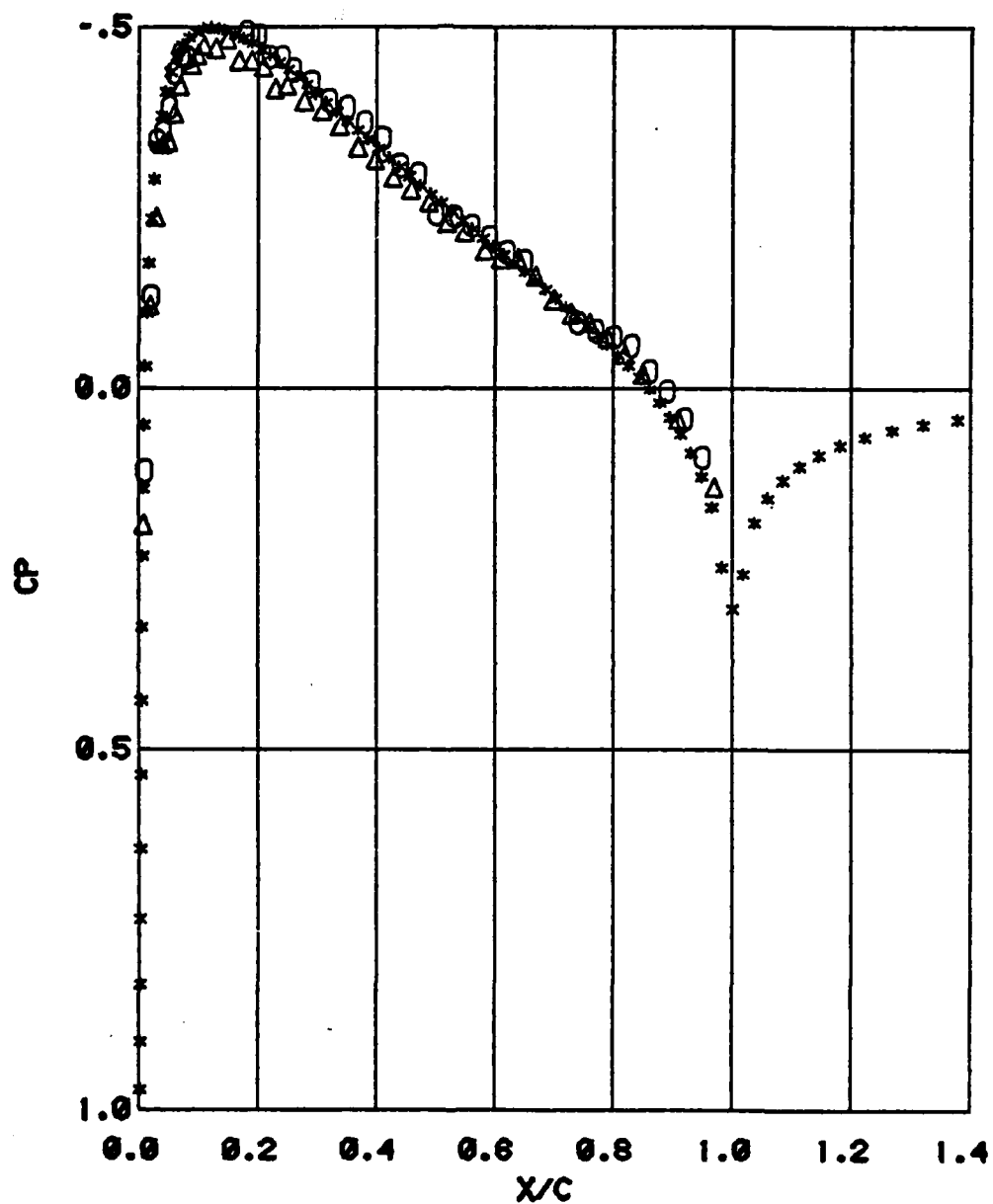
FIG. 9.11 EXPERIMENTAL AND PURE INVISCID PRESSURES
MINF= .490   RECH= 17.5E+06
NACA 0012 AIRFOIL .
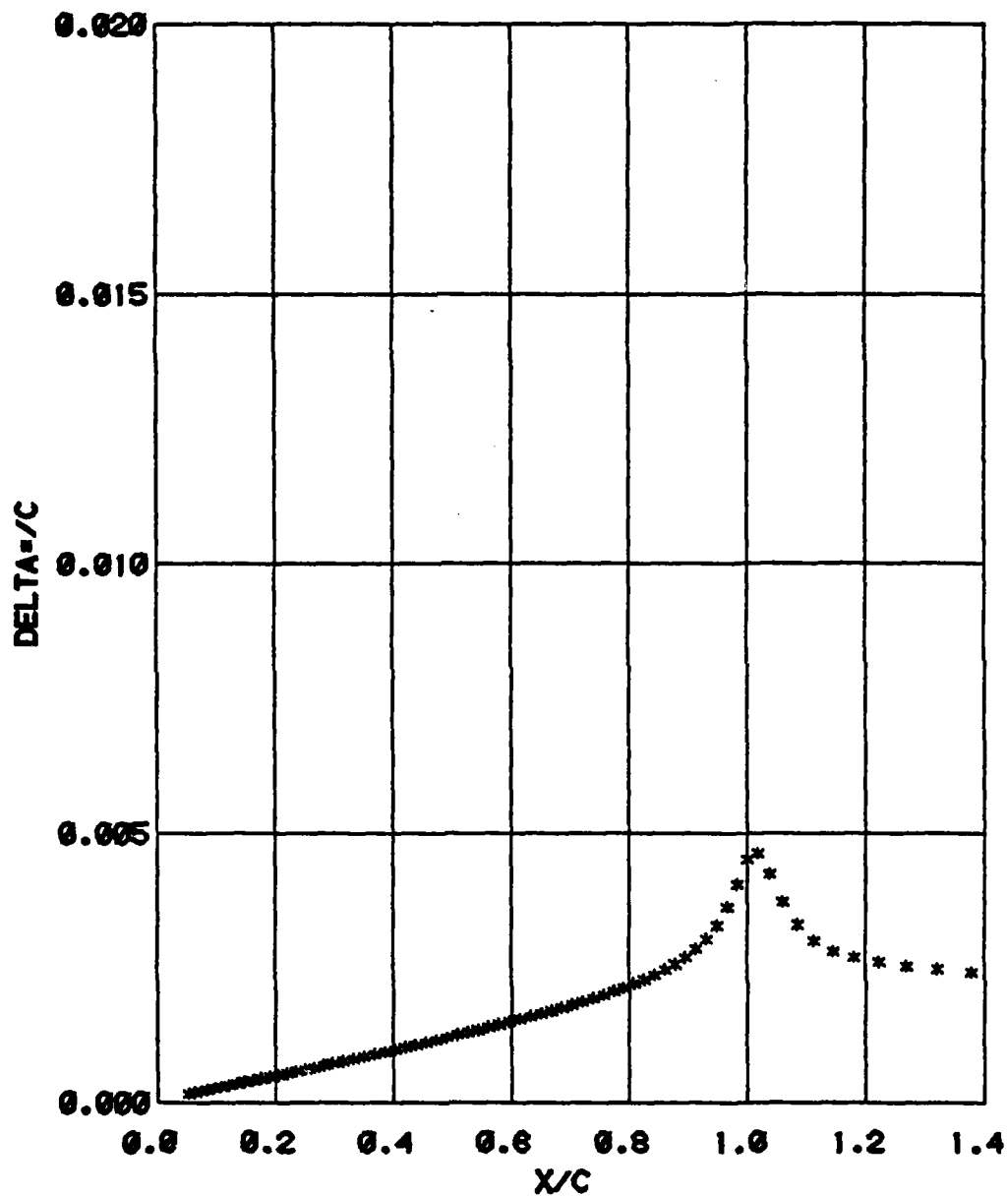
FIG. 9.12 DISPLACEMENT THICKNESS
MINF= .490   RECH= 17.5E+06
NACA 0012 AIRFOIL
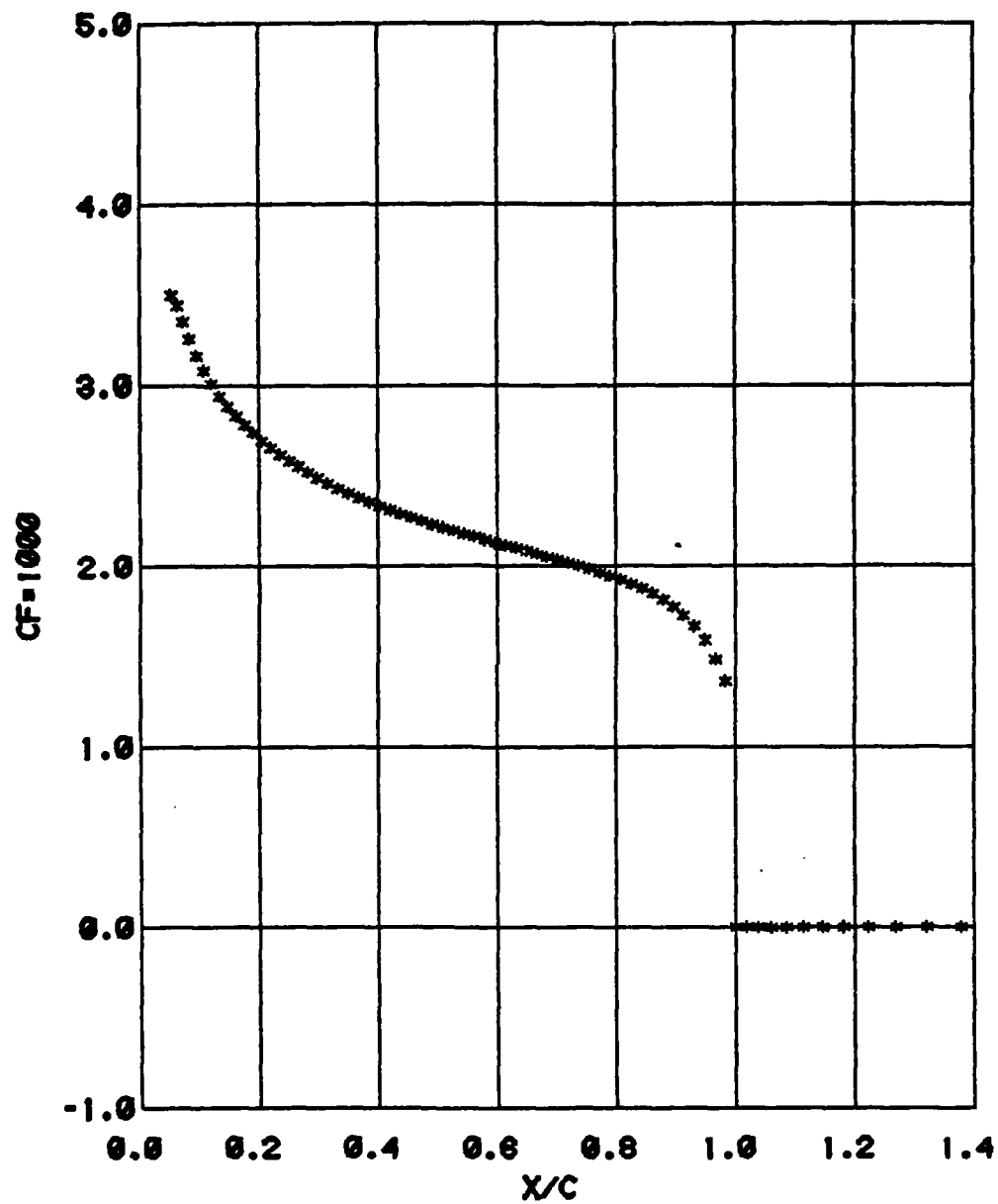
FIG. 9.13 SKIN FRICTION COEFFICIENT
MINF= .490   RECH= 17.5E+06
NACA 0012 AIRFOIL
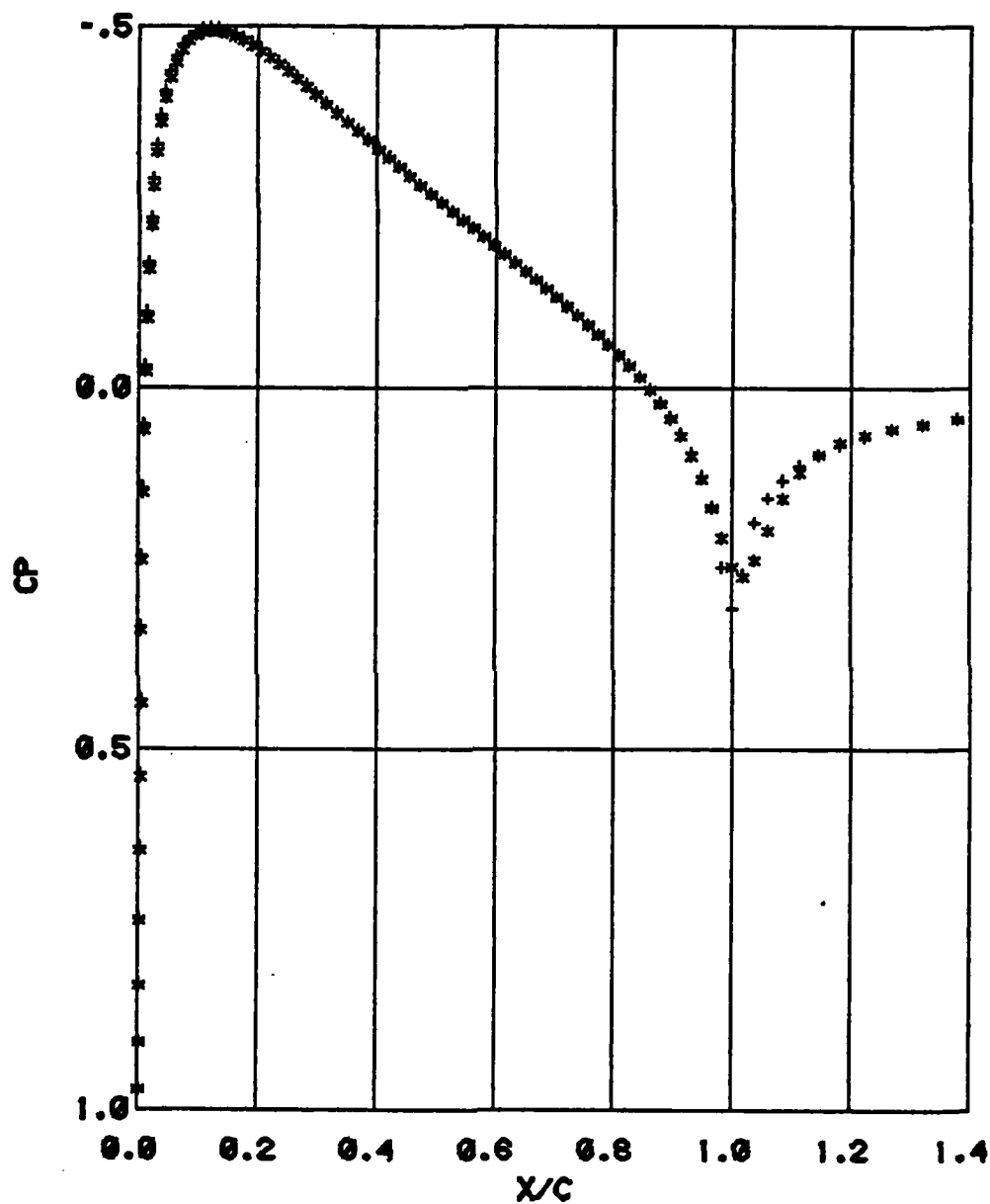
FIG. 9.14 PURE INVISCID PRESSURE
AND PRESSURE AFTER COUPLING
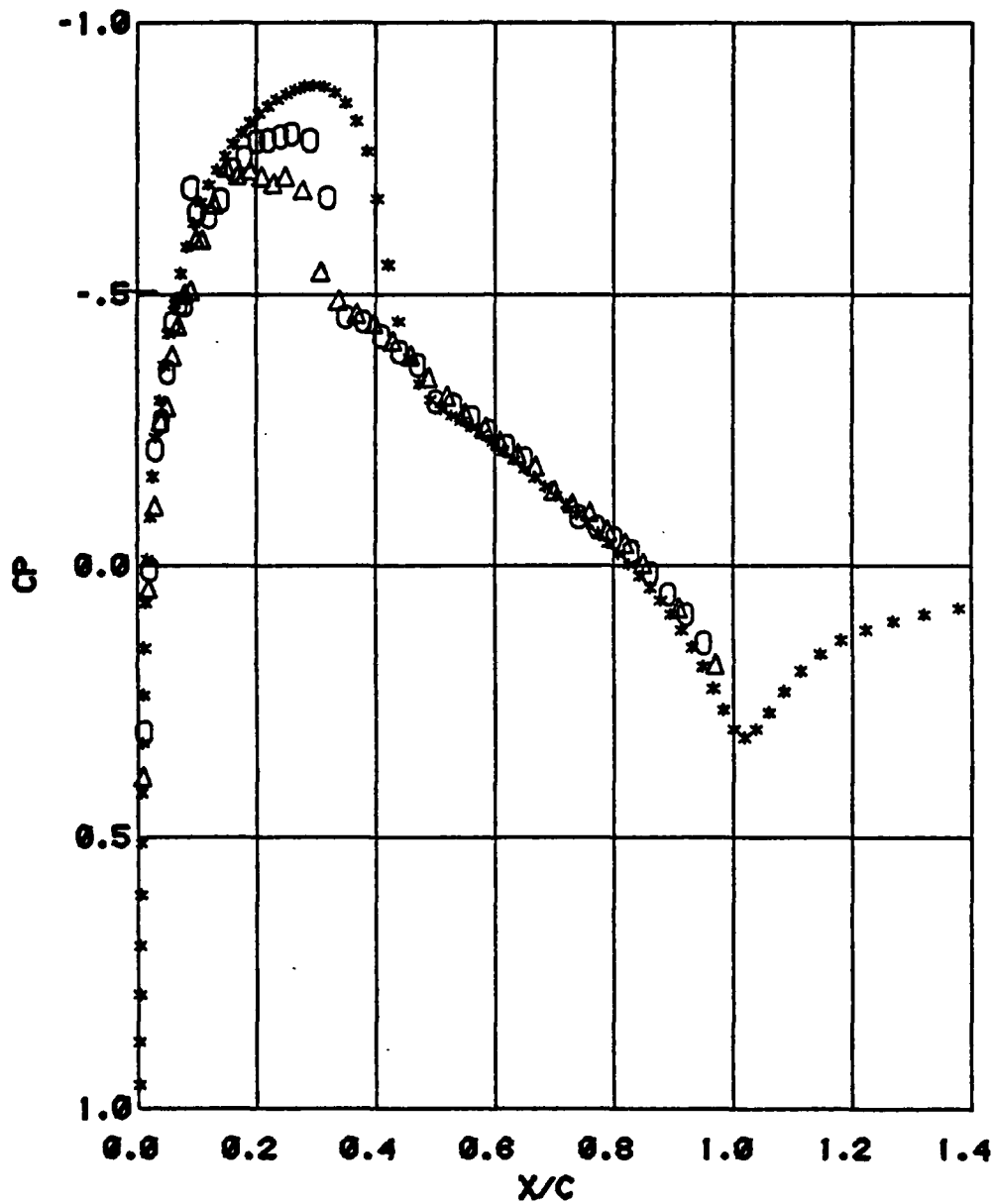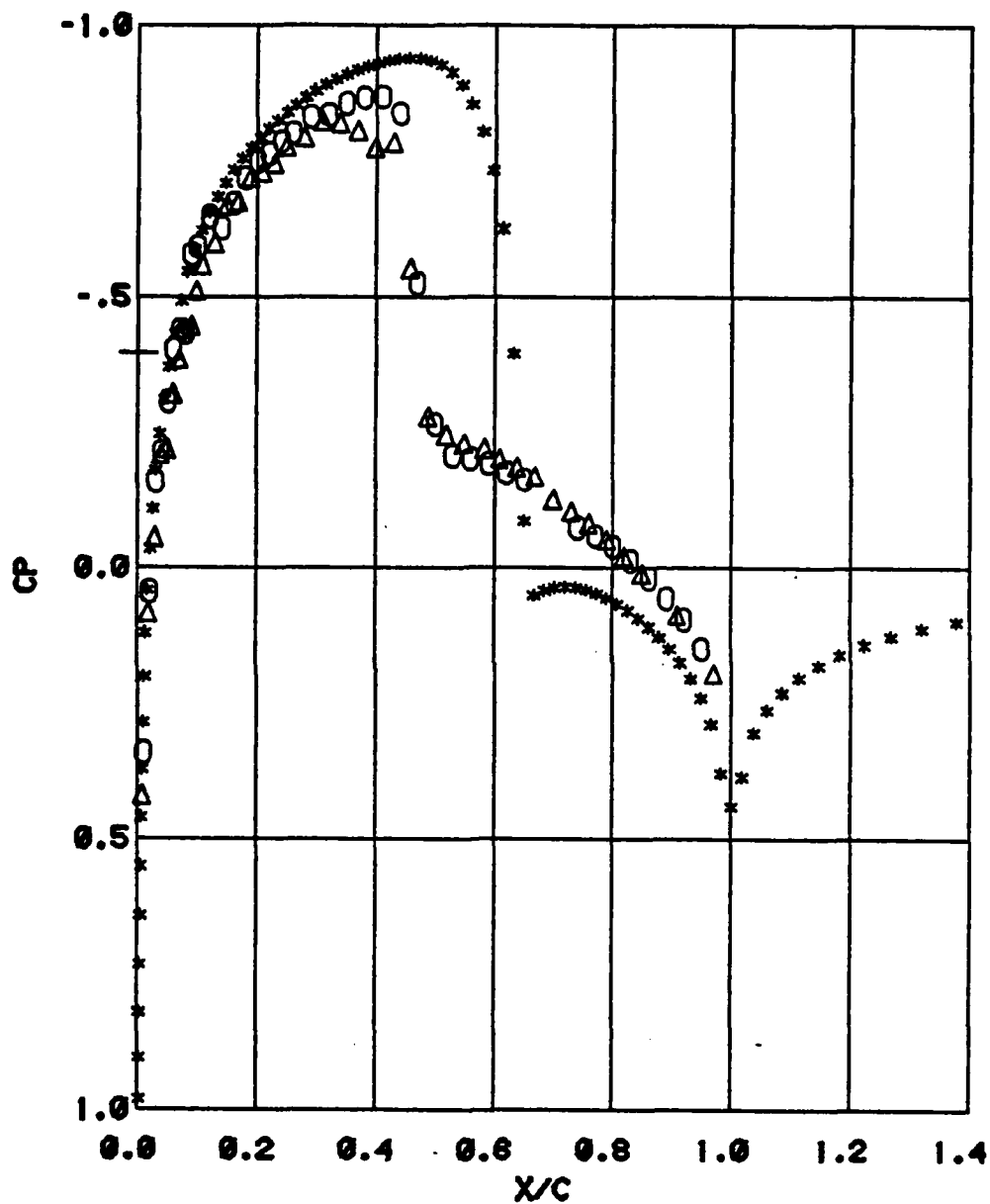MINF= .490   RECH= 17.5E+06
NACA 0012 AIRFOIL
■COUPLED   +INVISCID
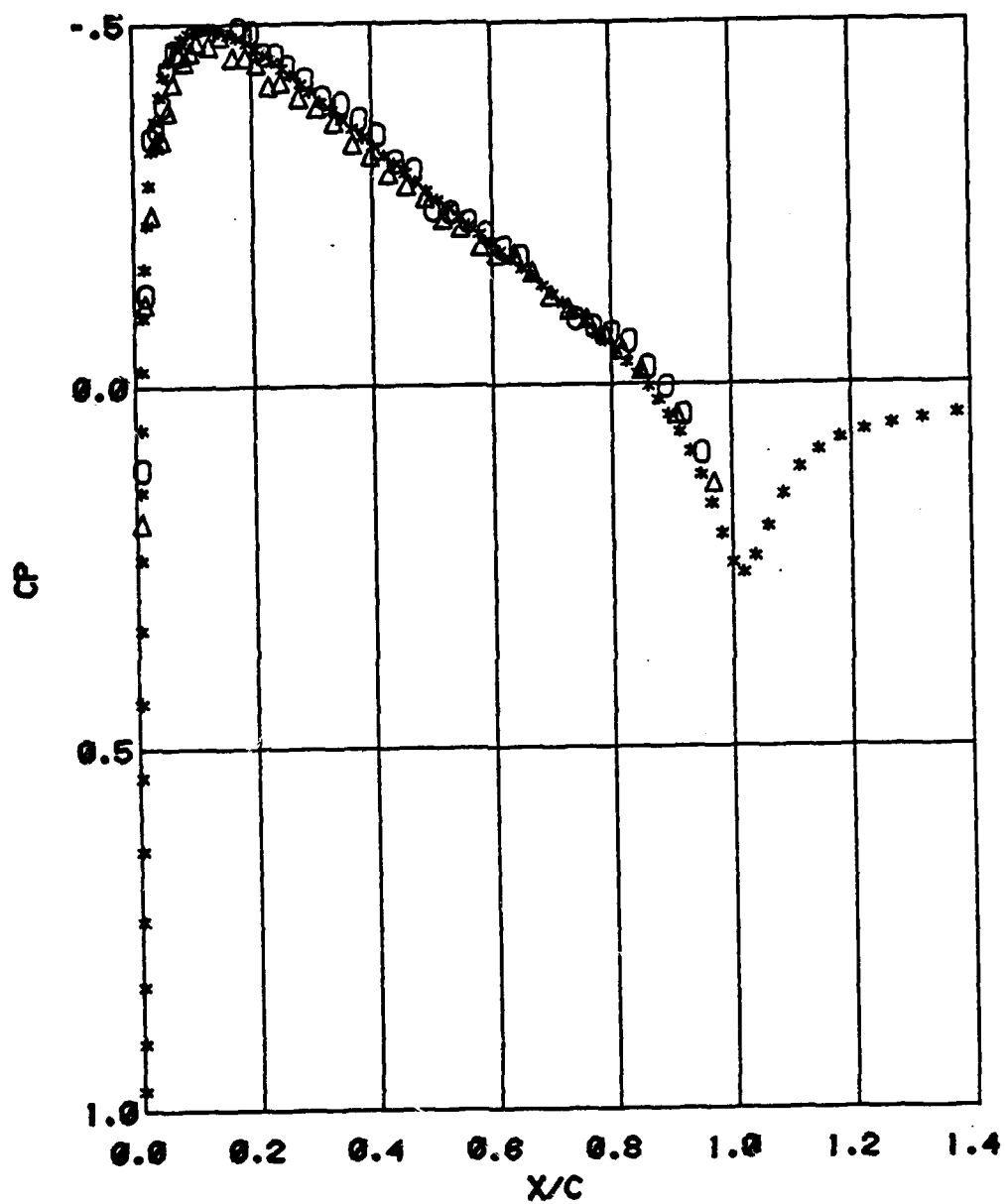
FIG. 9.15 EXPERIMENTAL AND COUPLED PRESSURES
MINF= .490   RECH= 17.5E+06
NACA 0012 AIRFOIL
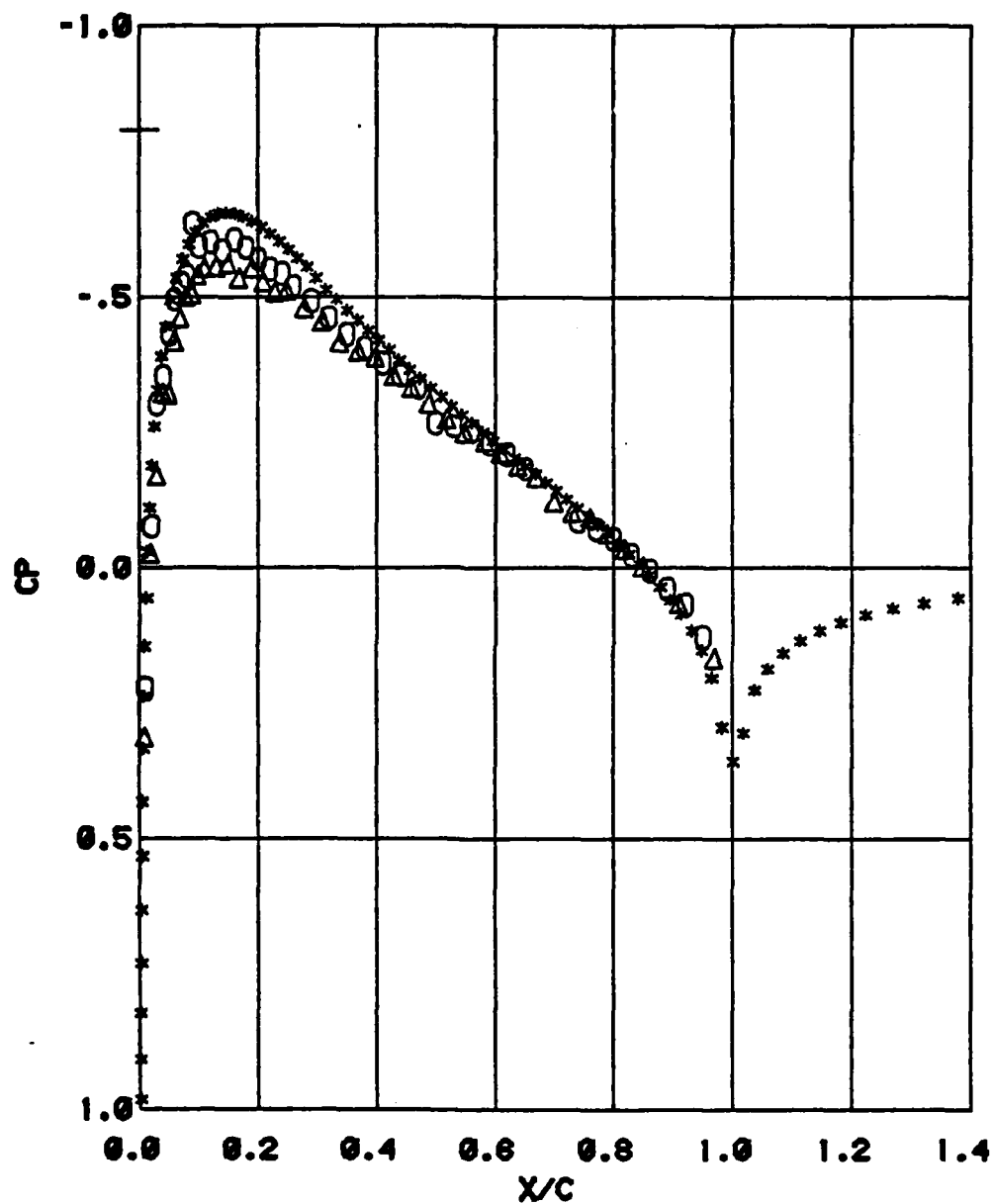
FIG. 9.21 EXPERIMENTAL AND PURE INVISCID PRESSURES
MINF= .693 RECH= 22.2E+06
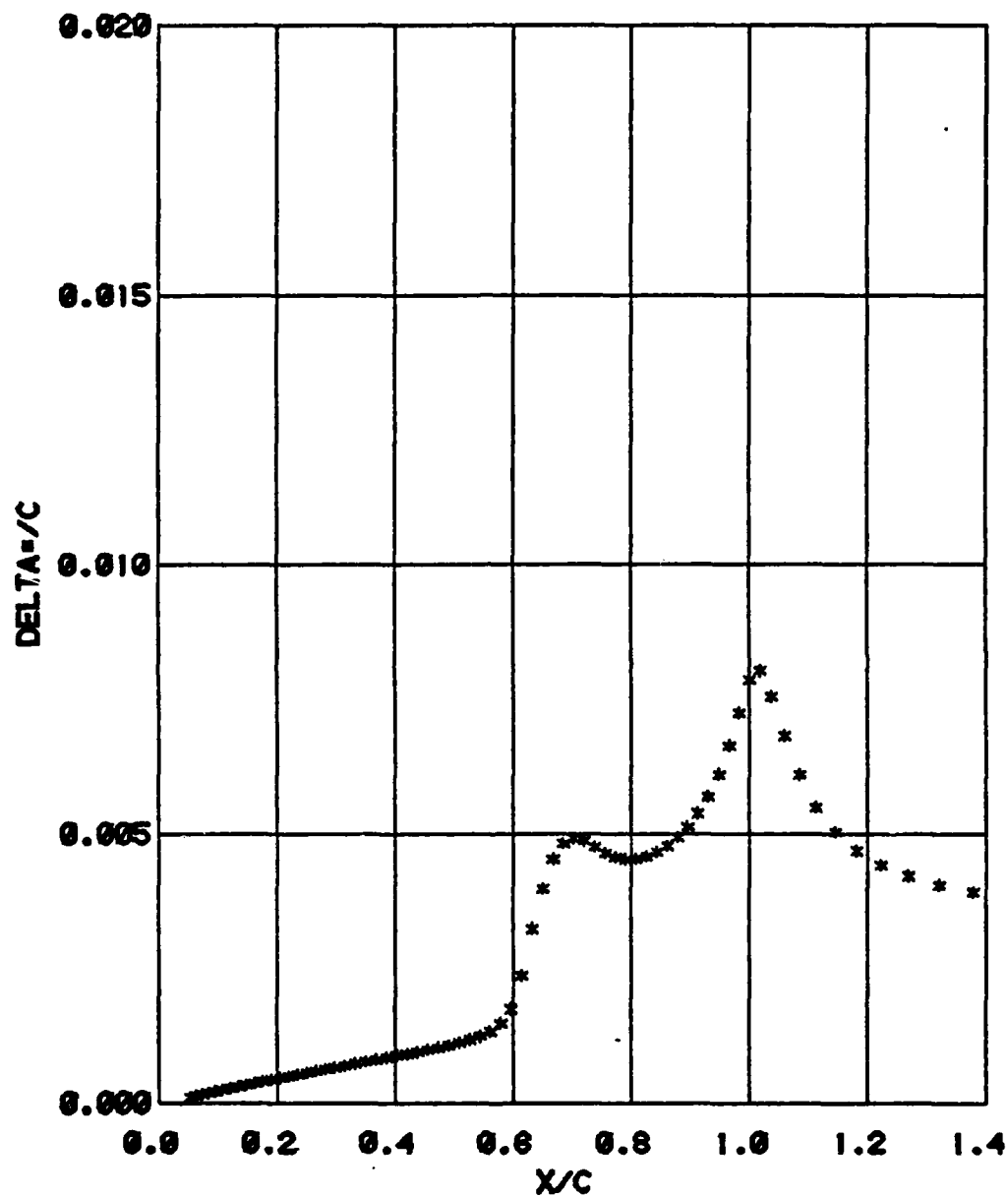NACA 0012 AIRFOIL
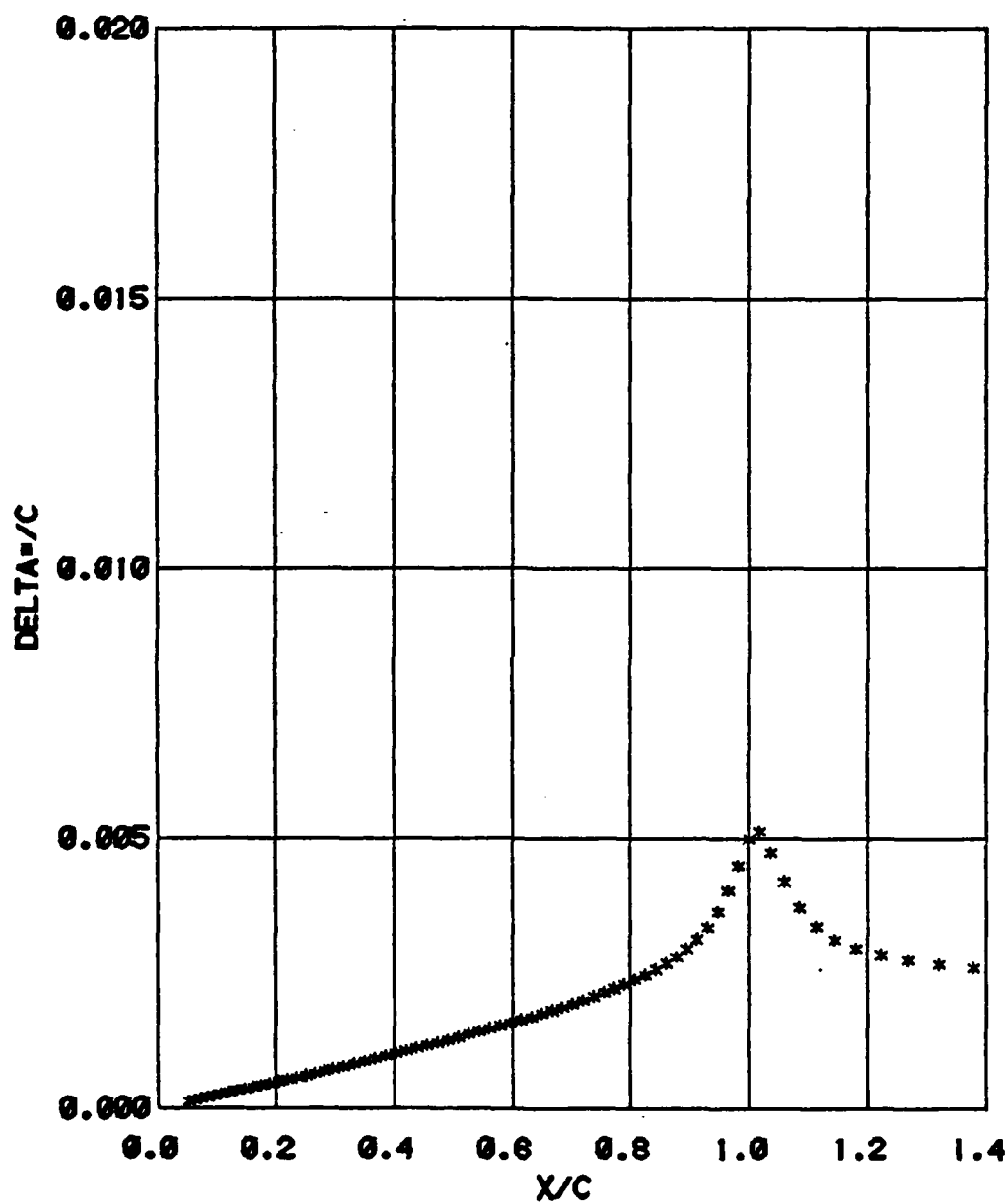
FIG. 9.22 DISPLACEMENT THICKNESS
MINF= .693   RECH= 22.2E+06
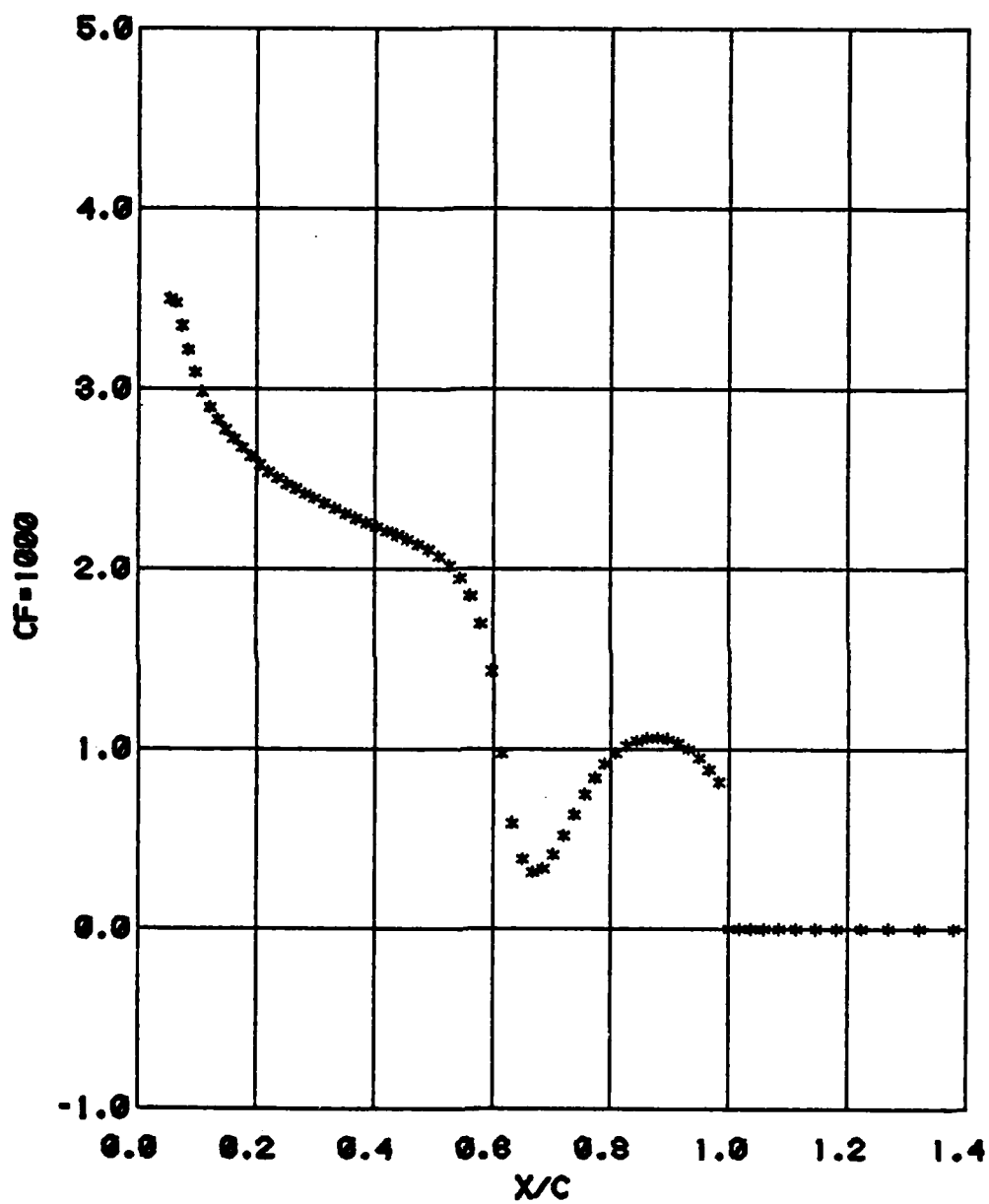NACA 0012 AIRFOIL
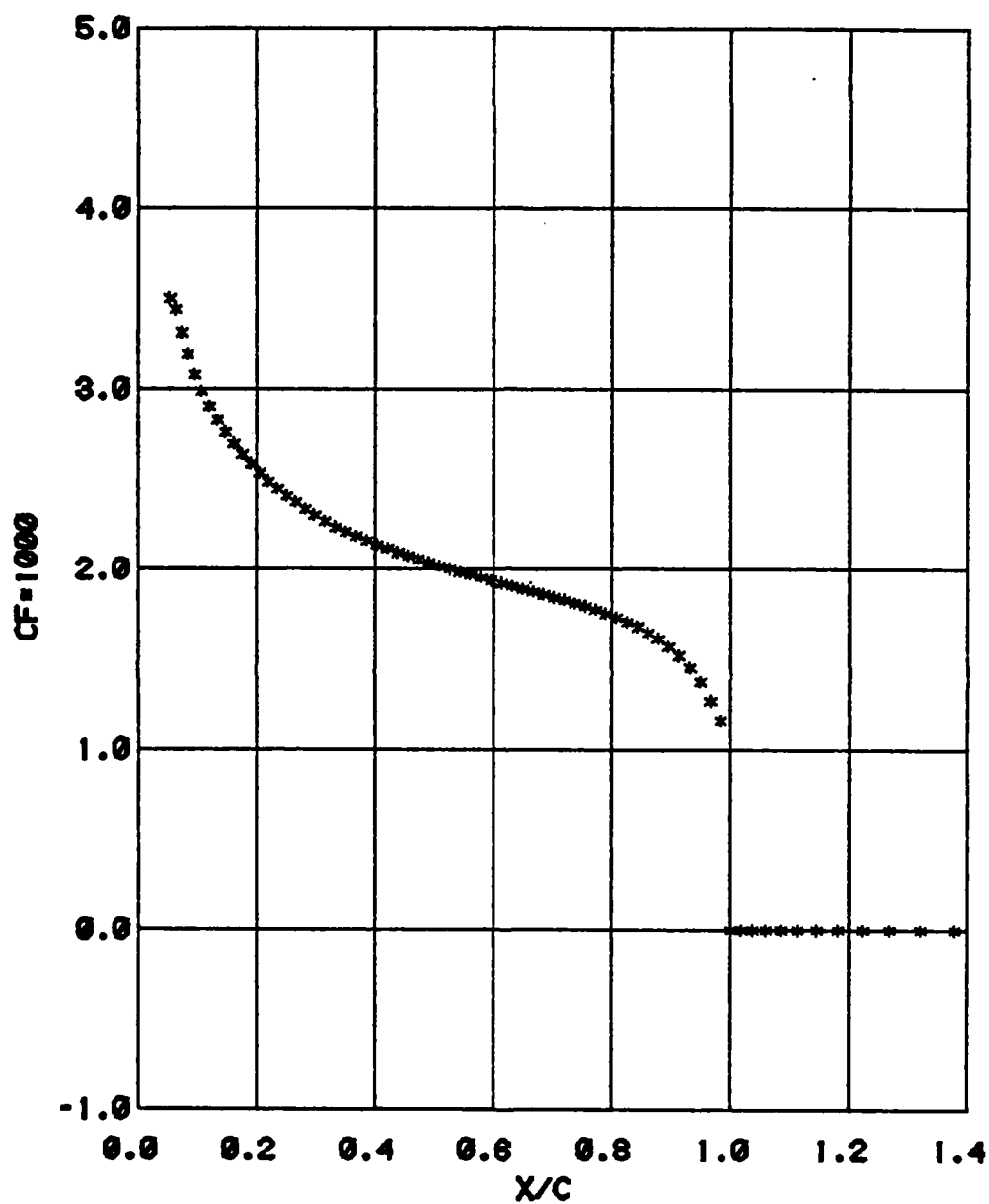
FIG. 9.23   SKIN FRICTION COEFFICIENT
            MINF= .693   RECH= 22.2E+06
            NACA 0012 AIRFOIL
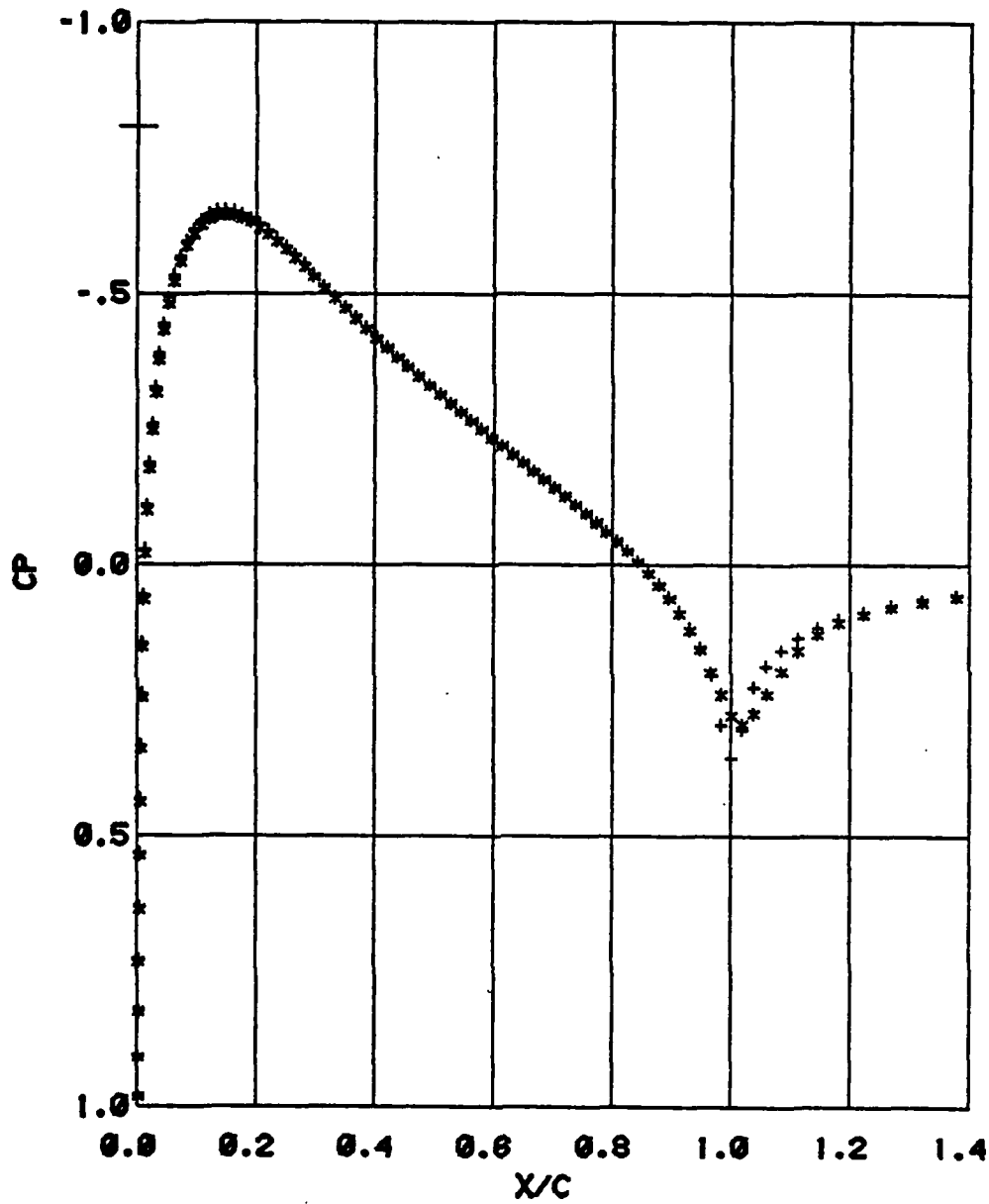
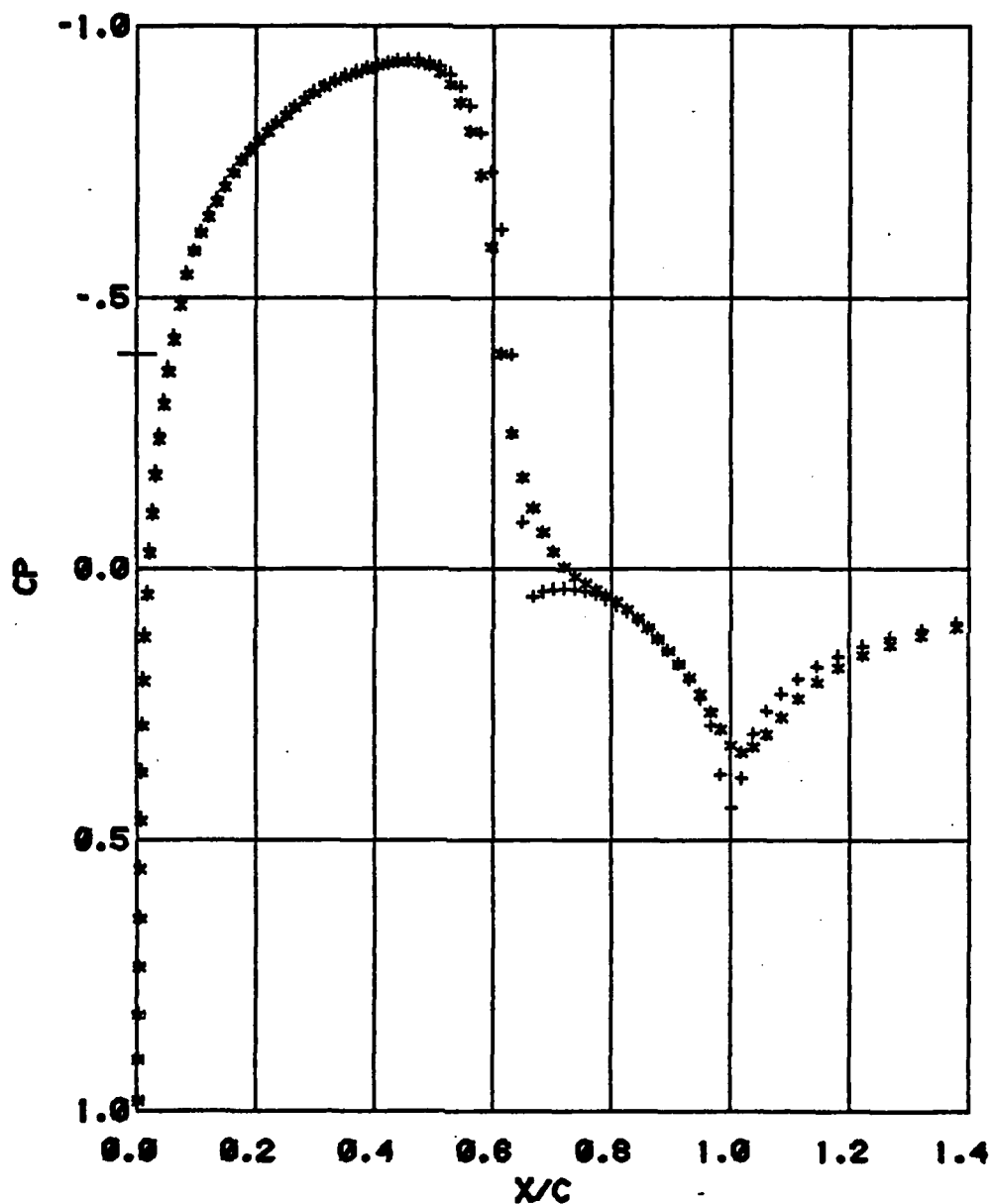FIG. 9.24   PURE INVISCID PRESSURE
AND PRESSURE AFTER COUPLING
MINF= .693   RECH= 22.2E+06
NACA 0012 AIRFOIL
▪COUPLED   •INVISCID
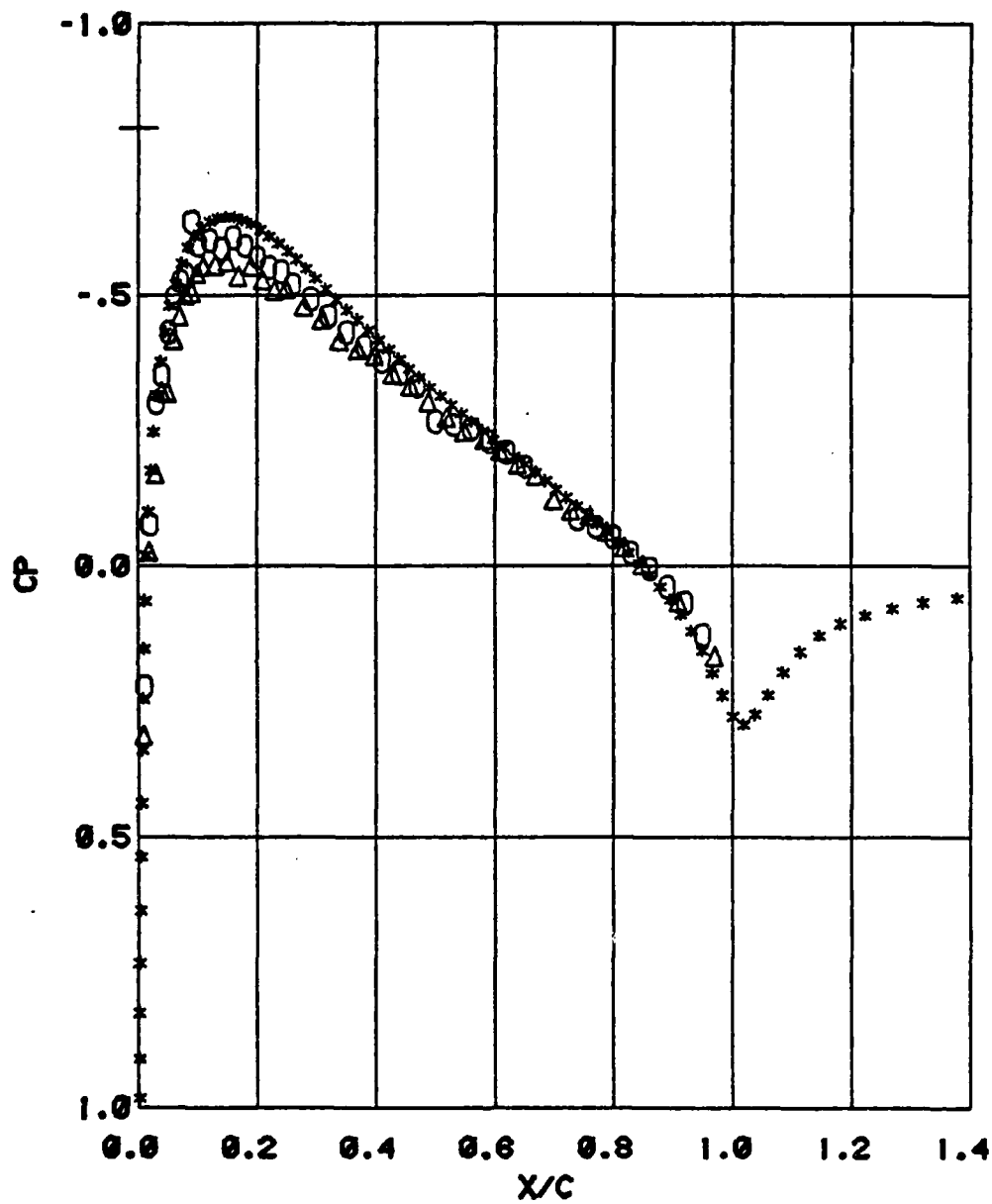
FIG. 9.25 EXPERIMENTAL AND COUPLED PRESSURES
MINF= .693   RECH= 22.2E+06
NACA 0012 AIRFOIL
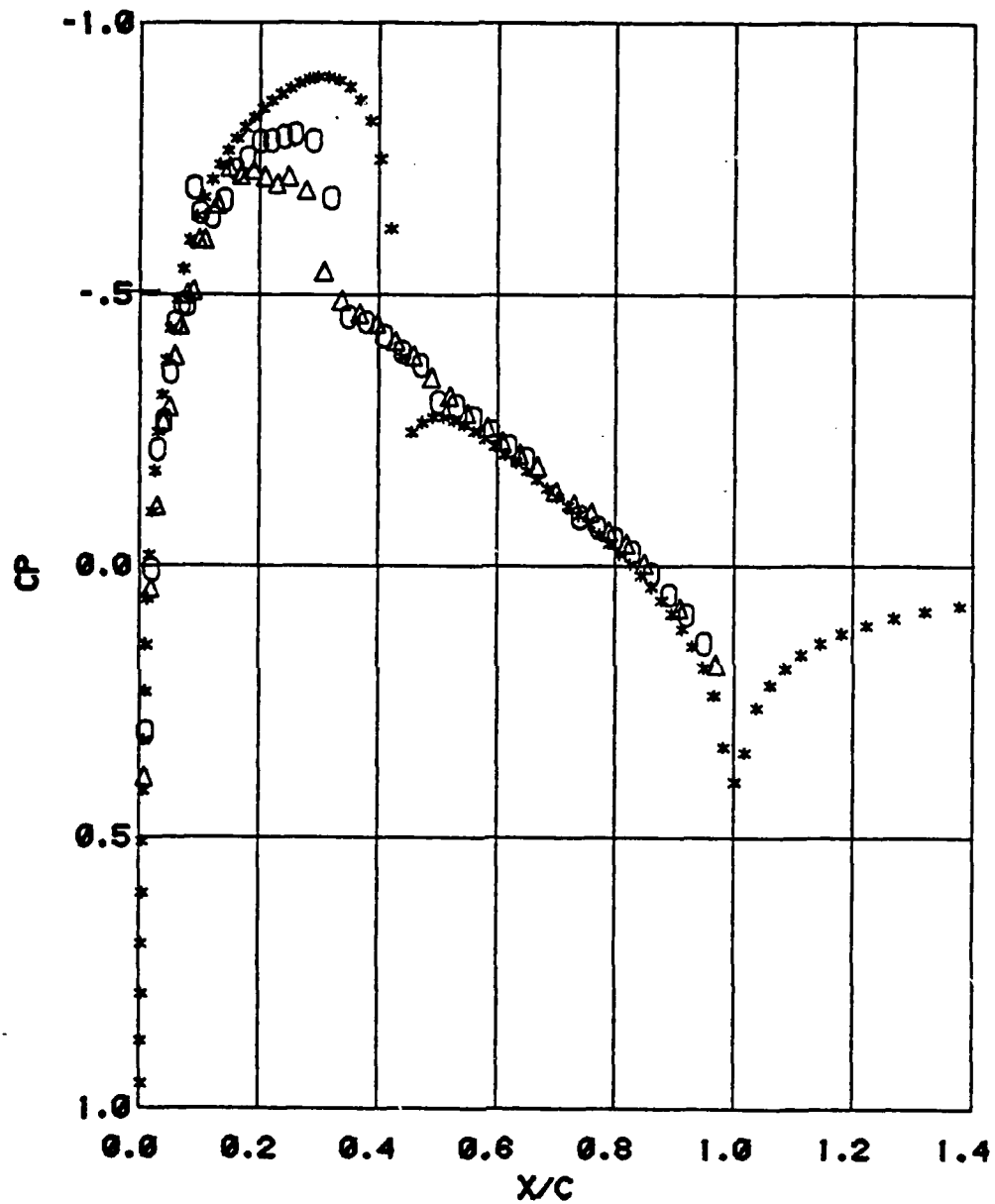
FIG. 9.31 EXPERIMENTAL AND PURE INVISCID PRESSURES
MINF= .776   RECH=   23.7E+06
NACA 0012 AIRFOIL
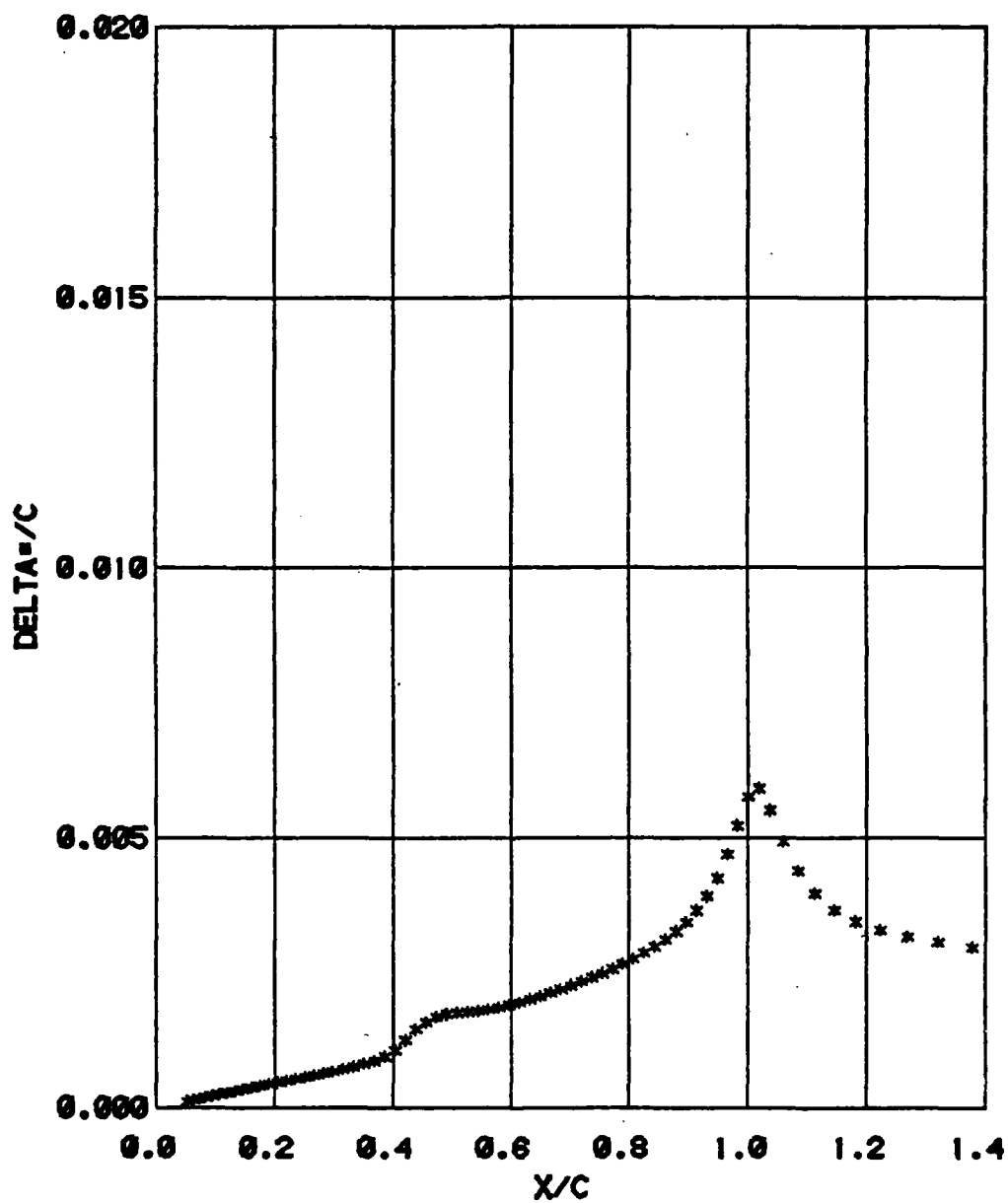
FIG. 9.32 DISPLACEMENT THICKNESS
MINF= .776   RECH= 23.7E+06
NACA 0012 AIRFOIL
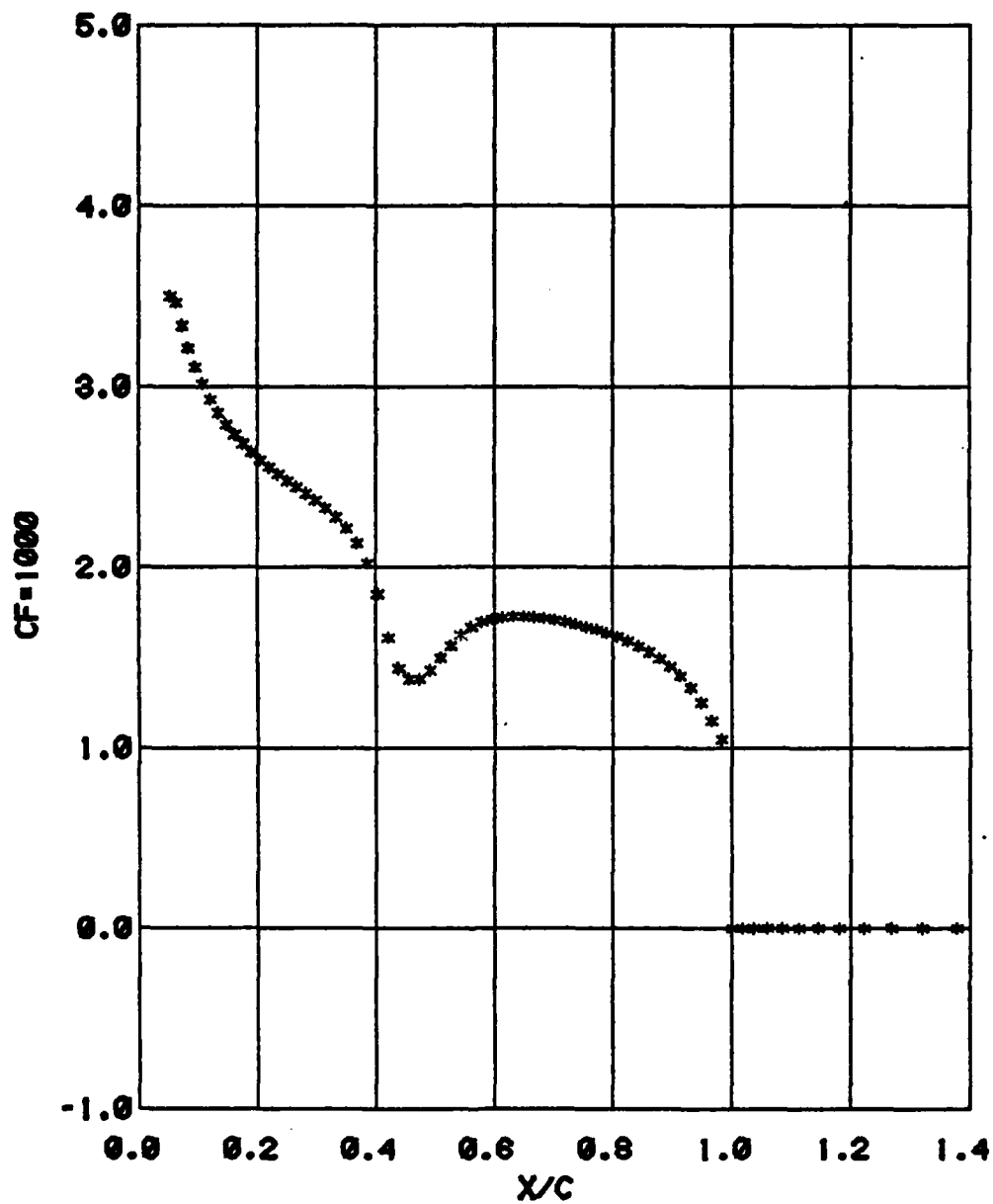
FIG. 9.33 SKIN FRICTION COEFFICIENT
MINF= .776   RECH= 23.7E+06
NACA 0012 AIRFOIL
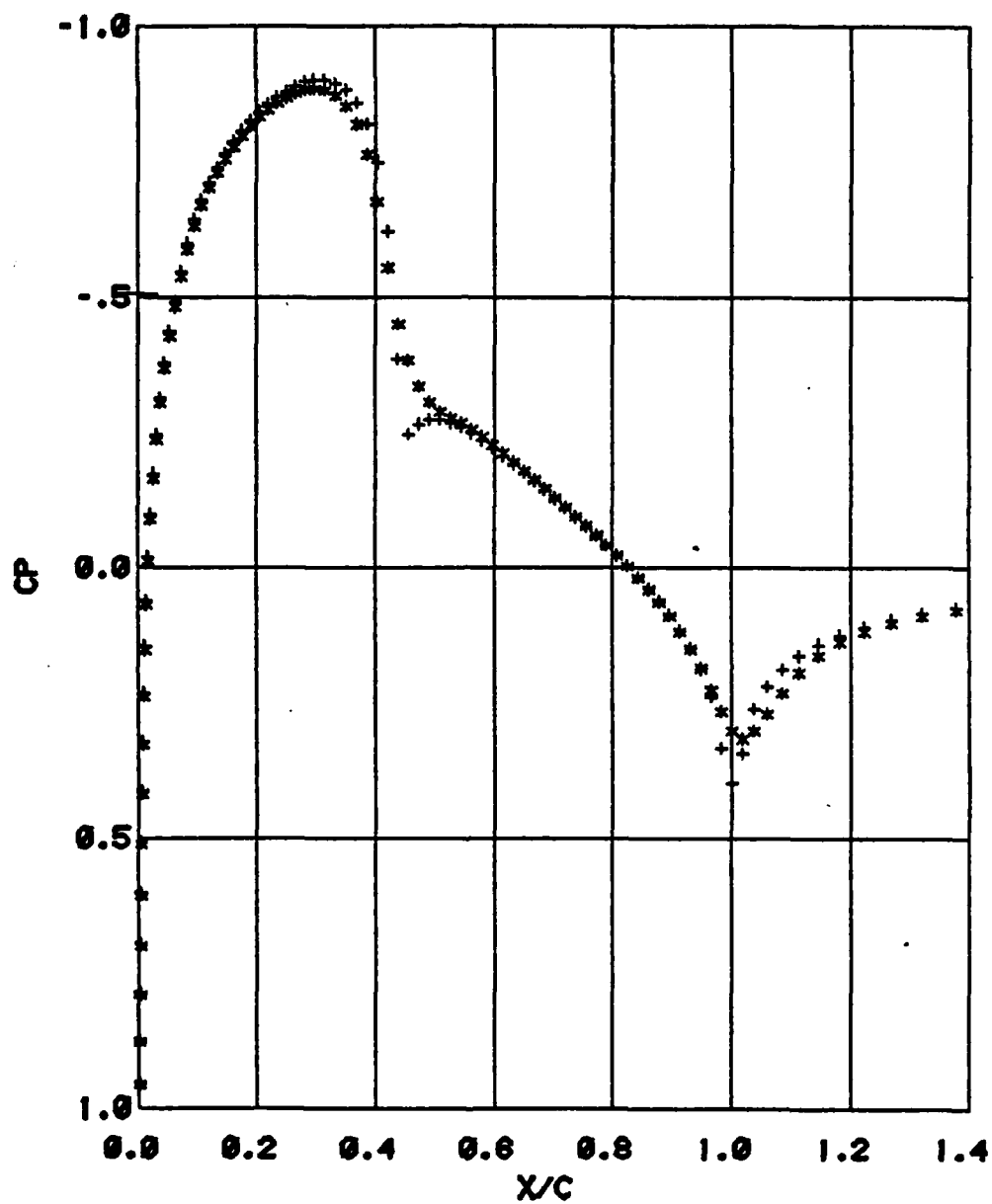
FIG. 9.34 PURE INVISCID PRESSURE
AND PRESSURE AFTER COUPLING
MINF= .776   RECH= 23.7E+06
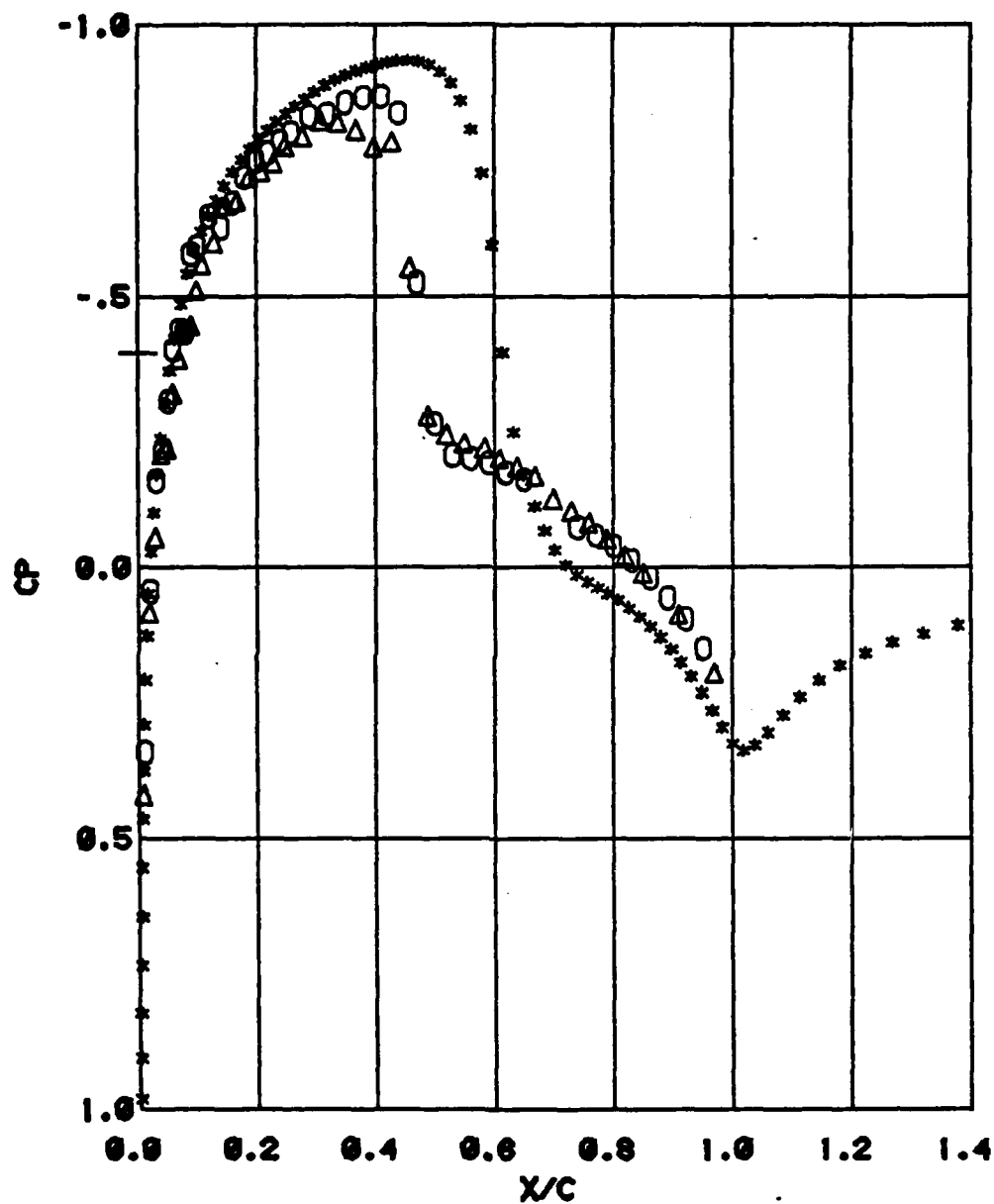NACA 0012 AIRFOIL
=COUPLED   •INVISCID

FIG. 9.35 EXPERIMENTAL AND COUPLED PRESSURES
MINF= .776 RECH= 23.7E+06
NACA 0012 AIRFOIL
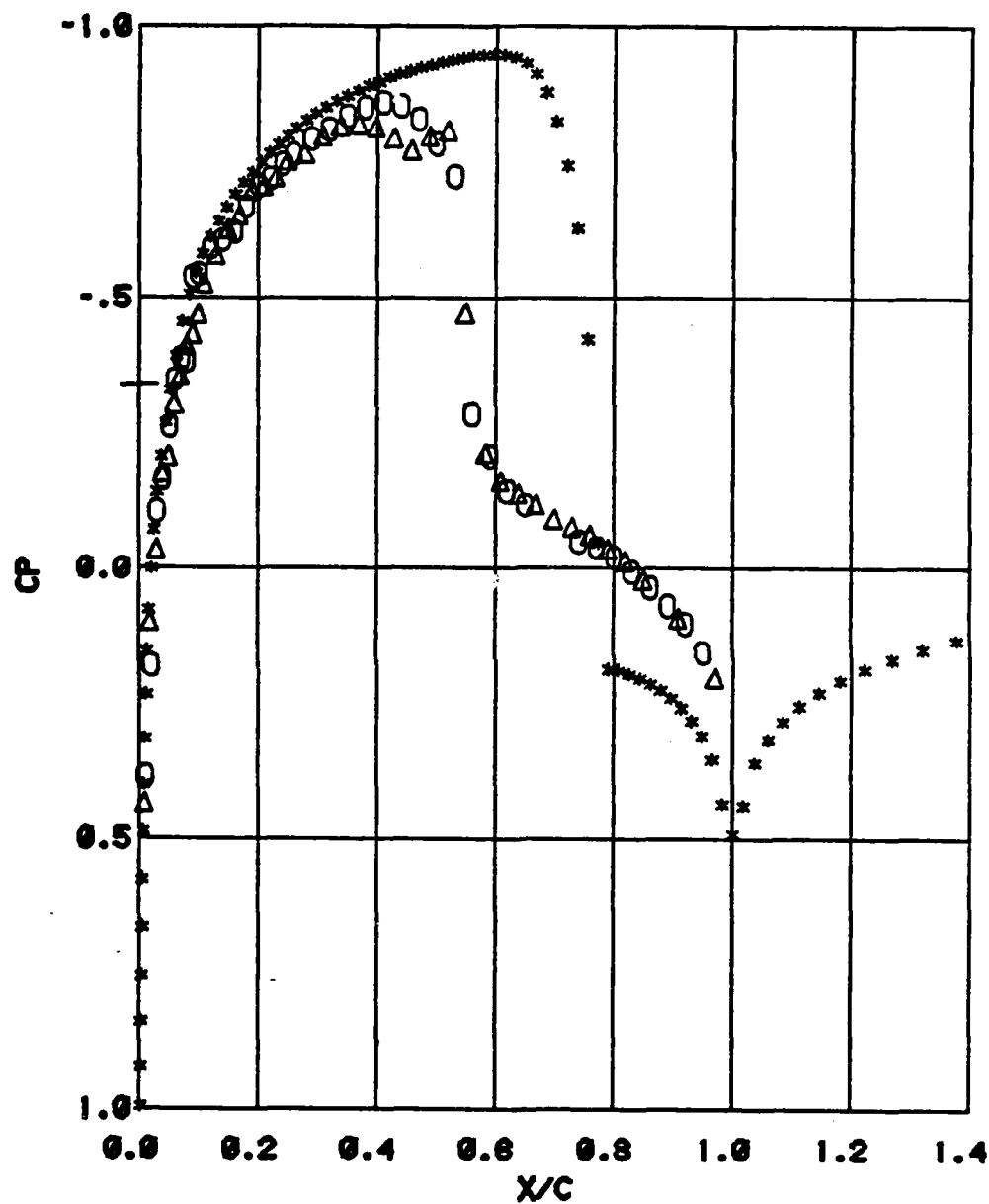
FIG. 9.41 EXPERIMENTAL AND PURE INVISCID PRESSURES
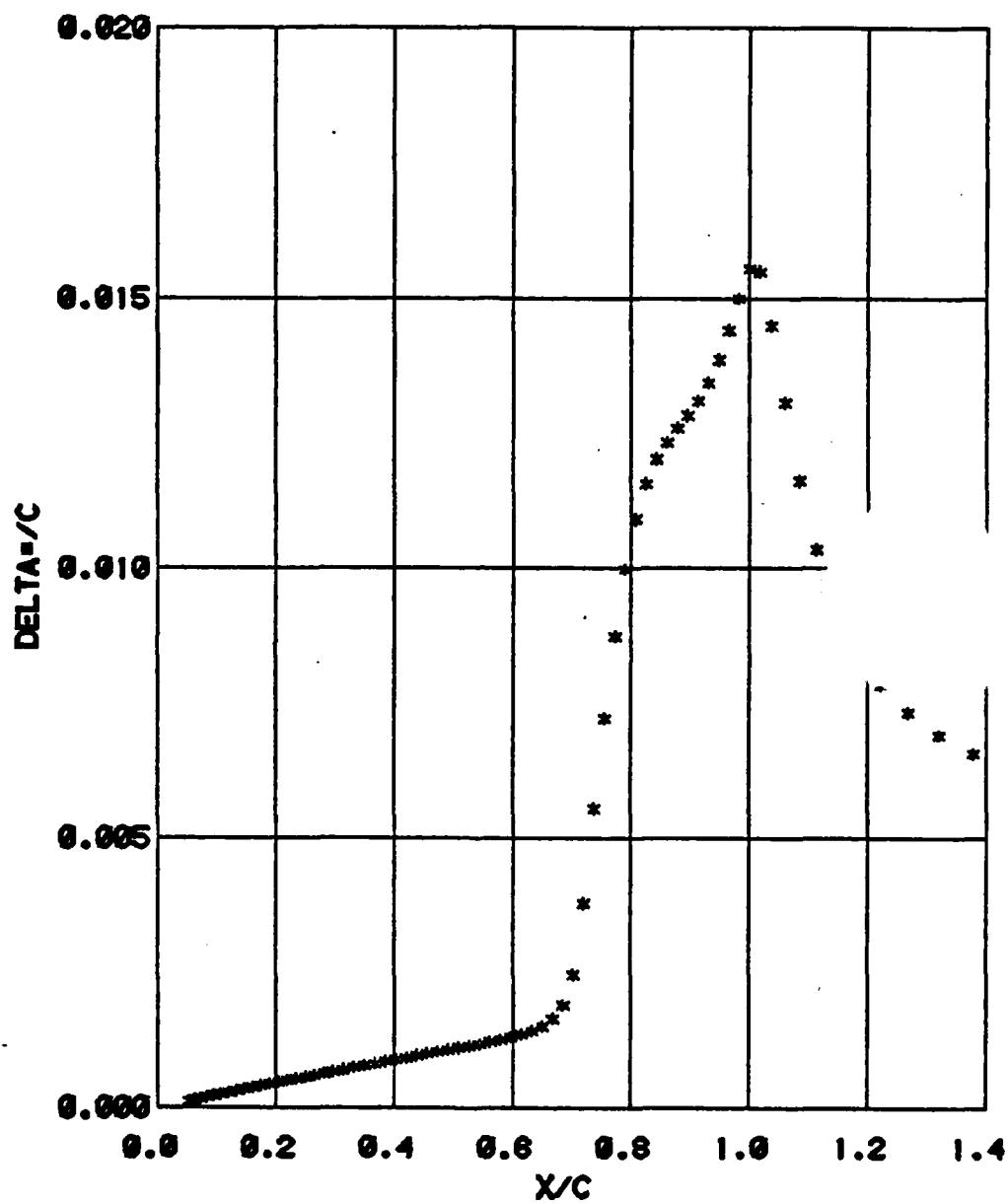MINF= .814   RECH= 24.7E+06
NACA 0012 AIRFOIL

FIG. 9.42 DISPLACEMENT THICKNESS
MINF= .814 RECH= 24.7E+06
NACA 0012 AIRFOIL
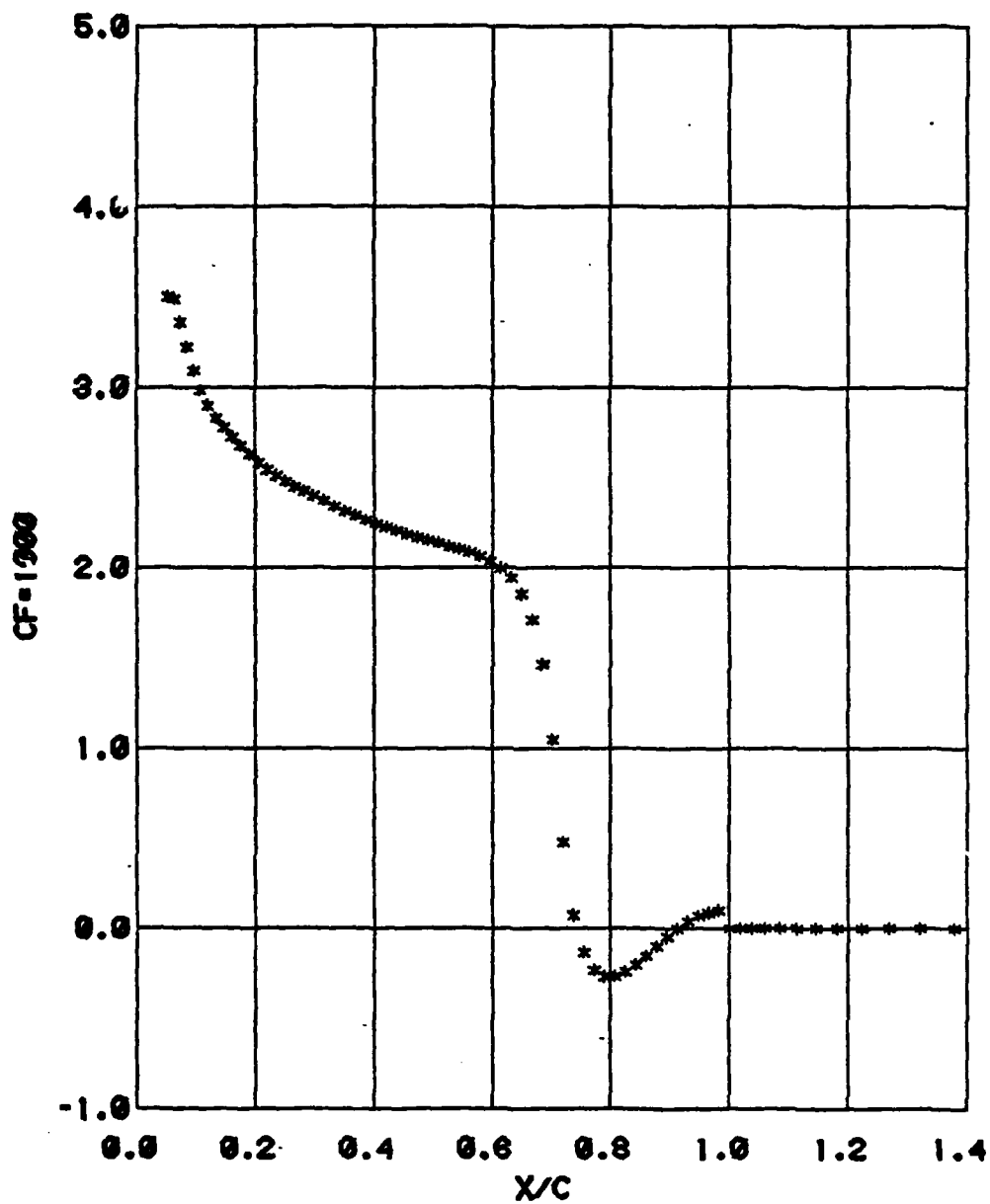
FIG. 9.43   SKIN FRICTION COEFFICIENT
MINF= .814   RECH= 24.7E+06
NACA 0012 AIRFOIL

FIG. 9.44   PURE INVISCID PRESSURE
AND PRESSURE AFTER COUPLING
MINF= .814   RECH= 24.7E+06
NACA 0012 AIRFOIL
=COUPLED   +INVISCID

FIG. 9.45   EXPERIMENTAL AND COUPLED PRESSURES
MINF= .814   RECH= 24.7E+06
NACA 0012 AIRFOIL

FIG. 9.51   EXPERIMENTAL AND PURE INVISCID PRESSURES
MINF= .835   RECH=   24.7E+06
NACA 0012 AIRFOIL

FIG. 9.52 DISPLACEMENT THICKNESS
MINF= .835   RECH= 24.7E+06
NACA 0012 AIRFOIL

FIG. 9.53 SKIN FRICTION COEFFICIENT
MINF= .835   RECH= 24.7E+06
NACA 0012 AIRFOIL
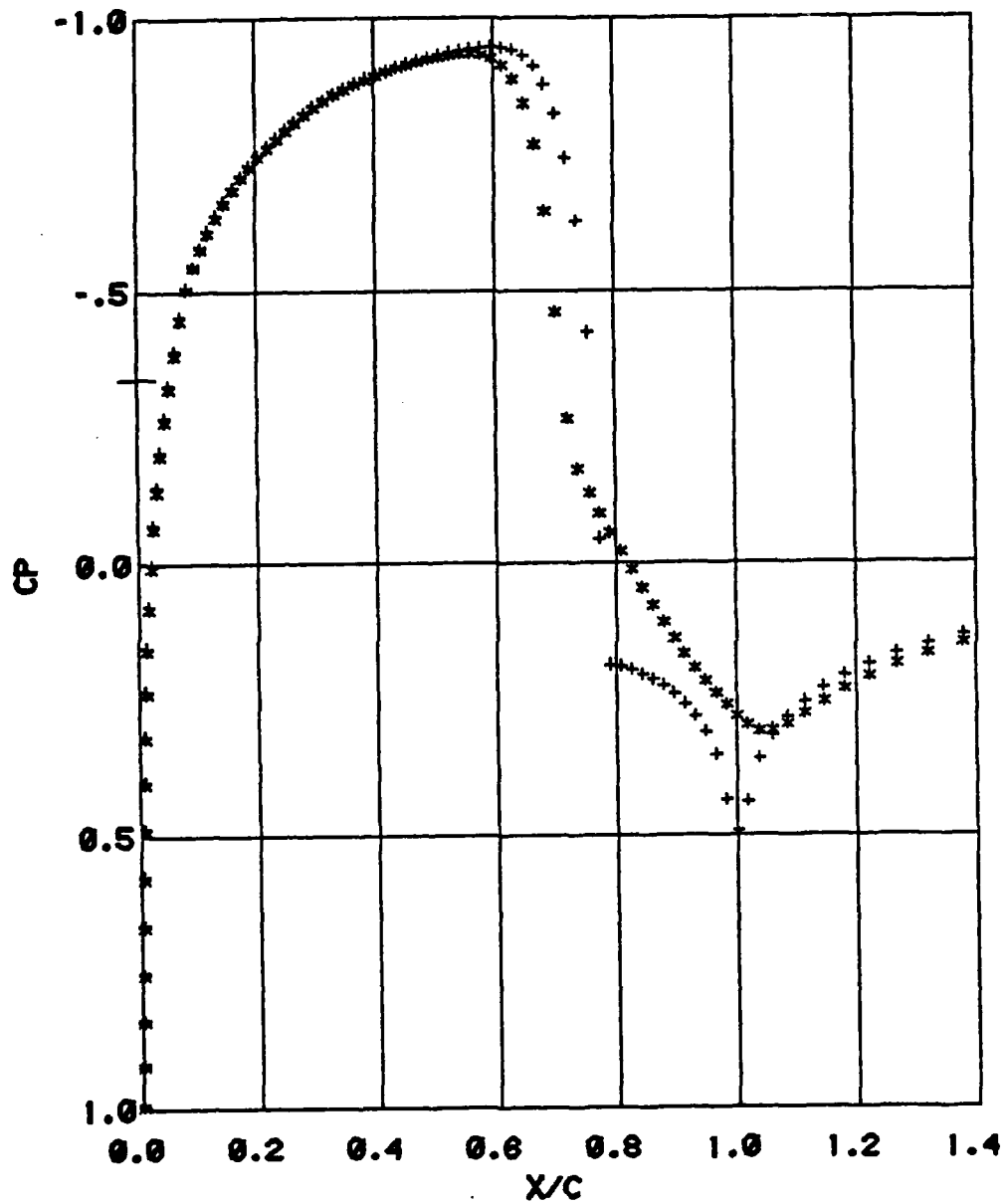
FIG. 9.54 PURE INVISCID PRESSURE
AND PRESSURE AFTER COUPLING
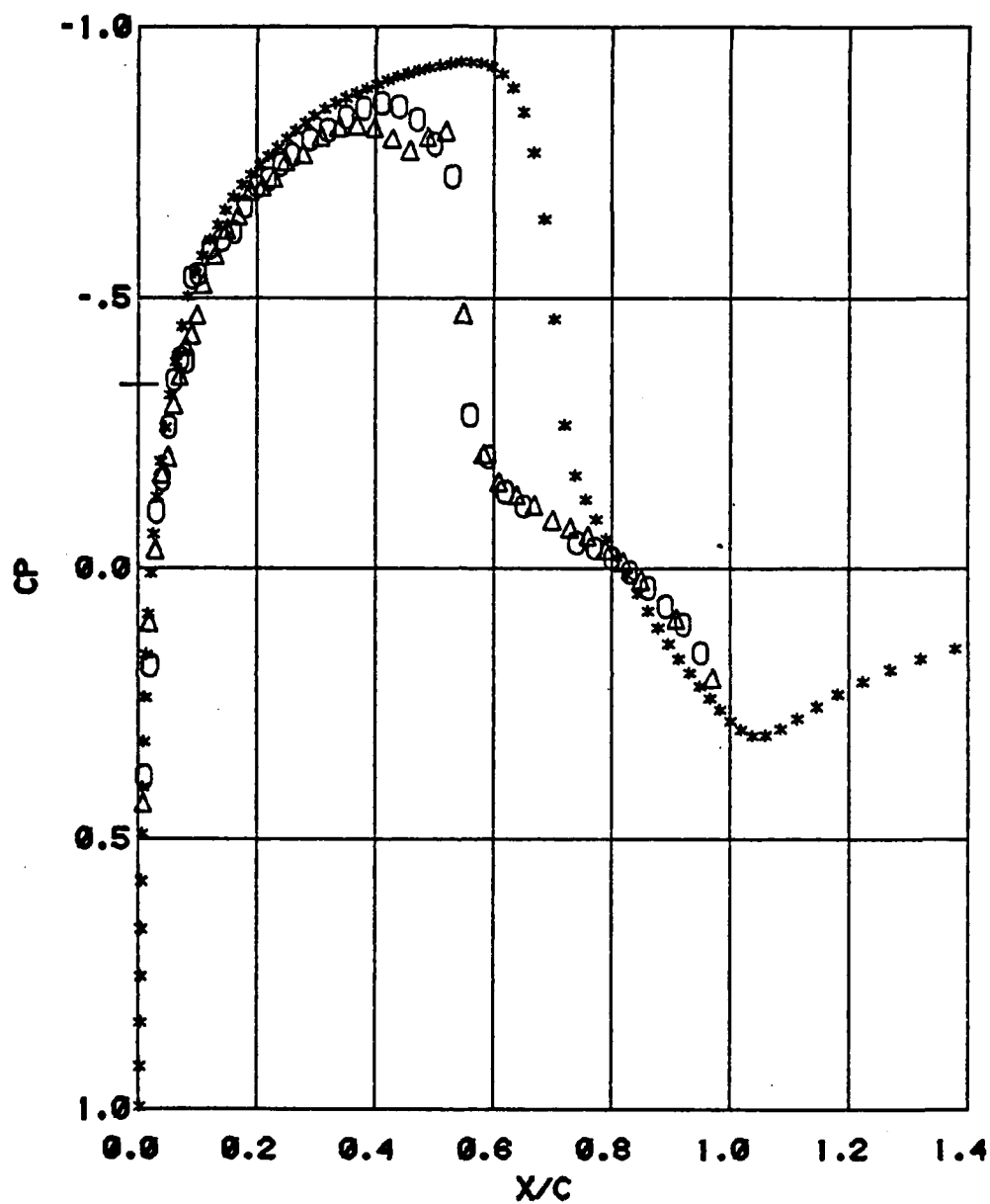MINF= .835   RECH= 24.7E+06
NACA 0012 AIRFOIL
*COUPLED   +INVISCID

FIG. 9.55   EXPERIMENTAL AND COUPLED PRESSURES
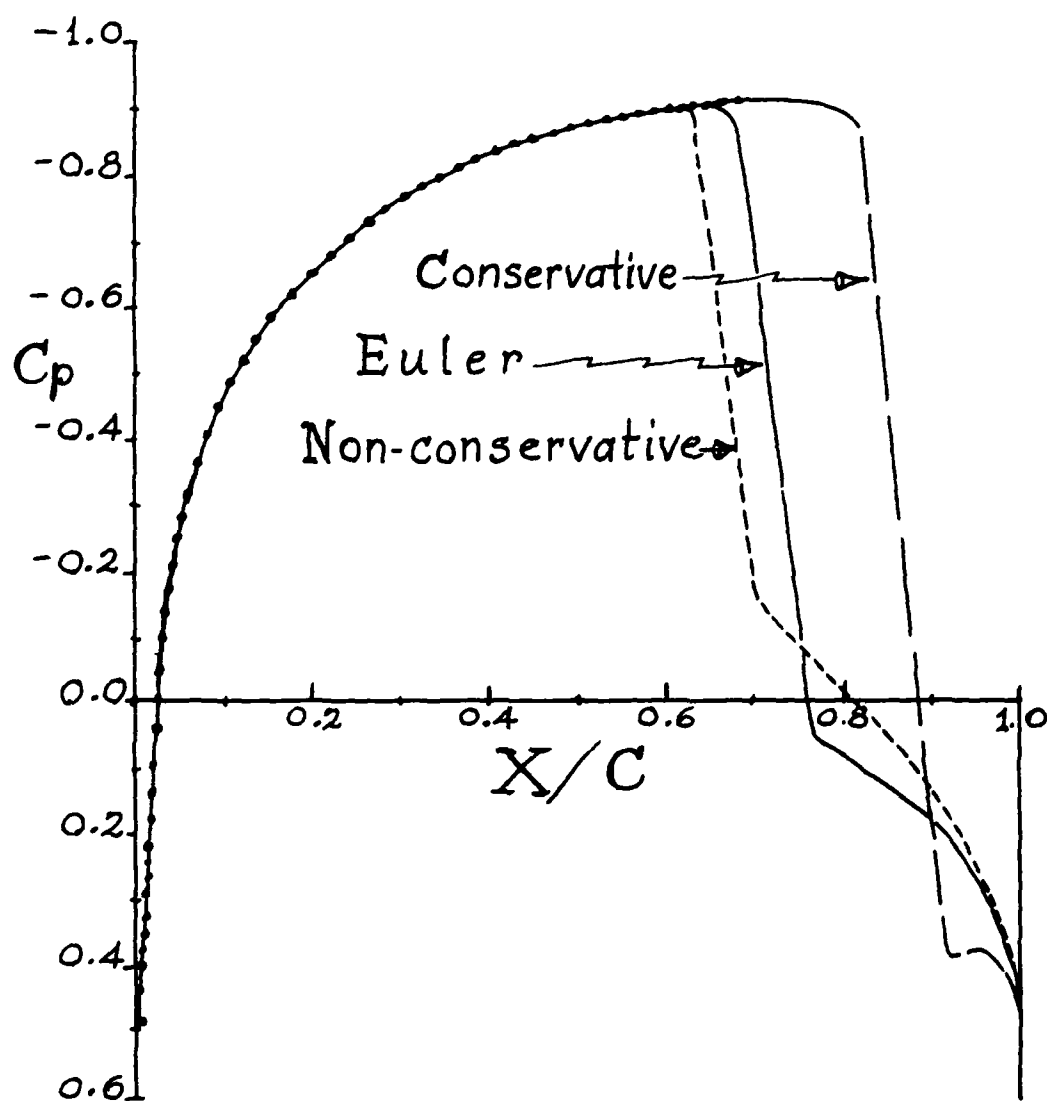MINF= .835   RECH= 24.7E+06
NACA 0012 AIRFOIL

Fig. 9.60   NACA 0012, MINF = .85
A Comparison Between Solutions
of the Euler and Potential Flow
Equations.

END

DATE
FILMED

7-81

DTIC